Contract No. – NAS9 – 16252
DRL – T – K19
Line Item No. 2
DRD – MA – 183TA
RCA – PRRL – 82 – CR – 1

ADVANCED MULTIPURPOSE RENDEZVOUS TRACKING SYSTEM STUDY

June 1, 1982

Richard J. Laurie
Project Scientist
Microwave Technology Center
RCA Laboratories

Fred Sterzer
Director
Microwave Technology Center
RCA Laboratories

RCA Laboratories

Princeton, New Jersey, 08540

PREFACE

This final report describes work performed at the Microwave Technology Center of RCA Laboratories for the Tracking and Communications Development Division of the Lyndon B. Johnson Space Center from November 11, 1980, to December 1, 1981, in fulfillment of NASA Contract NAS9-16252, Advanced Multipurpose Rendezvous Tracking System Study.

The Director of the Microwave Technology Center is F. Sterzer, the Project Supervisor was M. Nowogrodzki, and the Project Scientist was R. Laurie. A supporting study, "Space Missions Requiring Advanced Multipurpose Rendezvous Tracking Systems - 1985-1995," was performed by J. Preston Layton, an independent consultant, and is attached as the appendix.

SUMMARY

Rendezvous and docking (R&D) sensors are needed to support the future Earth-orbital operations of vehicles such as the Shuttle, the Teleoperator Maneuvering System (TMS), and the Orbital Transfer Vehicle (OTV). We investigated the form such sensors should take and whether a single, possibly modular, sensor could satisfy the needs of all three.

An R&D sensor must enable an interceptor vehicle to determine both the relative position and the relative attitude of a target vehicle. Relative-position determination is fairly straightforward and places few constraints on the sensor. Relative-attitude determination, however, is more difficult. The method we have selected is to calculate the attitude based on relative position measurements of several reflectors placed in a known arrangement on the target vehicle.

The constraints imposed on the sensor by the attitude-determination method are severe. Narrow beamwidth, wide field of view (fov), high range accuracy, and fast random-scan capability are all required to determine attitude by this method. A consideration of these constraints as well as others imposed by expected operating conditions and the available technology has led us to conclude that the sensor should be a cw optical radar employing a semiconductor-laser transmitter and an image-dissector receiver.

The performance obtainable from a representative sensor was compared to specifications generated during the study and the conclusion was that this type of sensor can meet the needs of future Earth-orbital operations. When specifications based on more exhaustive mission analyses are available, an optimum design can be generated and analyzed in accordance with the procedures developed.

Several of the components employed in the recommended R&D sensor require further development. The two most important are the image dissector with a GaAs photocathode and the high-power, cw, semiconductor-laser transmitter. Image dissectors with small, imperfect, GaAs photocathodes are available now. Space-qualified image dissectors with large, blemish-free, long-lived, GaAs photocathodes could be easily developed. The development of space-qualified high-power, cw, semiconductor-laser transmitters, however, will require a more extensive effort. Many fundamental aspects of their design have yet to be adequately investigated.

TABLE OF CONTENTS

TABLE OF CONTENTS (Continued)

LIST OF ILLUSTRATIONS

LIST OF ILLUSTRATIONS (Continued)

LIST OF ILLUSTRATIONS (Continued)

LIST OF ILLUSTRATIONS (Continued)

LIST OF TABLES

1. INTRODUCTION

Rendezvous and docking (R&D) capabilities will be required of the vehicles involved in future Earth-orbital operations. This fact was recognized very early in the U.S. space program, and a large part of NASA's efforts over the years has been devoted to the development of R&D procedures and equipment.

The Mercury program (ref. 1), which consisted of two suborbital and four orbital flights, began in 1958. The first suborbital flight took place on February 20, 1962. No rendezvous or docking sensors or capabilities were developed or required for this program.

The Gemini program launched its first spacecraft, an unmanned Gemini I, in 1964. Ten manned flights took place over the next two years. The Gemini program was a precursor to the Apollo program and was conducted, among other reasons, to develop the capability to rendezvous and dock in orbit.

The Gemini vehicles were equipped with a noncoherent pulse radar. Angle tracking was accomplished by the phase-comparison monopulse technique. The target vehicle, which was either another Gemini spacecraft or an Agena upper stage, carried a transponder to assist the radar in acquiring its target.

Rendezvous and docking were manual operations supported by range, range-rate, angle, and angle-rate radar measurements. During the docking maneuver, it was necessary for the astronauts to manually control their spacecraft, based on visual information, to maintain the proper relative attitude for successful docking. The first American rendezvous in space took place between Gemini VI-A and Gemini VII on December 15, 1965.

The first Gemini vehicle to dock was the Gemini VIII. It joined with an Agena target vehicle on March 16, 1966. Gemini IX was scrubbed, and Gemini IX-A, once it had rendezvoused with its target, an Agena upper stage, was unable to dock due to a shroud which had failed to separate from the target docking mechanism. Gemini X, XI and XII all successfully rendezvoused and docked with Agena target vehicles.

The Apollo program ran from 1969 to 1972 and consisted of eleven manned flights, six of which landed men on the Moon. The Apollo spacecraft was a three-man vehicle composed of three modules: the command module (CM), the service module (SM), and the lunar module (LM). The three modules traveled to the Moon as one vehicle. Once in lunar orbit, the LM, carrying two astronauts,

descended to the surface of the Moon. At the completion of the visit, the LM re-entered orbit to rendezvous and dock with the command and service module (CSM). Following the LM docking with the CSM, its two passengers returned to the CM. The LM was then jettisoned. The SM was jettisoned prior to re-entry into the earth's atmosphere.

The LM had to rendezvous and dock with the CSM. The LM was equipped with an X-band, amplitude-comparison monopulse, cw radar (ref. 2) to support these operations. The CM carried a transponder that frequency shifted and amplified the radar pulse before retransmitting it.

The LM rendezvous radar determined range from the phase shifts on three tones (200 Hz, 6.4 kHz, and 204.8 kHz) that phase modulated the X-band carrier. Range rate was determined from the carrier Doppler shift. Angles were determined by the amplitude-comparison monopulse technique. Angle rate was measured by rate gyros mounted on the radar pedestal.

The rendezvous radar had a maximum range of several hundred miles and a minimum range of 50 ft. Over that range its errors were:

- Range: < 1%
- Range Rate: < 1 ft/s
- Angle: 2 mrad
- Angle Rate: < 0.3 mrad/s

Rendezvous and docking were manual operations supported by radar measurements and visual observations. The relative attitude of the two vehicles, in particular, was determined visually.

Soon after the conclusion of the lunar Apollo flights, NASA began the Skylab program which involved the flight of three 3-man crews to a workshop in Earth orbit. Orginally, this had been called the Apollo Applications Program, and was to have run concurrently with the lunar flights. The spacecraft used to take the Skylab pilots to the space station and back was an Apollo CSM, so Skylab could be considered part of the Apollo program.

There were four launches conducted during the Skylab program. The first launch inserted the space station into orbit; the next three brought the crews. During each of the visits, the rendezvous and docking maneuvers employed the same techniques and equipment developed during the Apollo program.

In 1972 NASA embarked on the major program of the 1970s -- the development of a reusable space transportation system based on the Shuttle. The Shuttle is

now completing its final testing and will soon be entering regularly scheduled service. The Shuttle will eventually require the ability to rendezvous and dock if its potential is to be fully realized. The Shuttle will be equipped, shortly, with a rendezvous radar.

The Shuttle rendezvous radar (refs. 3, 4) is a Ku-band, pulse-Doppler radar which doubles as a communications transceiver. Range is determined from pulse transit time; range rate is determined from carrier Doppler shift. Angle is determined by the amplitude-comparison monopulse technique. Angle rates are measured by gyros mounted on the antenna pedestal.

The Shuttle rendezvous radar has a maximum range of 300 nmi if the target has a transponder and 12 nmi if it doesn't. The minimum range is 100 ft in either case. The errors (3σ) within the operating range are:

- Range: 80 ft or 1% (whichever is greater)
- Range Rate: 1 ft/s
- Angle: 8 mrad
- Angle Rate: 0.14 mrad/s

The rendezvous radar is not accurate enough to support close-in station-keeping or docking. Efforts are currently underway (ref. 5) to develop supplemental techniques and sensors to support these operations.

Over the years, several rendezvous and/or docking sensors were developed to various stages, short of deployment. The greatest amount of effort went into ITT's optical radar, the Scanning Laser Radar (SLR) (refs. 6-12). This sensor, which was designed to support both rendezvous and docking, was brought to an advanced (for the time) stage of development under NASA sponsorship.

The ITT SLR went through several generations, but it was essentially a noncoherent, pulsed optical radar with a GaAs-laser transmitter and an image-dissector receiver. Higher accuracy than that achievable from a pulse system was obtained at short ranges from a tone-ranging system based on a cw intensity-modulated LED transmitter.

An optical docking sensor (refs. 13-15) for the Shuttle was proposed and studied in some detail by NASA's Manned Spacecraft Center (now the Johnson Space Center). The sensor had an LED (later changed to an Nd:YAG) transmitter and an image-dissector receiver. In operation, the entire field of view was illuminated by a broad intensity-modulated beam from the transmitter while the

image dissector focused on the returns from individual reflectors arranged around the docking port.

Range was determined from the phase shift on the modulation tones. Angles were determined from the location of the reflector's image on the image dissector's photocathode; there was no closed-loop angle tracking. Range and angle rates were calculated from incremental displacements of the corresponding quantities.

The optical docking sensor investigated by the Manned Spacecraft Center was never constructed, although some experiments were carried out using a borrowed image-dissector-based star tracker.

The Russians, of course, were conducting a space program (Soyuz) at the same time as the United States. One very interesting aspect of the Soyuz program was the development for the first, and only, time of fully automated orbital rendezvous and docking. The Russian approach (ref. 16) to automating these operations employed two similar vehicles: one, the interceptor, equipped with a radar and the other, the target, equipped with a transponder and search beacon.

The automatic rendezvous began with the interceptor radar searching space for the broad beam emitted by the target beacon. Once the target acquired the beacon, the radar began to provide the interceptor with the relative range, bearing, and rate measurements that were the basis for the ensuing rendezvous maneuvers.

As the vehicles closed, the target independently aligned itself with the line of sight (LOS) between itself and the interceptor. The interceptor also aligned itself with the LOS. In this way the relative pitch and yaw attitude angles required for docking were established without either direct measurements of the target's attitude by the interceptor radar or communication between the two vehicles. The roll angle required for docking was established by the interceptor, based upon direct roll-angle measurements made by a supplemental roll-angle sensor.

The Soyuz rendezvous radar was an amplitude-modulated cw radar. Range was determined from the phase shift on the returned modulation tones. Range rate was determined from the carrier Doppler shift. Angles were determined by the amplitude-comparison monopulse technique. Angle rates were measured by gyros mounted on the antenna pedestal.

It might appear that the Russians have already solved the automatic rendezvous and docking problem. However, this is not the case. First, the automatic rendezvous demonstrated no more capability than that possessed by the Apollo spacecraft. The LM rendezvous with the CSM was essentially automatic; the astronauts' primary function being to press the CONTINUE button at various check points in the maneuver.

Second, and more importantly, the Russian automatic docking required that the target have much more capability than could be expected in general. The target not only had to carry a transponder and beacon, it also had to determine its own attitude relative to the LOS and then align itself properly to it. The size, cost, and power consumption of the target equipment would make it impractical for all but the largest vehicles. In addition, some vehicles, such as a space station, could not be expected to alter their relative attitude to enable another vehicle to dock with them.

The present situation with regard to R&D sensors is that we have one operating vehicle, the Shuttle, equipped with a limited-capability rendezvous radar, and two planned vehicles, the Teleoperator Maneuvering System (TMS) and the Orbital Transfer Vehicle (OTV), whose needs have received little attention, up to now.

The purpose of this project was to investigate the future needs for R&D sensors of vehicles such as the Shuttle, TMS, and OTV, and to see whether one, possibly modular, sensor could be developed for all of them. Since a requirement for rendezvous and docking with all types of vehicles, from small communications satellites to large space stations, was envisioned, emphasis was placed on limiting the equipment and capability required of the target. The target should not have to carry more than a few passive aids, such as reflectors, in addition to some kind of docking fixture.

In the following pages we present the results of our investigation. We began by looking at the data required to support rendezvous and docking. This effort is described in the next section.

2. FUTURE EARTH-ORBITAL OPERATIONS

Future Earth-orbital operations will require sensors capable of supporting rendezvous, stationkeeping, and docking between various vehicles, satellites, and space stations. Some representative operations and the entities involved are classified in Table 2-1.

TABLE 2-1. FUTURE SPACE ACTIVITIES

	Satellites	Space Stations	Vehicles	Unknown Objects
Deployment	X		X	
Construction		X	X	
Operation	X	X	X	
Inspection	X	X	X	X
Repair	X	X	X	
Retrieval	X	X	X	X

The need for rendezvous, stationkeeping, and docking capability to perform these operations is indicated in Table 2-2.

TABLE 2-2. CAPABILITIES REQUIRED FOR FUTURE SPACE MISSIONS

	Rendezvous	Stationkeeping	Docking
Deployment			
Construction	X	X	X
Operation	X	X	X
Inspection	X	X	
Repair	X	X	X
Retrieval	X	X	X

There are several terms used when discussing rendezvous, stationkeeping, and docking which require definition. Generally, these operations involve two vehicles: a passive vehicle which does nothing other than maintain its present state, and an active vehicle which moves to effect the operation. The passive vehicle is called the target and the active vehicle is called the interceptor.

The target vehicle may be cooperative or noncooperative. A cooperative target assists the interceptor by helping it to obtain the information needed for the intended operation. The target can help by carrying aids such as reflectors, or transponders, or by making measurements with its own sensors and transmitting the information to the interceptor. Passive aids are those that require no power from the target. Active aids are those that require power from the target. Passive aids are preferable but may not always be feasible.

2.1 Future Earth-Orbital Vehicles

The three vehicles shown in Figure 2-1, the Shuttle, the TMS, and the OTV, will be used to support most future Earth-orbital operations. The Shuttle is in operation today and will be the primary means to deliver objects into lower earth orbit (LEO) in the future. The TMS will ride in the Shuttle cargo bay and will be used for Shuttle-proximity operations. The OTV will be used to move objects from LEO to higher orbit (such as geosynchronous orbit [GEO]). The precise forms that the TMS and the OTV will take has not been settled but the need for them is clear.

The Space Operations Center (SOC), shown in Figure 2-2, will be a key element in future space operations. It will be placed in LEO by the shuttle and will support operations such as the assembly and servicing of satellites. The OTV would probably be based at the SOC.

All three vehicles will eventually require the capability to rendezvous, stationkeep, and dock. A single R&D sensor able to support these operations for all three vehicles must be able to provide the data required by each of them and must be physically compatible with all of them. The TMS is the smallest of the three vehicles and imposes the most severe size and power limitations.

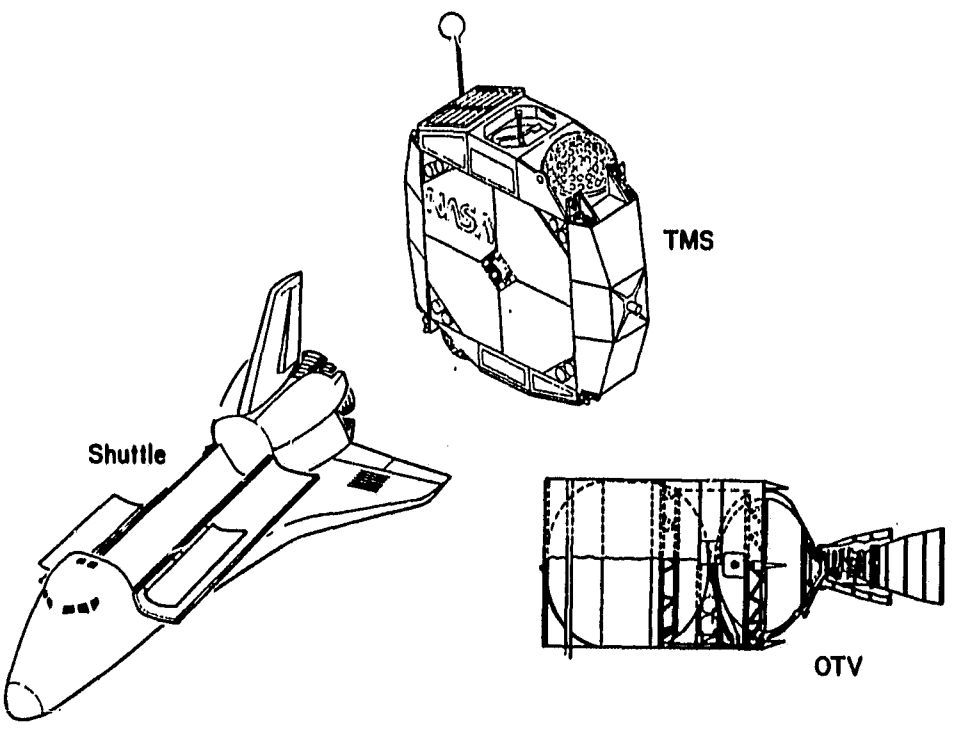

Figure 2-1. Future space vehicles.

2.2 Rendezvous

Rendezvous (refs. 17-22) is the maneuvering of the interceptor into the same orbit and phase as the target. Rendezvous requires that the interceptor match both the target's position and velocity as opposed to interception, in the military sense, which merely requires that the positions be identical.

For our purposes, a rendezvous maneuver can be considered to have two steps. Initially, the target is beyond the range of the interceptor's sensors. The interceptor obtains the target's state either from a third party (such as a ground station) or from the target itself. The interceptor then calculates a trajectory designed to effect a rendezvous, based upon knowledge of both its own and the target's states. Due to various errors, the rendezvous maneuver will not deliver the interceptor to the precise position, relative to the target, that is desired.

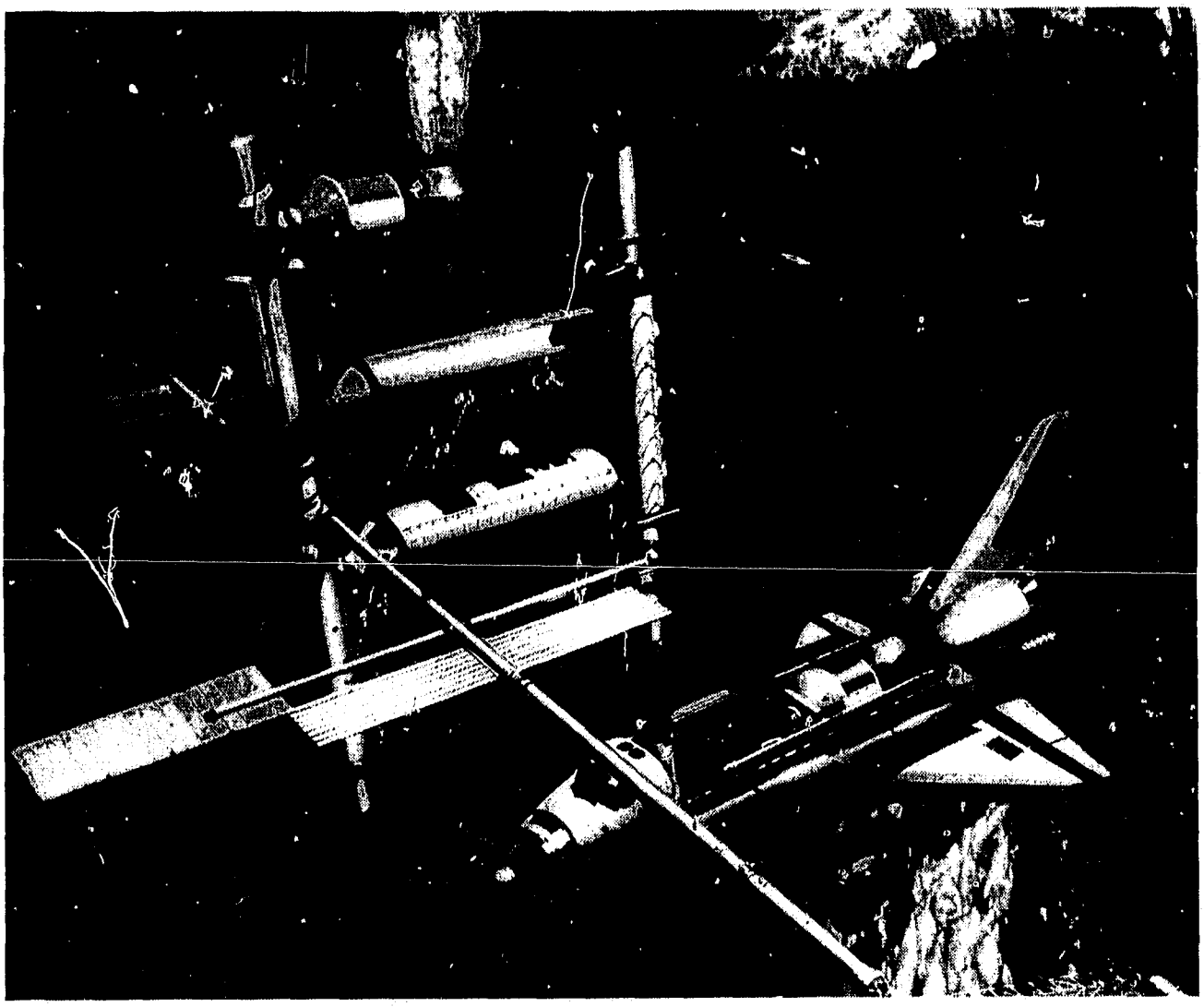

Figure 2-2. The Space Operations Center.

Once the target comes within range of the interceptor's sensors, the second phase of the rendezvous begins. The interceptor now conducts maneuvers based upon direct measurements of the relative position of the target. The errors in the original trajectory are corrected and the rendezvous is completed when the two vehicles are within about 100 m of one another.

Rendezvous requires that the relative range and bearing (and rates) of the two vehicles be known, but does not require knowledge of their relative attitude. The most critical item is the maximum range since this directly affects the

sensor size and weight. The rendezvous data requirements we have assumed are shown in Table 2-3. The 50-km maximum range is justified by the improved navigational systems, such as the Global Positioning System (GPS), that will be coming into use shortly.

TABLE 2-3. RENDEZVOUS DATA REQUIREMENTS

Parameter	Limits	Accuracy (3σ)
Range	0.1-50 km	0.01 x Range
Range Rate	±50 m/s	0.1 m/s
Angle	±0.25 rad	10 mrad
Angle Rate	±20 mrad/s	0.1 mrad/s

2.3 Docking

Docking (refs. 23-25) is the physical joining of the interceptor and the target. Since each vehicle must contain a docking mechanism of some sort (even if it's just a grappling fixture), docking requires a cooperative target. A cooperative target is also required because successful docking requires data accuracy beyond that achievable without aids.

There are two types of docking mechanisms: hard (impact) and soft (non-impact). Hard-docking mechanisms can tolerate nonzero impact velocities. In fact, hard-docking mechanisms are designed to use the energy of impact to latch up. Soft-docking mechanisms are designed to operate with a zero-impact velocity.

In the past, hard-docking mechanisms have been employed. These are suitable for the docking of two small- or medium-size vehicles; this has been the case up to now. In the future, we can expect docking between large, medium, and small vehicles in all possible combinations and, in many cases, a soft-docking mechanism will be required. A general-purpose R&D sensor should provide the type of data required for soft docking.

Docking requires that the target's range, bearing, and attitude (and rates) be known. This is in contrast to rendezvous which does not require attitude. Typical data required to support a soft docking are shown in Table 2-4. The maximum range for the docking data is 100 m, which is the range at which the docking maneuver is expected to begin. The minimum range is 2 m, which is the range between the R&D sensor and the target aids at the time the docking mechanisms first contact.

TABLE 2-4. DOCKING DATA REQUIREMENTS

Parameter	Limits	Accuracy (3σ)
Range	2-100 m	0.01 x Range
Range rate	±1 m/s	0.01 m/s
Angle	±0.25 rad	10 mrad
Angle rate	±20 mrad/s	0.1 mrad/s
Attitude (P,Y)	±0.5 rad	30 mrad
Attitude (R)	± π rad	30 mrad
Attitude rate	±20 mrad/s	0.1 mrad/s

The docking range-rate limits are lower than those for rendezvous since the vehicles are expected to have a lower relative velocity at the start of the maneuver. The range-rate accuracy required for docking is higher because the velocity must be reduced to near zero as the vehicles come together.

The attitude-data requirements are primarily functions of the docking mechanism design. The requirements shown in Table 2-4 are believed to be adequate for any foreseeable mechanism.

2.4 Stationkeeping

Stationkeeping is the maintenance of constant relative positions, and possibly attitudes, between the interceptor and the target. Stationkeeping would normally take place within 10-1000 m of the target. It is assumed that any sensor that provides data adequate to support rendezvous and docking will also support stationkeeping.

2.5 R&D Docking Sensor Requirements

The information required to support rendezvous and docking (and, therefore, station-keeping), given in Tables 2-3 and 2-4, has been combined in Table 2-5. Our task was to identify which type of sensor could provide this information and would be suitable for use by either the Shuttle, the TMS or the OTV. Sensors that required passive aids were considered but those that required active aids were not because active aids are not suitable for all targets.

TABLE 2-5. RENDEZVOUS AND DOCKING DATA REQUIREMENTS

Parameter	Limits	Accuracy (3σ)
Range	2m-50 km	0.01 x Range
Range rate	±50 m/s	0.01 m/s ($R \leq 1$m/s)
		0.1 m/s ($R > 1$m/s)
Angle	±0.25 rad	10 mrad
Angle rate	±20 mrad/s	0.1 mrad/s
Attitude (P,Y)	±0.25 rad ($R < 100$ m)	30 mrad
Attitude (R)	$\pm \pi$ rad ($R < 100$ m)	30 mrad
Attitude rate	±20 mrad/s ($R < 100$ m)	0.1 mrad/s

3. ATTITUDE DETERMINATION

Docking requires that the interceptor be able to determine the relative attitude of the target. There are only two ways to do this within the passive-aid constraint. The first method determines attitude from range and bearing measurements to three (or more) reflectors in a known configuration on the target. The second method determines attitude from bearing-only measurements to four (or more) reflectors in a known configuration on the target.

The first method (range and bearing measurements) was selected because range measurement capability is needed anyway (to support rendezvous), the required bearing accuracy is less than required by the second method, and fewer reflectors are needed. The coplanar docking aids (reflectors) are assumed to be placed in a known arrangement around the circumference of a 1-m-diameter, or smaller, circle, as shown in Figure 3-1.

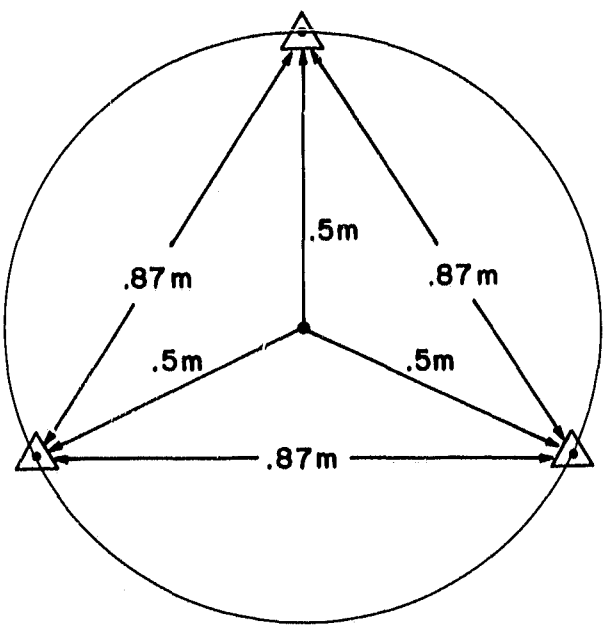

Figure 3-1. Reflector arrangement.

The reflector pattern shown in fig. 3-1 would result in a roll-angle ambiguity since the reflectors cannot be distinguished from one another. This problem can be eliminated by employing an unsymmetric arrangement or by using different size reflectors. If a docking mechanism with the proper symmetry were used, the ambiguity would not be a problem. In any case, this is considered a minor matter and was not specifically studied.

3.1 Calculating Attitude from Range and Bearing

The range, R_i, and bearing, θ_{ei} and θ_{ai}, of each reflector in the array are measured and then the attitude of the target is calculated from this data. There are several ways to describe the relative attitude of two vehicles. Euler's angles are frequently used in analytical mechanics but for our purposes, pitch, θ_p, yaw, θ_y, and roll, θ_r, as shown in Figure 3-2, are employed.

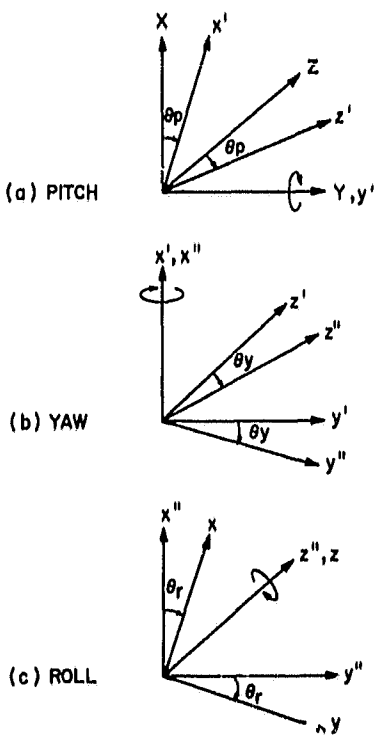

Figure 3-2. Attitude angles.

The relationship between the coordinates of a point in the x, y, z reference frame and in the X,Y,Z frame are

$$\begin{bmatrix} X \\ Y \\ Z \end{bmatrix} = A_1 \begin{bmatrix} x' \\ y' \\ z' \end{bmatrix} \tag{3-1}$$

$$\begin{bmatrix} x' \\ y' \\ z' \end{bmatrix} = A_2 \begin{bmatrix} x'' \\ y'' \\ z'' \end{bmatrix} \tag{3-2}$$

$$\begin{bmatrix} x'' \\ y'' \\ z'' \end{bmatrix} = A_3 \begin{bmatrix} x \\ y \\ z \end{bmatrix} \tag{3-3}$$

and

$$\begin{bmatrix} X \\ Y \\ Z \end{bmatrix} = A \begin{bmatrix} x \\ y \\ z \end{bmatrix} \tag{3-4}$$

where
$$A_1 = \begin{bmatrix} \text{Cos } \theta_p & 0 & -\sin \theta_p \\ 0 & 1 & 0 \\ \sin \theta_p & 0 & \cos \theta_p \end{bmatrix} \tag{3-5}$$

$$A_2 = \begin{bmatrix} 1 & 0 & 0 \\ 0 & \cos \theta_y & -\sin \theta_y \\ 0 & \sin \theta_y & \cos \theta_y \end{bmatrix} \tag{3-6}$$

$$A_3 = \begin{bmatrix} \cos\theta_r & -\sin\theta_r & 0 \\ \sin\theta_r & \cos\theta_r & 0 \\ 0 & 0 & 1 \end{bmatrix} \tag{3-7}$$

and $A = A_1 A_2 A_3$

$$= \begin{bmatrix} \cos\theta_p\cos\theta_r - \sin\theta_p\sin\theta_y\sin\theta_r & -\cos\theta_p\sin\theta_r - \sin\theta_p\sin\theta_y\cos\theta_r & -\sin\theta_p\cos\theta_y \\ \cos\theta_y & \cos\theta_y\cos\theta_r & -\sin\theta_y \\ \sin\theta_p\cos\theta_r + \cos\theta_p\sin\theta_y\sin\theta_r & -\sin\theta_p\sin\theta_r + \cos\theta_p\sin\theta_y\cos\theta_r & \cos\theta_p\cos\theta_y \end{bmatrix} \tag{3-8}$$

If there are two vectors, P_0P_1 and P_0P_2, having a known orientation in the x, y, z frame, as shown in Figure 3-3, then we can determine A as

$$A = \begin{bmatrix} (X_1 - X_0) & (X_2 - X_0) & (X_3 - X_0) \\ (Y_1 - Y_0) & (Y_2 - Y_0) & (Y_3 - Y_0) \\ (Z_1 - Z_0) & (Z_2 - Z_0) & (Z_3 - Z_0) \end{bmatrix} \times \begin{bmatrix} x_1 & x_2 & x_3 \\ y_1 & y_2 & y_3 \\ z_1 & z_2 & z_3 \end{bmatrix}^{-1} \tag{3-9}$$

where*

$$\begin{bmatrix} x_3 \\ y_3 \\ z_3 \end{bmatrix} = \begin{bmatrix} x_1 \\ y_1 \\ z_1 \end{bmatrix} X \begin{bmatrix} x_2 \\ y_2 \\ z_2 \end{bmatrix} \tag{3-10}$$

The values of the elements of A may be all we need. If the actual angles, θ_p, θ_y, θ_r, are needed they can be determined numerically. When more reflectors are employed, A can be computed in as many independent ways as possible and the results averaged.

*X indicates the vector cross-product operation.

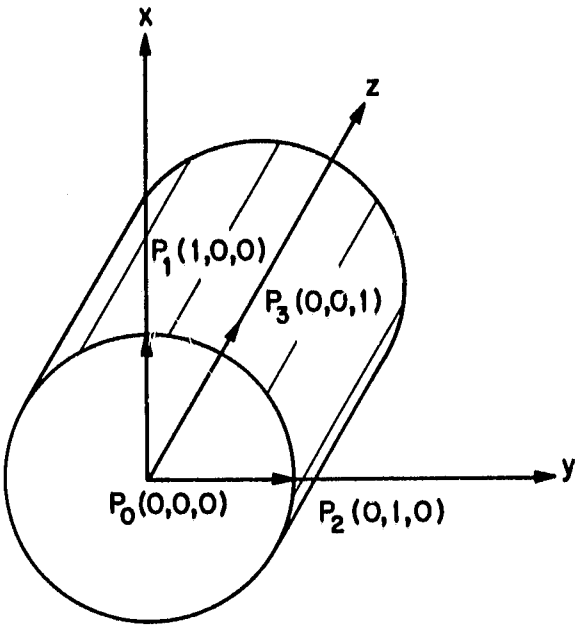

Figure 3-3. Reference vectors for attitude determination.

The rectangular components of each point, P_i, X_i, Y_i and Z_i, are determined from the on-axis azimuth and elevation angles, θ_{ei} and θ_{ai}, as shown in Figure 3-4. The relationships are

$$X_i = \frac{R_i \sin \theta_{ei} \cos \theta_{ai}}{(1 - \sin^2 \theta_{ei} \sin^2 \theta_{ai})^{1/2}} \tag{3-11}$$

$$Y_i = \frac{R_i \sin \theta_{ai} \cos \theta_{ei}}{(1 - \sin^2 \theta_{ei} \sin^2 \theta_{ai})^{1/2}} \tag{3-12}$$

and

$$Z_i = \frac{R_i \cos \theta_{ai} \cos \theta_{ei}}{(1 - \sin^2 \theta_{ei} \sin^2 \theta_{ai})^{1/2}} \tag{3-13}$$

The relations above are expressed in terms of the on-axis bearing angles. A particular sensor may actually measure θ_a and θ_e' (elevation over azimuth), θ_a'

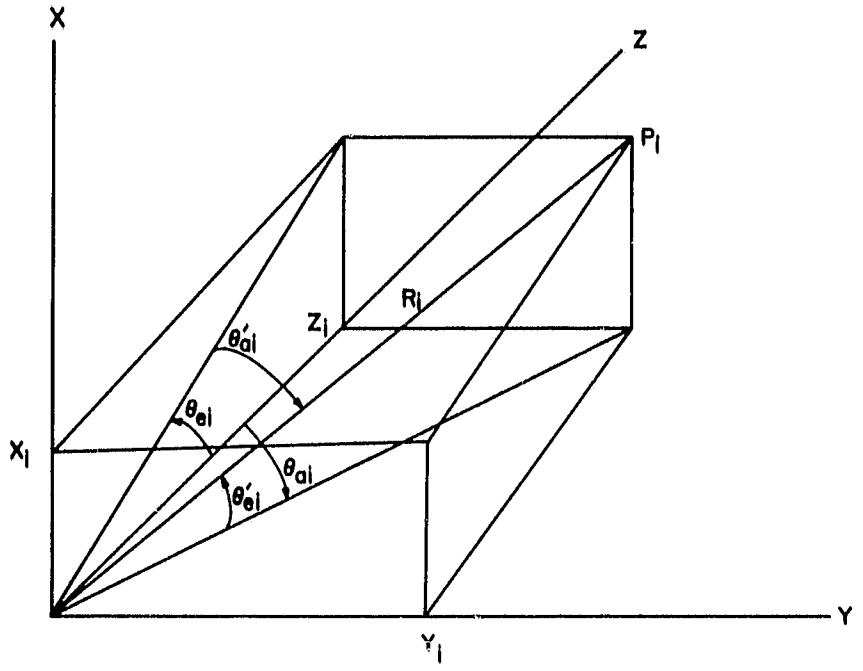

Figure 3-4. On-axis (unprimed) and off-axis (primed) bearing angles.

and θ_e (azimuth over elevation), or θ_a and θ_e (electronic beamsteering). The relations between the on-axis and off-axis bearing angles are

$$\sin \theta_e = \sin \theta'_e / \cos \theta'_a \tag{3-14}$$

and

$$\sin \theta_a = \sin \theta'_a / \cos \theta'_e. \tag{3-15}$$

3.2 Range and Bearing Accuracy Requirements

The accuracy required of the range and bearing measurements for an attitude accuracy of 10 mrad (1σ) was determined by studying the simplified situation depicted in Figure 3-5. We assume that R_1, θ_1, R_2, and θ_2 are measured and that we then calculate ϕ as

$$\phi = \tan^{-1} (y/x) \tag{3-16}$$

where

$$y = y_2 - y_1 \tag{3-17}$$

$$x = x_2 - x_1 \tag{3-18}$$

and

$$x_1 = R_1 \cos \theta_1 \tag{3-19}$$

$$y_1 = R_1 \sin \theta_1 \tag{3-20}$$

$$x_2 = R_2 \cos \theta_2 \tag{3-21}$$

$$y_2 = R_2 \sin \theta_2 \tag{3-22}$$

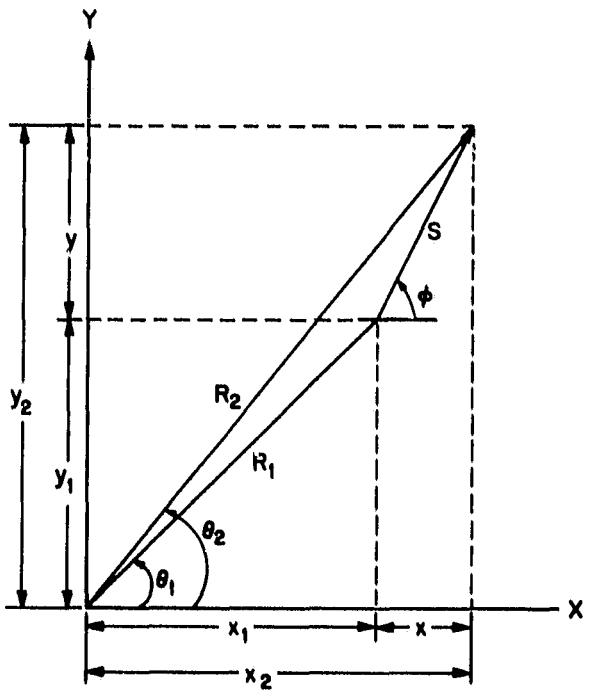

Figure 3-5. Quantities involved in attitude determination from range and bearing measurements.

If there were no errors, ϕ could be determined exactly. However, there is a range-measurement error, σ_R, and a bearing-measurement error, σ_θ. These errors propagate through the calculations as

$$\sigma_\phi^2 = \frac{\sin^2\phi}{S^2} \cdot \sigma_x^2 + \frac{\cos\phi^2}{S^2} \cdot \sigma_y^2 \tag{3-23}$$

where

$$\sigma_x^2 = \sigma_{x1}^2 + \sigma_{x2}^2 \tag{3-24}$$

$$\sigma_y^2 = \sigma_{y1}^2 + \sigma_{y2}^2 \tag{3-25}$$

and

$$\sigma_{xi}^2 = \cos^2\theta_i \cdot \sigma_R^2 + R_i^2 \sin^2\theta_i \cdot \sigma_\theta^2 \tag{3-26}$$

$$\sigma_{yi}^2 = \sin^2\theta_i \cdot \sigma_R^2 + R_i^2 \cos^2\theta_i \cdot \sigma_\theta^2. \tag{3-27}$$

The method used to determine σ_ϕ for a given value of σ_R and σ_θ was:

1. Pick S, θ_1, R_1, σ_θ, σ_R, ϕ

2. Calculate x_1 and y_1
   $x_1 = R_1 \cos\theta_1$
   $y_1 = R_1 \sin\theta_1$

3. Calculate x and y
   $x = S \cos\phi$
   $y = S \sin\phi$

4. Calculate x_2 and y_2
   $x_2 = x_1 + x$
   $y_2 = y_1 + y$

5. Calculate θ_2, R_2
   $\theta_2 = \tan^{-1}(y_2/x_2)$
   $R_2 = \left(x_2^2 + y_2^2\right)^{1/2}$

6. Calculate σ_{xi}^2, σ_{yi}^2

$$\sigma_{xi}^2 = \cos^2 \theta_i \cdot \sigma_R^2 + R_i^2 \sin^2 \theta_i \cdot \sigma_\theta^2$$

$$\sigma_{yi}^2 = \sin^2 \theta_i \cdot \sigma_R^2 + R_i^2 \cos^2 \theta_i \cdot \sigma_\theta^2$$

7. Calculate σ_x^2, σ_y^2

$$\sigma_x^2 = \sigma_{x1}^2 + \sigma_{x2}^2$$

$$\sigma_y^2 = \sigma_{y1}^2 + \sigma_{y2}^2$$

8. Calculate σ_ϕ^2

$$\sigma_\phi^2 = \frac{\sin^2 \phi}{S^2} \cdot \sigma_x^2 + \frac{\cos^2 \phi}{S^2} \cdot \sigma_y^2$$

Some typical results from this procedure are shown in Figure 3-6 where the allowable errors in range and bearing measurements to yield σ_ϕ = 10 mrad for a reflector spacing, S, of 1 m and a range, R_1, of 10 m are shown for $\theta_1 = 45°$ and $\phi = 0°$. This is a representative case and, based upon it and others, a range accuracy of 5 mm and a bearing accuracy of 0.4 mrad were determined to be necessary.

Figure 3-7 shows how σ_ϕ varies with range for σ_R = 5 mm and σ_θ = 0.4 mrad in a typical case. Figure 3-8 shows the effect of reduced reflector spacing on σ_ϕ.

3.3 Sensor Requirements Assuming Attitude Calculation

The method we have selected to determine target attitude is by calculation, based on range and bearing measurements to three (or more) reflectors arranged in a known configuration. We have determined that within the range at which attitude information will be required (2-100 m), range should be measured to within 5 mm (1σ) and bearing to within 0.4 mrad (1σ). The resulting requirements for an R&D sensor that will result in the same performance as specified

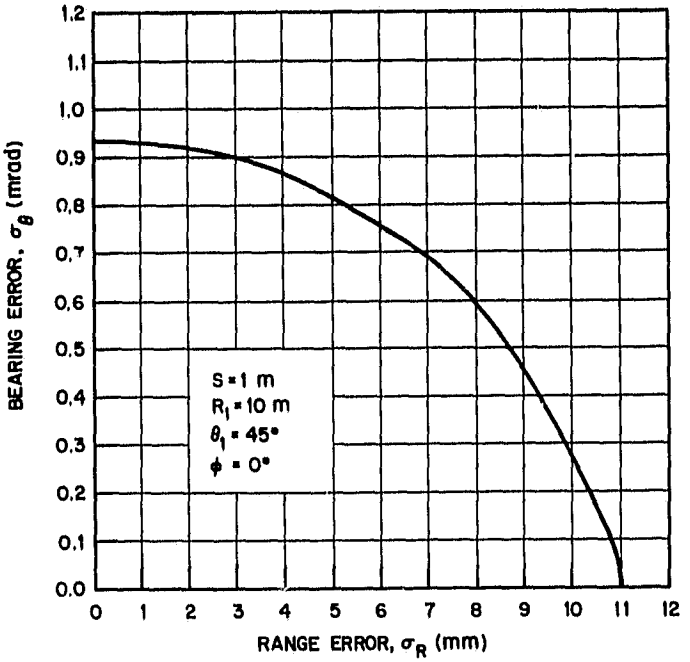

Figure 3-6. Required range and bearing accuracy to result in an attitude error of 10 mrad (σ_ϕ = 10 mrad).

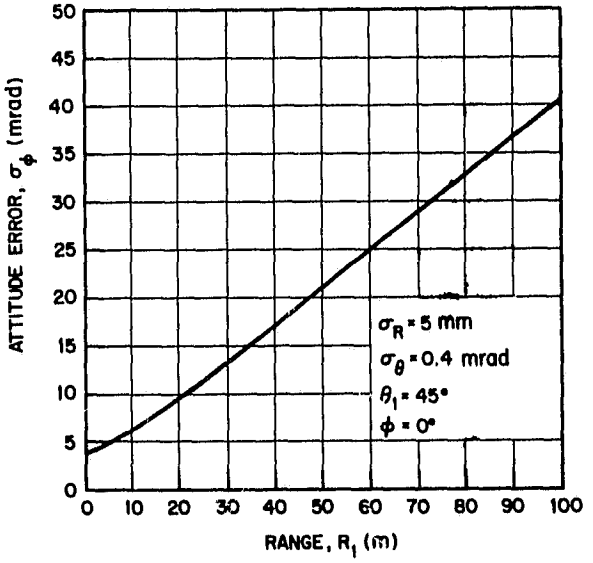

Figure 3-7. Attitude error as a function of range for σ_R = 5 mm, σ_θ = 0.4 mrad, θ_1 = 45°, and ϕ = 0°.

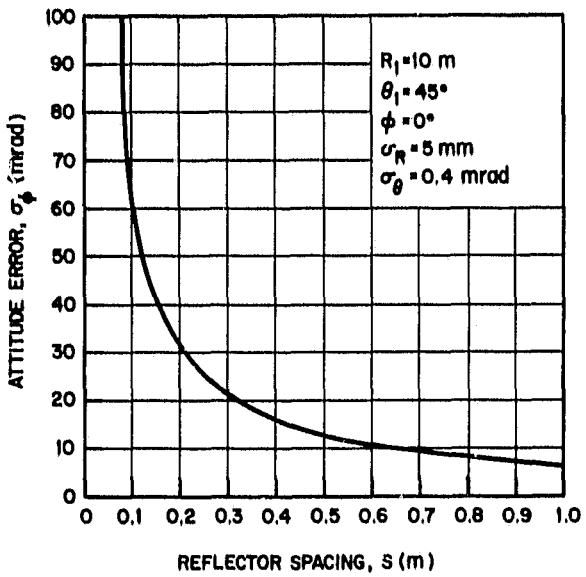

Figure 3-8. Attitude error as a function of reflector spacing for σ_R = 5 mm, σ_θ = 0.4 mrad, R_1 = 10 m, θ_1 = 45°, and ϕ = 0°.

in Table 2-5 are shown in Table 3-1. The required range accuracy is shown in Figure 3-9.

TABLE 3-1. PERFORMANCE REQUIREMENTS FOR THE R&D SENSOR

Parameter	Limits	Accuracy (3σ)
Range	2 m - 50 km	0.00015 x Range (R>100m)
		15 mm (2 m<R<100 m)
Range rate	±50 m/s	0.01 m/s (R ≤ 1 m/s)
		0.1 m/s (R>1 m/s)
Angle	±0.25 rad	1.2 mrad
Angle rate	±20 mrad/s	0.1 mrad/s

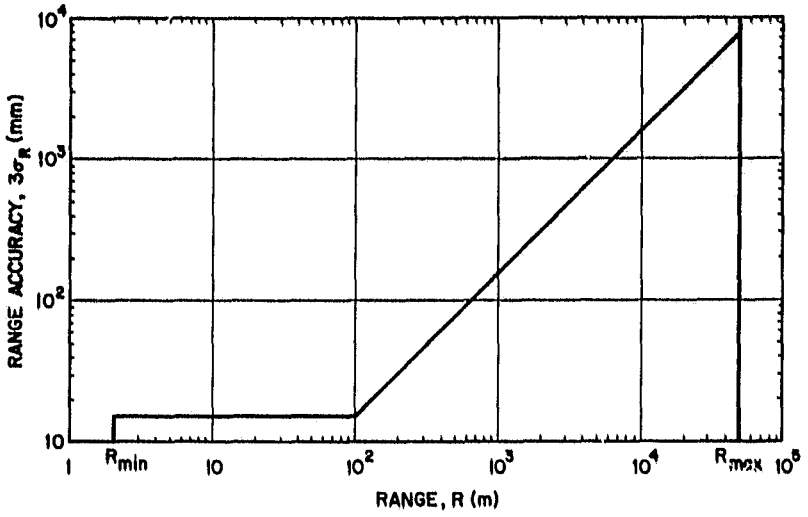

Figure 3-9. Required range accuracy.

4. PRELIMINARY SENSOR DESIGN

So far the only constraint that we have placed on the R&D sensor is that it be able to measure range and bearing over the limits and to the accuracies, specified in Table 3-1. There are a variety of sensors that can be used to measure range and bearing. In the following pages we will attempt to narrow the field by examining the performance requirements, the conditions of use, and the available technology. Specifically, we will examine each of the following topics in an attempt to identify suitable candidates:

- Illumination source
- Beamwidth
- Carrier frequency
- Field of view
- Background radiation
- Transmitter source
- Modulation techniques
- Receiver scanning mechanism

4.1 Illumination Source

All sensors have a receiver that senses radiation originating from the target. Active sensors illuminate the target themselves. Passive sensors depend on some other source of illumination, such as the Sun. A passive R&D sensor would have to depend on the Sun to illuminate the target. Sunlight, however, is not always available. Figure 4-1 illustrates the shadow cast by the Earth.

The diameter of the shadow, d_s, at an altitude A_o above the Earth's surface is

$$d_s = 2\left[r_e - \frac{r_s}{X}(r_e + A_o)\right] \qquad (4\text{-}1)$$

This relationship is shown in Figure 4-2. Clearly, the Earth's shadow is too large to rely upon the Sun to illuminate the target. Therefore only active sensors are considered further.

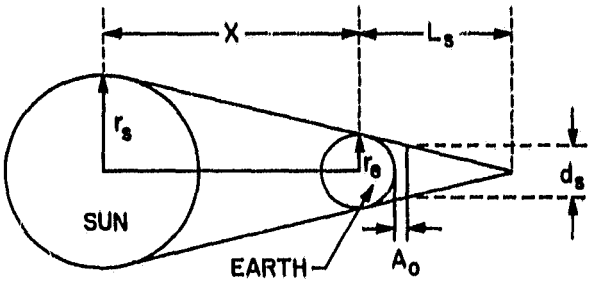

$r_e = 6731$ km
$r_s = 6.96 \times 10^5$ km
$X = 1.496 \times 10^8$ km

Figure 4-1. The Earth's shadow.

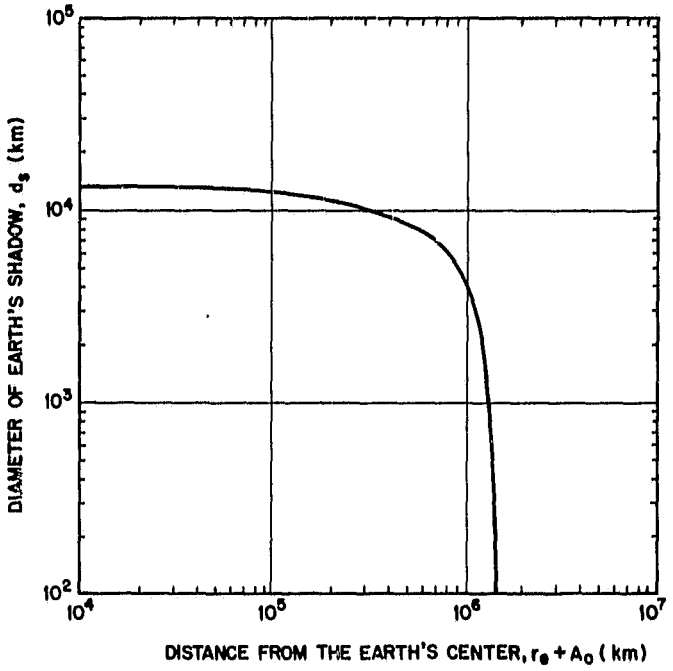

Figure 4-2. The diameter of the Earth's shadow as a function of altitude.

4.2 Beamwidth

There are two beamwidths associated with any active sensor (one that provides its own source of illumination): that of the transmitter and that of the receiver. The most efficient operation is achieved when the transmitter and receiver beamwidths are identical. We have restricted our considerations to sensors with identical transmitter and receiver beamwidths and therefore the term beamwidth will be used henceforth without further qualification.

The beamwidth of the sensor is determined by the requirement that the reflectors on the target be resolvable at 100 m. Figure 4-3 illustrates the angular separation existing between two reflectors separated by 1 m for several inclination angles.

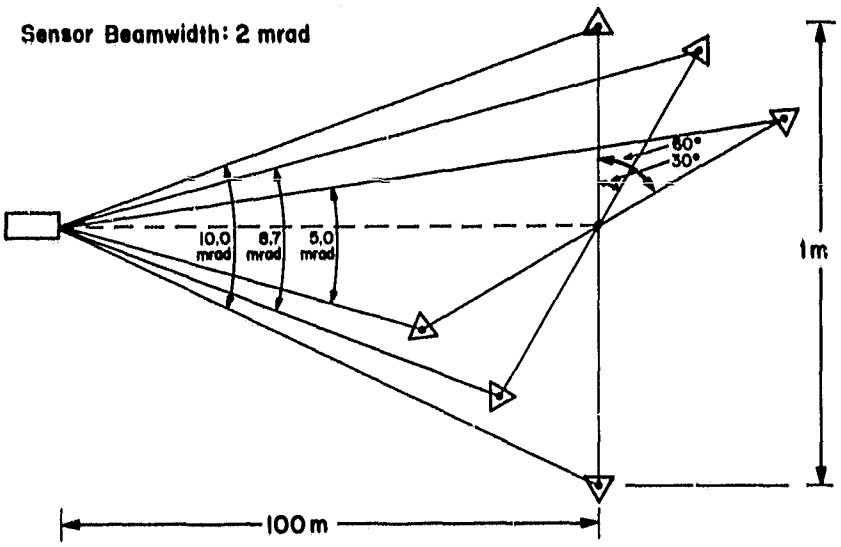

Figure 4-3. Angular separation at 100 m of reflectors spaced 1 m apart.

The minimum angular separation at 100 m between any two reflectors arranged around a 1-m-diameter circle normal to the line of sight is

$$\theta_{min} = \frac{\sin (\pi/n)}{100} \qquad (4\text{-}2)$$

where n is the number of reflectors. The value of θ_{min} for several values of n are:

n	θ_{min} (mrad)
2	10.0
3	8.7
4	7.1
5	5.9

In view of the number of reflectors most likely to be employed (3 or 4) and the initial inclination angles expected, a beamwidth of 2 mrad was selected for the sensor.

4.3 Carrier Frequency

Active sensors capable of measuring range and bearing can operate at frequencies from the lower microwave to visible light. The one parameter that restricts the allowable operating frequency is beamwidth. The minimum beamwidth achievable from a circular aperture occurs when it is uniformly illuminated. This beamwidth (ref. 26) is

$$\theta_b \cong \frac{\lambda}{D} \tag{4-3}$$

where λ = wavelength

D = aperture diameter

θ_b = beamwidth between half-intensity points

There is another beamwidth, θ_b', which is the angular diameter of the Airy disk. This beamwidth is

$$\theta_b' = \frac{2.44\ \lambda}{D} \tag{4-4}$$

but it is not the one we are interested in.

Figure 4-4 shows the minimum beamwidths achievable from uniformly illuminated circular apertures of various sizes as a function of wavelength. If we limit the sensor-aperture diameter to 0.1 m and if we assume that the actual beamwidth will be twice the minimum, we see that a wavelength of 100 μm or less will be necessary. The R&D sensor must therefore be an optical radar operating somewhere between the visible and infrared.

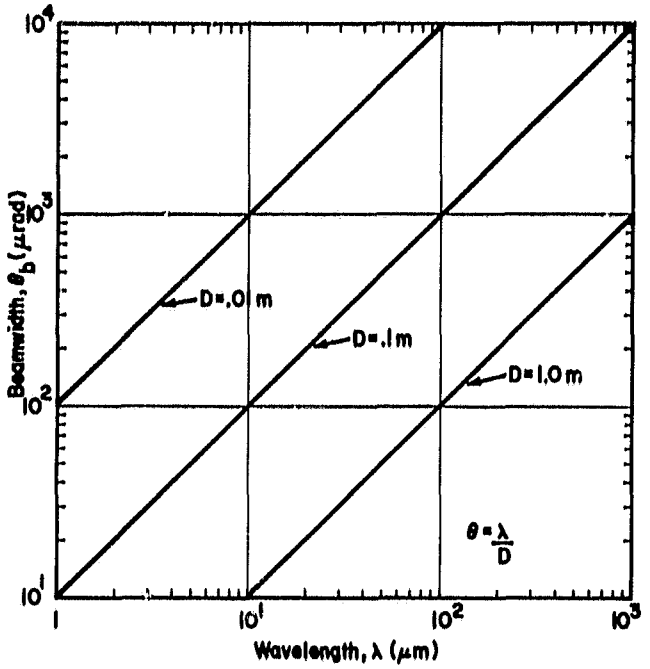

Figure 4-4. The beamwidth of the radiation from a uniformly illuminated circular aperture.

4.4 Field of View

As the interceptor approaches the target a point will eventually be reached where the angle subtended by the reflector array exceeds the total sensor field of view (fov) as depicted in Figure 4-5. Figure 4-6 shows the angle subtended by an array of reflectors arranged around a 1-m-diameter circle as a function of range. For a 0.5-rad fov, the array will be visible to within about 2 m from the array plane. This should be acceptable.

If range and bearing are required at distances less than 2 m, a single reflector can be placed in the center of the array. If attitude information is also required at shorter ranges, a smaller array can be installed within the larger one.

4.5 Background Radiation (ref. 27)

There are two important sources of background radiation: the Earth and the Sun. The sensor should function properly with the Earth in the background.

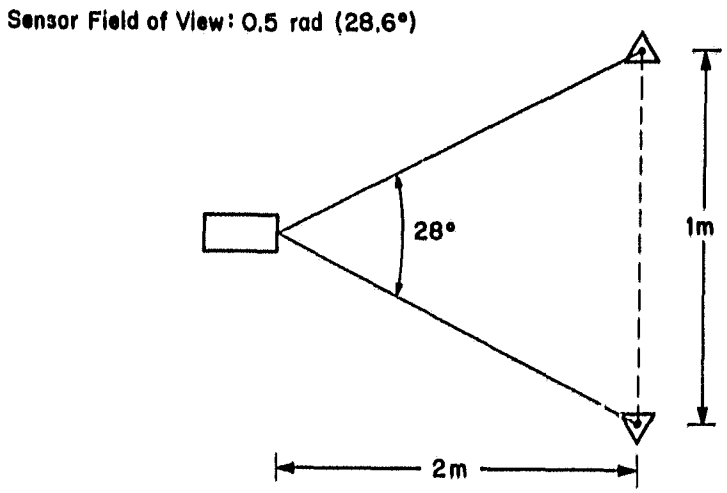

Figure 4-5. The angle subtended by the reflector array at the minimum range.

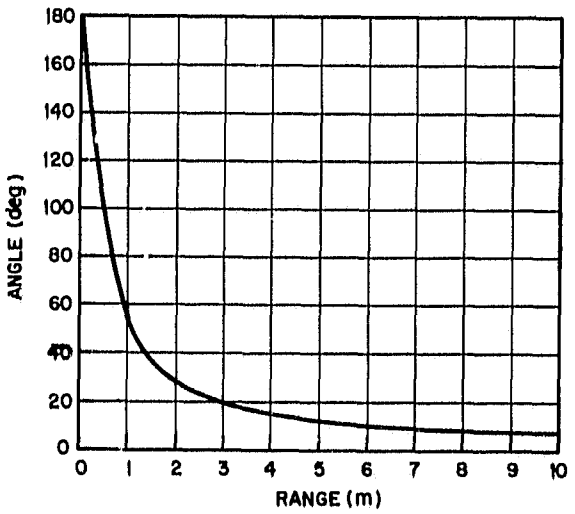

Figure 4-6. The angle subtended by a 1-m-diameter reflector array as a function of range.

The sensor need not function properly when the Sun is in the background, but it should not suffer any damage.

The worst case with regard to the Earth-background radiation occurs when the Earth fills the entire receiver beamwidth. Figure 4-7 shows the angle subtended by the Earth as a function of the distance from the Earth's surface. For most orbital operations and receiver beamwidths, the Earth could fill the entire beam.

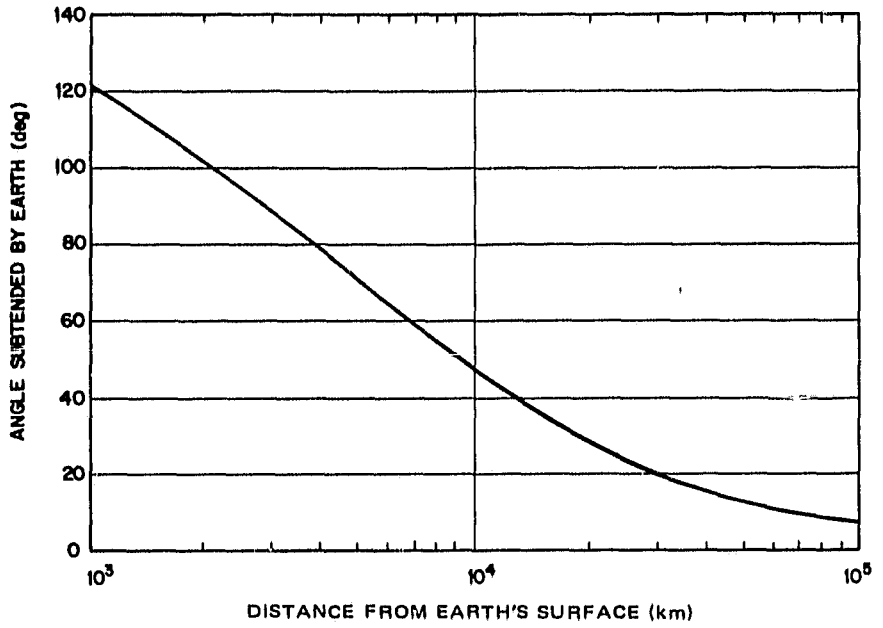

Figure 4-7. The angle subtended by the Earth.

The background radiation received from the Earth when it fills the entire receiver beam is

$$P_{be} = \frac{B_o \, \theta_b^2 \, W_e \, A_r}{4} \qquad (4\text{-}5)$$

where P_{be} = background radiation from Earth (W)
B_o = optical filter bandwidth (μm)
θ_b = receiver beamwidth (rad)

W_e = Earth's radiance at wavelength of interest (W/cm^2 μm) (See Figure 4-8)

A_r = receiver aperture area (cm^2)

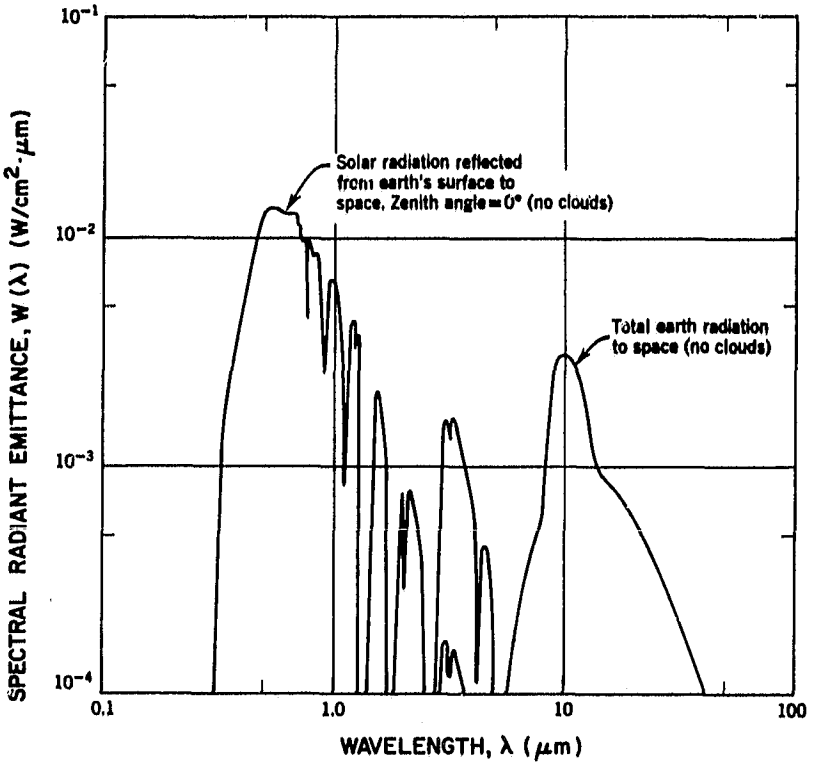

Figure 4-8. The Earth's radiance.

The Sun subtends a constant angle of approximately 4.7 mrad from anywhere in the vicinity of the Earth. If the receiver beamwidth is larger than the angle subtended by the Sun, the total power received from the Sun will be

$$P_{bs} = B_o A_r H_s \qquad (4\text{-}6)$$

where B_o = bandwidth of optical filter (μm)

A_r = receiver aperture (cm^2)

H_s = Sun's spectral irradiance (W/cm^2 μm) (See Figure 4-9).

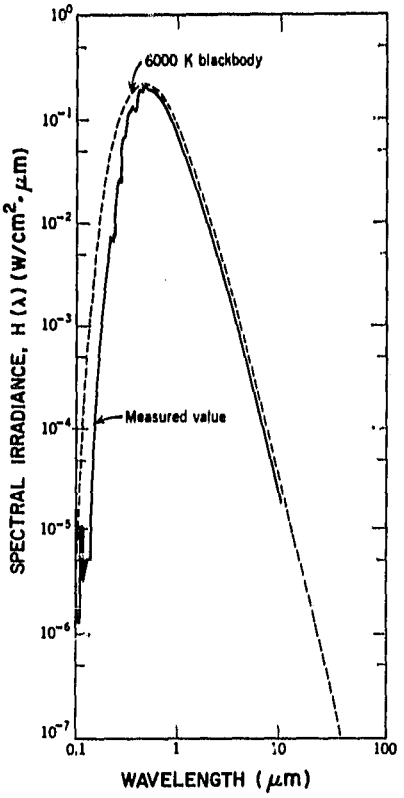

Figure 4-9. The Sun's spectral irradiance.

If the receiver beamwidth is smaller than the angle subtended by the Sun, the power due to the Sun will be

$$P_{bs} = \frac{B_o \, \theta_b^{\,2} \, W_s \, A_r}{4} \tag{4-7}$$

where

$$W_s = \frac{4 \, H_s}{\theta_s^{\,2}} \tag{4-8}$$

θ_s = angle subtended by the Sun (rad).

The background radiation due to various stars is shown in Figure 4-10. This radiation is insignificant compared to that from the Earth and Sun.

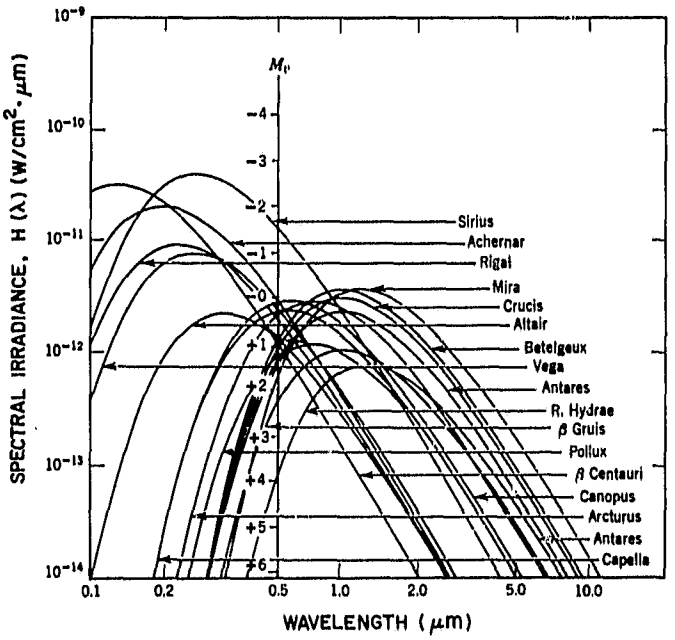

Figure 4-10. The spectral irradiance of various stars.

4.6 Transmitter Source

In Section 4.3 we showed that a carrier wavelength shorter than 100 μm was required to achieve a 2-mrad beamwidth within the transmitter-aperture size limitations. The only sources of coherent radiation operating in that region of the spectrum are lasers, and there are only three types of lasers that have the output power level, efficiency, and lifetime required for an optical radar: the CO_2 laser, the Nd:YAG laser, and the (GaAlAs) semiconductor laser.

The characteristics of these lasers are compared in Table 4-1. The semiconductor laser is considered superior to the other two because it does not require active cooling (like the Nd:YAG laser does for all but the lowest power levels), its associated detector does not require cooling (as do those associated with the CO_2 laser), it has high efficiency (unlike the Nd:YAG laser), and it does not require an external modulator (as do both the CO_2 and Nd:YAG lasers). The one disadvantage of the semiconductor laser is the present maximum output power limit of about 50 mW. However, this level will undoubtedly be exceeded in the future and, if necessary, the outputs of several lasers can be combined to reach higher power levels.

TABLE 4-1 CANDIDATE LASERS FOR THE R&D SENSOR

Laser	Wavelength	P^*_{max}	Mode	Efficiency	Lifetime	Detection	Detector	Modulation
CO_2	10,600 nm	100 mW	cw, Pulse	20 %	10^4 h	Heterodyne	Cooled	External
Nd:YAG	1,060 nm	10 mW	cw, Pulse	1 %	10^4 h	Direct	Uncooled	External
GaAlAs	830 nm	50 mW	cw, Pulse	10 %	10^5 h	Direct	Uncooled	Direct

*Without active cooling

It is interesting to note that while most of the intersatellite optical-communication systems that have been studied or developed in the past have employed Nd:YAG (ref. 28) or CO_2 lasers (ref. 29), a consensus is gradually emerging that, in the long run, the transmitters should, and will, employ semiconductor lasers.

Our selection of the semiconductor laser as the R&D sensor transmitter source places two severe restrictions on the overall system design. First, since the operating wavelength is about 830 nm, we must select only detectors that respond in that region of the spectrum. Second, the only type of modulation that can be employed with the semiconductor laser is intensity modulation (IM).

While the semiconductor laser is monochromatic (coherent) compared to most sources of light (such as lamps of any sort), it does not have a narrow spectrum compared to the modulating frequencies that would be employed for ranging. A 0.1-nm spectral width at 830 nm, which is narrow for a semiconductor laser, is the same as a 43.5-GHz spectral width in accordance with the relationship between wavelength and frequency bandwidths:

$$\Delta f = \frac{C\,\Delta\lambda}{\lambda^2} \tag{4-9}$$

where Δf = frequency bandwidth
$\Delta\lambda$ = wavelength bandwidth
λ = center wavelength
$C = 3\times10^8$ m/s

Therefore, it is not possible to phase (or frequency) modulate the output of a semiconductor laser. In the next section we give some consideration to those types of IM that can be employed with the semiconductor laser.

4.7 Ranging Modulation

The transmitted signal will be modulated so that the range to the target can be determined. Since we have selected a directly modulated semiconductor laser as the transmitter source, only intensity modulation (IM) can be employed.

There are two basic types of IM: pulse and cw. Pulse IM is preferred in those instances where either system will do because it allows for range discrimination and requires less average power. However, pulse IM has two characteristics that render it unsuitable for our application. First, pulse systems have a minimum range greater than the specified 2 m. Second, pulse systems do not have the required range accuracy.

Pulse-modulated systems have a larger minimum range than cw-modulated systems because time must be allowed for the transmitted pulse to clear the antenna and for the receiver to settle before the return pulse can be properly received. Pulse-modulated systems have difficulty in making highly precise range measurements because their precision is directly proportional to the resolution of the clock measuring the pulse travel time. A 10-mm resolution would require a 30-GHz clock, which is not practical.

There are several different types of IM that could be employed. The first distinction that we can make is between subcarrier IM and baseband IM. Subcarrier IM is employed when we first modulate a subcarrier, such as a microwave tone, with a ranging modulation and then modulate the optical carrier with the subcarrier. This method has three advantages. First, the subcarrier can be high enough in frequency to allow direct radial velocity determination from the Doppler shift on the subcarrier. Second, other subcarriers could be used for communication purposes. Third, modulation techniques, such as phase and frequency, that are not possible with baseband intensity modulation can be used.

There are two disadvantages with the subcarrier modulation scheme, however. First, since the subcarrier would normally be in the near-microwave band, a very wideband receiver is needed. Second, the final recovered modulation power is lessened because some power resides in the subcarrier, which is ultimately discarded. We decided not to consider the subcarrier-modulation technique at this time. If serious problems arose with the baseband-modulation technique we would reconsider the use of subcarrier modulation.

There are two basic types of baseband cw IM. The first method, tone ranging, requires the transmission of a sinusoidal or squarewave ranging tone and the measurements of the phase shift on the return signal to determine range. The second method requires the transmission of a pseudo-noise (PN) code and the determination of range from the time delay that must be imposed on the transmitted modulation so that it correlates with the returned modulation. The second method is not acceptable because its range resolution is as poor as that of the pulse system, and for the same reasons.

We have selected the baseband cw IM tone-ranging system for the R&D sensor. The sinusoidal-tone-based system is assumed in the following analysis and is henceforth referred to as the tone-ranging system. The various modulation schemes that have been considered and their relationships to one another are depicted in Figure 4-11.

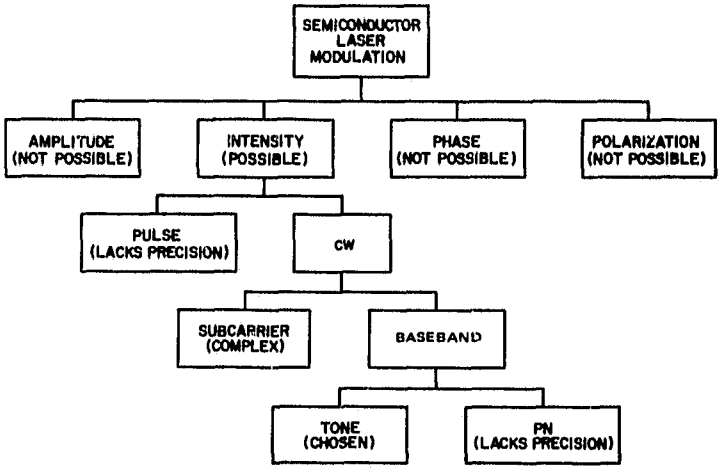

Figure 4-11. Modulation schemes considered for the R&D sensor.

4.8 Tone Ranging (refs. 30, 31)

Tone ranging has been selected for the R&D sensor because it is practical, relatively simple, has no minimum range requirement, and has the necessary precision. Tone-ranging systems do have three limitations, however, that must be considered.

The first limitation is that they have no range discrimination. The return from a nearby object of no interest can mask the return from a distant object of interest, and vice versa. In fact, it is possible for returns from the atmosphere or dust in the sensor optics to mask return signals of interest. This limitation is acceptable for the R&D sensor since it will be used in space, where there is very little atmosphere and the density of potential targets is low.

The second limitation of tone ranging is that there is no way to distinguish between a phase ϕ and a phase $2\pi\ n + \phi$, where n is an integer. Therefore, if only one tone is used, its wavelength would have to be less than 2 R_{max}, where R_{max} is the maximum expected target range. The corresponding maximum allowable frequency of this tone could not exceed f_{max}, where

$$f_{max} = \frac{C}{2\ R_{max}} \qquad (4\text{-}10)$$

Figure 4-12 shows the maximum unambiguous range as a function of modulation frequency.

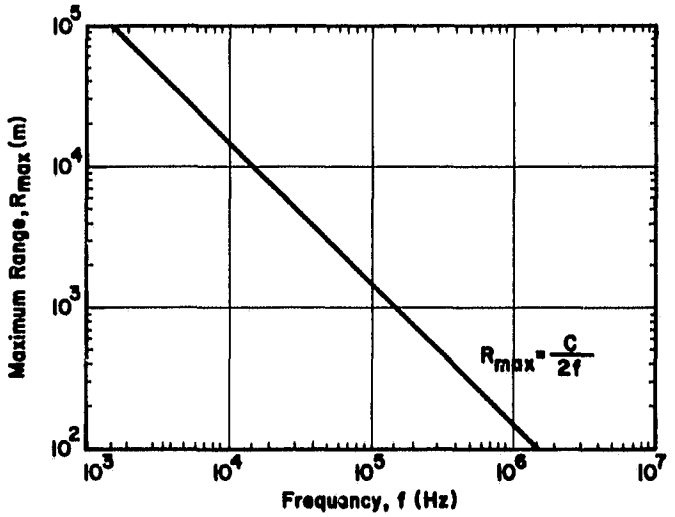

Figure 4-12. Maximum allowable range to avoid ambiguity in the single-tone ranging system.

The third limitation is that, in a single-tone system, the modulation frequency must exceed f_{min}, where

$$f_{min} = \frac{C}{(2\pi/\Delta\theta)\Delta R} \tag{4-11}$$

and

$\Delta\theta$ = resolution with which the phase-shift can be measured (rad)

ΔR = desired range resolution

For example, if our phase-measuring method could measure 1 part in 1000 ($2\pi/\Delta\theta$ = 1000), then f_{min} would have to be 60 MHz for ΔR = 5 mm. Figure 4-13 shows f_{min} as a function of ($2\pi/\Delta\theta$) for ΔR = 5 mm.

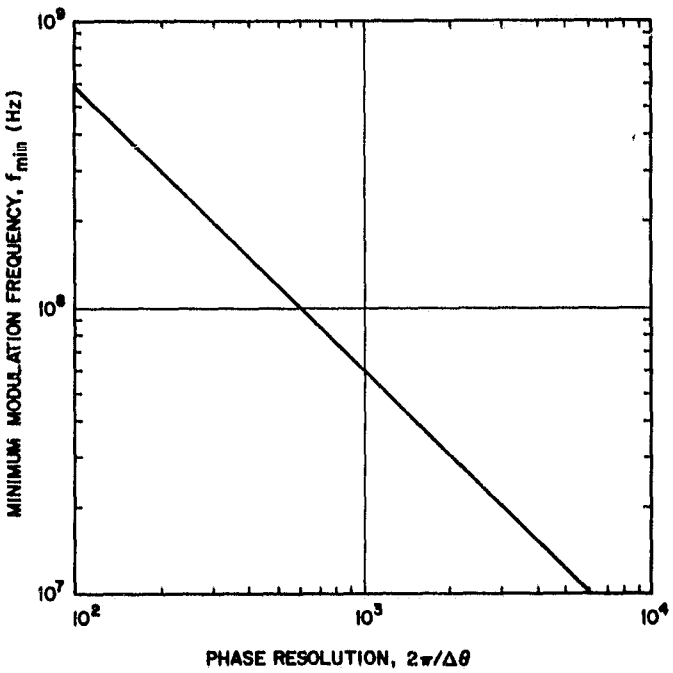

Figure 4-13. Minimum allowable modulation frequency in the single-tone ranging system for ΔR = 5 mm.

One might question why we have assumed, in the analysis above, that the phase resolution remains constant while the carrier frequency changes. After

all, for a given clock period the phase resolution will halve as the carrier frequency is doubled if the phase of the carrier is measured directly. The reason we say that increasing the carrier frequency improves resolution is that, in high-accuracy tone-ranging system, all the modulation tones will be heterodyned down to a fixed, low frequency, such as 1 kHz, before making phase measurements. This process is depicted in Figure 4-14.

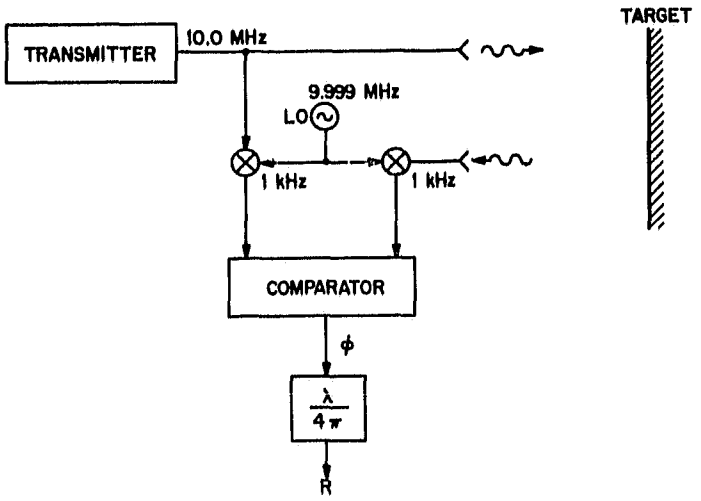

Figure 4-14. Tone-ranging system employing heterodyning prior to phase measurement.

It is usually not possible to employ a single-tone ranging system that simultaneously satisfies the maximum range and resolution requirements. The solution is to employ a multitone modulation system. The highest frequency establishes the resolution and, therefore, the accuracy, of the system, while the other tones are used to resolve the ambiguities that would result if the highest frequency tone were used alone.

4.9 Accuracy in Tone Ranging

There are three sources of errors in the tone-ranging system. First, the return signal will contain noise which will corrupt its waveform; second, there will be phase shifts in different system components that will vary with time

and temperature; and third, the finite resolution of the clock used to make the phase measurements will contribute an error of ± 1 clock period. An analysis of the errors due to the first cause, random noise, is presented below. We assume that the errors due to the second cause can be removed by a continuous calibration procedure and that the errors due to the third cause will be negligible.

The error analysis that follows assumes the use of a phase detector such as the one shown in Figure 4-15.

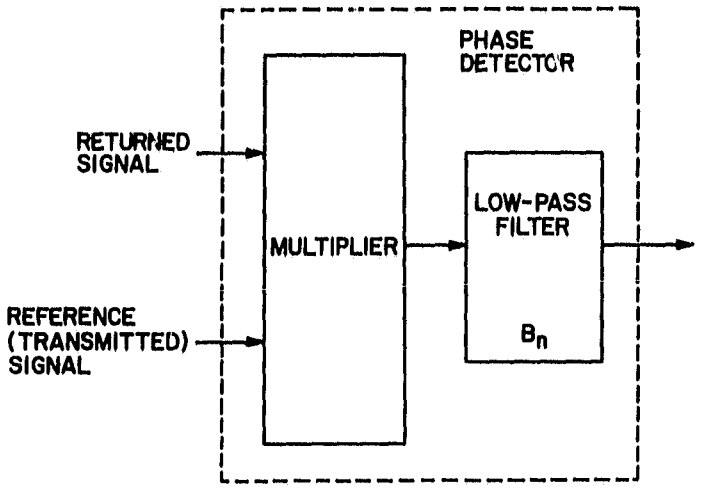

Figure 4-15. The elements of a tone-ranging system involved in the error analysis.

The two input signals involved are $S_t(t)$, the transmitted signal, given by

$$S_t(t) = A_t \cos(\omega_m t) \tag{4-12}$$

and $S_r(t)$, the received signal, given by

$$S_r(t) = A_r \sin(\omega_m t + \phi) + n(t) \tag{4-13}$$

where

$$\phi = \frac{4\pi R}{\lambda_m}$$

$n(t)$ = additive, Gaussian noise

The Gaussian noise, n(t), can be resolved into two independent components,

$$n(t) = n_c(t) \cos \omega_m t + n_s(t) \sin \omega_m t \tag{4-14}$$

where

$$\sigma_{nc}^2 = \sigma_{ns}^2 = \sigma_n^2 \tag{4-15}$$

and

$$\Phi_{nc}(f) = \Phi_{ns}(f) = 2 N_0 \tag{4-16}$$

where N_0 is the (assumed) constant one-sided spectral density of n(t). The phase detector multiplies the two input signals and then filters out all the signals at the modulation frequency or above. The product of the two signals is

$$v_p(t) = K [V_r V_t \sin (\omega_m t+\phi) \cos \omega_m t + V_t n_c(t) \cos^2 \omega_m t \tag{4-17}$$

$$- V_t n_s(t) \sin \omega_m t \cos \omega_m t]$$

$$= K \left[\frac{V_r V_t}{2} \sin \phi + \frac{V_r V_t}{2} \sin (2\omega_m t + \phi) + \frac{V_t n_c(t)}{2} \right. \tag{4-18}$$

$$\left. + \frac{V_t n_c(t) \cos 2\omega_m t}{2} - \frac{V_t n_s(t) \sin 2\omega_m t}{2} \right]$$

The output of the detector is

$$v_d(t) = K \left[\frac{V_r V_t}{2} \sin \phi + \frac{V_t n_c(t)}{2} \right] \tag{4-19}$$

If we assume that ϕ is small, then we can use the approximation

$$\sin \phi \cong \phi \tag{4-20}$$

and, therefore,

$$v_d(t) = \frac{K V_r V_t \phi}{2} + \frac{K V_t n_c(t)}{2} \tag{4-21}$$

The noise spectral density of $v_d(t)$ is

$$\Phi_{vd} = \left(\frac{K^2 V_t^2}{4} \right) \Phi_{nc} = \frac{K^2 V_t^2 N_0}{2} \tag{4-22}$$

The noise power out of the low-pass filter of noise bandwidth, B_n, is

$$\sigma_{vd}^2 = \frac{K^2 V_t^2 N_0 B_n}{2} \tag{4-23}$$

The signal power out of the low-pass filter is

$$\overline{v_d}^2 = \frac{K^2 V_r^2 V_t^2 \phi^2}{4} \tag{4-24}$$

The phase estimate, $\tilde{\phi}$, is determined from the measured value $v_d(t)$ as

$$\tilde{\phi} = \frac{2 v_d(t)}{K V_r V_t} \tag{4-25}$$

The range estimate, $\tilde{R}$, is determined from the phase estimate, $\tilde{\phi}$, by

$$\tilde{R} = \frac{\lambda_m \tilde{\phi}}{4\pi} \tag{4-26}$$

The variance of the range estimate, $\sigma_{\tilde{R}}^2$, is

$$\sigma_{\tilde{R}}^2 = \frac{\lambda_m^2 \sigma_{\tilde{\phi}}^2}{4^2 \pi^2} \tag{4-27}$$

$$= \frac{\lambda_m^2 4 \sigma_{vd}^2}{4^2 \pi^2 K^2 V_r^2 V_t^2} \tag{4-28}$$

$$= \frac{4 \lambda_m^2 K^2 V_t^2 N_0 B_n}{32\pi^2 K^2 V_r^2 V_t^2} \tag{4-29}$$

$$= \frac{\lambda_m^2 N_0 B_n}{8\pi^2 V_r^2} \tag{4-30}$$

$$= \frac{\lambda_m^2}{8\pi^2 \left(V_r^2 / N_0 B_n \right)} \tag{4-31}$$

$$= \frac{\lambda_m^2}{16\pi^2 (S/N)} \tag{4-32}$$

where S/N is the signal-to-noise ratio of the received signal

$$S/N = \frac{V_r^2}{2 N_0 B_n} \tag{4-33}$$

The standard deviation of the range estimate is, therefore,

$$\sigma_{\tilde{R}} = \frac{\lambda_m}{4\pi \sqrt{S/N}} \tag{4-34}$$

For a given S/N, the range error is a constant fraction of the modulating wavelength as shown in Figure 4-16,

$$\frac{\sigma_{\tilde{R}}}{\lambda_m} = \frac{1}{4\pi \sqrt{S/N}} \tag{4-35}$$

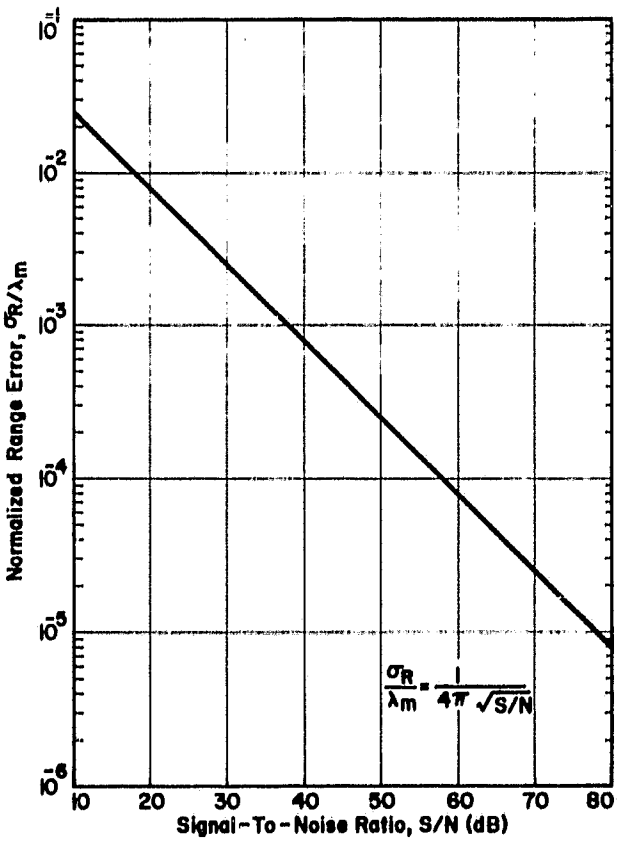

Figure 4-16. The accuracy of the tone-ranging system.

We might suppose that we could achieve any accuracy we desire, for a given S/N, by utilizing a high enough modulating frequency. However, as we increase the highest modulating frequency, the number of required intermediate frequencies between the highest and lowest -- which is fixed by the maximum expected target range -- increases. Each time we add another modulating tone, the S/N for each one is reduced since the available transmitting power must be shared among all the modulating tones. Transmitting the tones sequentially (one at a time) would eliminate this problem but would increase the measurement time.

4.10 Effect of Target Velocity on the Tone-Ranging System

When an electromagnetic wave of frequency f strikes an object moving at a velocity V_r in the direction of the radiation, it experiences a Doppler frequency shift, f_d, where

$$f_d = \frac{2\ V_r\ f}{C} \tag{4-36}$$

(This relationship is shown in Figure 4-17.)

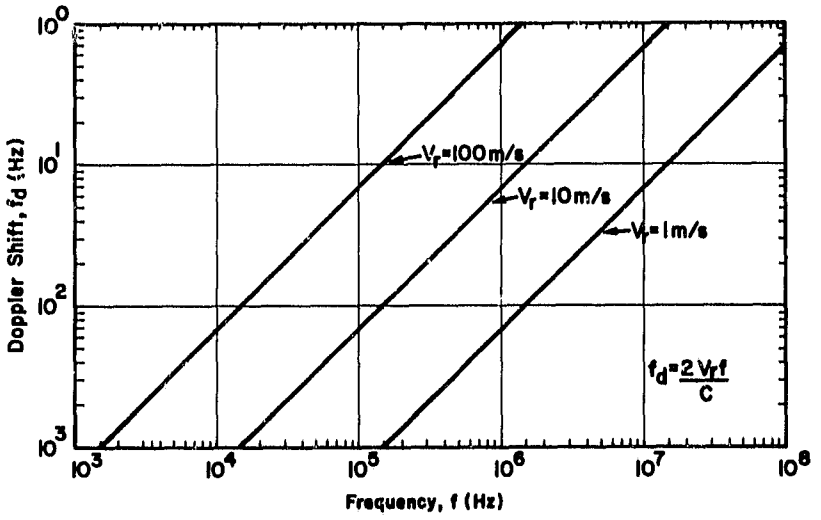

Figure 4-17. Effect of target radial velocity on ranging tones.

Since a change in frequency of a signal will result in a change in phase over time, the accuracy of the tone-ranging system can be expected to be reduced for moving targets. Since the Doppler shift is proportional to frequency we might also expect that the higher the ranging tone the worse the effect. We will in fact show that, for the ranges and velocities that we have assumed, the Doppler shift will not significantly affect the accuracy of the range measurements. Furthermore, we shall see that the errors are not a function of the ranging tone's frequency.

First, we should point out that, even though the ranging tones are not transmitted directly but are used instead to modulate an optical carrier, they do experience the same Doppler shift that they would if they were transmitted directly. The optical carrier also experiences a Doppler shift, a much greater one than that of the ranging tone. However, since the optical carrier is directly detected, this Doppler shift is of no consequence.

We will now determine the extent the range measurement is affected by the phase shift resulting from the returned signal's Doppler shift. The modulating signal leaving the transmitter can be expressed as

$$S_t = \cos\ (2\pi f_m\ t) \tag{4-37}$$

This signal arrives at the target a time R/C later as S_t' where

$$S_t' = \cos\ [2\pi f_m\ t + 2\pi(R/C)f_m] \tag{4-38}$$

If the target has no radial velocity the signal returns to the receiver a time R/C later as

$$S_r = \cos\ [2\pi f_m\ t + 4\pi(R/C)f_m] \tag{4-39}$$

and the phase shift, due solely to the range, is

$$\phi_R = 4\pi(R/C)f_m \tag{4-40}$$

If, however, the target has a radial velocity, V_r, then the reflected signal is

$$S_t' = \cos\ [2\pi(f_m+f_d)\ t + 2\pi(R/C)f_m] \tag{4-41}$$

where

$$f_d = \frac{2\ V_r\ f_m}{C}$$

The received signal in this case is S_r', where

$$S_r' = \cos [2\pi(f_m+f_d)\ t + 2\pi(R/C)(f_m+f_d) + 2\pi(R/C)f_m] \quad (4\text{-}42)$$

The phase shift due to both Doppler and range is

$$\phi_T = 2\pi(R/C)f_d + 4\pi(R/C)f_m \quad (4\text{-}43)$$

$$\phi_T = \phi_d + \phi_R \quad (4\text{-}44)$$

where

$$\phi_d = 2\pi(R/C)f_d \quad (4\text{-}45)$$

The effect of ϕ_d on the measurement of range is proportional to ϕ_d/ϕ_R where

$$\frac{\phi_d}{\phi_R} = \frac{f_d}{2\ f_m} = \frac{V_r}{C} \quad (4\text{-}46)$$

For the maximum specified velocity of 50 m/s, $\phi_d/\phi_R = 1.7\text{x}10^{-7}$, which represents a negligible error. Furthermore, we see that increasing f_m does not directly increase the error due to Doppler shifts. This is because the phase shift due to the Doppler grows at the same rate as the phase shift due to the range when the modulating frequency is increased.

The analysis above of the effect of Doppler shift on range measurement has assumed that the phase of the received signal is determined instantaneously. In some measurement methods the phase is determined from measurements made over a time interval of, perhaps, several milliseconds. The effect of measuring phase over a time T is that ϕ_T is increased to

$$\phi_T = 2\pi(R/C)f_d + 2\pi f_d T + 4\pi(R/C)f_m = \phi_d' + \phi_R \quad (4\text{-}47)$$

where

$$\phi_d' = 2\pi f_d(R/C + T) \quad (4\text{-}48)$$

The ratio ϕ_d'/ϕ_R is now

$$\frac{\phi_d'}{\phi_R} = \frac{f_d(R/C+T)}{2f_m(R/C)} \quad (4\text{-}49)$$

$$\frac{\phi_d'}{\phi_R} = \frac{(V_R/C)(R/C+T)}{R/C} \tag{4-50}$$

$$\frac{\phi_d'}{\phi_R} = \left(\frac{V_r}{C}\right) + \left(\frac{V_r}{R}\right) T \tag{4-51}$$

For $T < 10$ ms, $V_r < 50$ m/s, and $V_r/R < 0.1$, $\phi_d'/\phi_R < 10^{-3}$, which is still acceptable.

4.11 Receiver Scanning Mechanism

In the previous sections we have tried to define, as much as possible, the form the R&D sensor must take. Some of these properties have a direct effect on the type of receiver scanning mechanism that can be employed. Specifically, we have concluded that the receiver must be able to:

- Scan a narrow (2 mrad) beam almost instantaneously, at random, over a 0.5-rad fov. (At close ranges the individual reflectors will lie at the extremes of the fov.)
- Have a large enough ($\geq$ 50 mm) aperture to gather a useable signal at the maximum range of 50 km.
- Operate in the portion of the spectrum around 830 nm.

Within the selected spectral range there are only two scanning mechanisms that can move from point to point in the fov quickly enough. The first method, mechanical beamsteering, uses mirrors mounted on piezoelectric deflectors or galvanometers to steer the optical beam; the sensor itself does not move. The second method, electron beamsteering, uses magnetic coils to steer the photoelectrons emitted by a photocathode which has the sensor fov imaged upon it. This is the method used in the image-dissector receiver.

The first method has one drawback: it cannot be used with both a large aperture and a large fov. The capability of a beamsteerer can be expressed in terms of an aperture-fov product. By the use of telescopes, the task of steering a large aperture over a small fov can be accomplished with a beamsteerer that steers a small aperture over a large fov and vice versa. Unfortunately, the aperture-fov capability we require is beyond that possible with mechanical beamsteerers.

The second method, electron beamsteering as employed in the image dissector, is our remaining choice. A representation of an R&D sensor with an image-dissector receiver is shown in Figure 4-18.

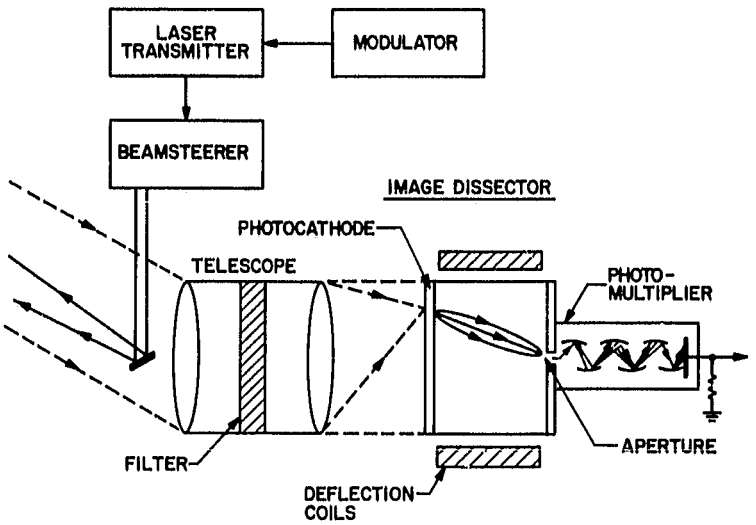

Figure 4-18. R&D sensor with an image-dissector receiver.

We have said nothing here about the transmitter beamsteerer. As we shall see, the requirements of the transmitter beamsteerer are not so stringent. The aperture, in particular, only has to be large enough to allow a 2-mrad beamwidth and this will be less than the 50-mm minimum specified for the receiver. A mechanical beamsteerer will be satisfactory for the transmitter.

4.12 Summary

We have tried, in Section 4, to determine, as much as possible, the form that the R&D sensor must take. We have determined, as a result of these efforts, the following characteristics:

- Target type: Cooperative, 3 or more reflectors in a known planar configuration around a 1-m (maximum) -diameter circle
- Sensor type: Active
- Background radiation: Should function normally with Earth occupying total beam; should survive presence of Sun in beam.

- Beamwidth (transmitter and receiver): 2 mrad
- fov (transmitter and receiver): 500 mrad
- Transmitter source: Semiconductor laser (830 nm typical)
- Modulation type: cw IM (tone ranging)
- Receiver: Image dissector

The sensor must be long-lived, small, and low-power if it is to support the operations of the Shuttle, OTV, and TMS. The following specifications have been established for these items:

- Volume: 0.1 m^3
- Mass: 10 kg
- Power: 50 W
- Lifetime: 10^4 h

5. KEY COMPONENTS

Now that we have some idea what the R&D sensor should look like, it is time to discuss, in some detail, its components. Specifically, the following items will be examined:

- Semiconductor lasers
- Beamsteerers
- Reflectors
- Telescopes
- Optical filters
- Image dissectors

The items above are all electro-optical components. Many purely electrical components, such as filters, phase-lock loops, computer-based controllers, power supplies, etc., are not discussed because they are less critical to the eventual development of the R&D sensor and because the audience to whom this report is addressed is generally familiar with them.

In discussing the electro-optical components listed above, the emphasis will be on those characteristics that would affect their performance as an element of the R&D sensor. There are several characteristics that must be considered for every element. These are:

- Size
- Lifetime (reliability)
- Power requirements
- Radiation tolerance
- Ambient requirements

These parameters will be discussed only in those instances where a problem is foreseen.

5.1 Semiconductor Lasers (ref. 32)

The semiconductor laser is the radiation source that has been selected for the R&D sensor's transmitter. The semiconductor laser has many desirable properties for this application. It is small, efficient, reliable, easily modulated, and emits at a convenient wavelength. On the other hand, the

semiconductor laser emits its radiation in a rather wide elliptic beam and it has a power limit, at this time, below the level that will probably be required. Methods of dealing with these problems will be discussed later.

The semiconductor laser, as shown in Figure 5-1, has the same basic structure as any other laser; it consists of an optical resonator containing an amplifying medium. The optical resonator is a small chip of a semiconductor compound, such as GaAs, having two rough (sawn) facets and two smooth (cleaved) facets. The two cleaved facets act as partially reflecting mirrors; they and the material between them constitute a Fabry-Perot etalon. The amplifying medium is the region around a p-n junction in the material. When current flows through the junction, the minority carriers (mostly electrons) injected across it create a region of population inversion which acts as an amplifier to the optical wave in the cavity.

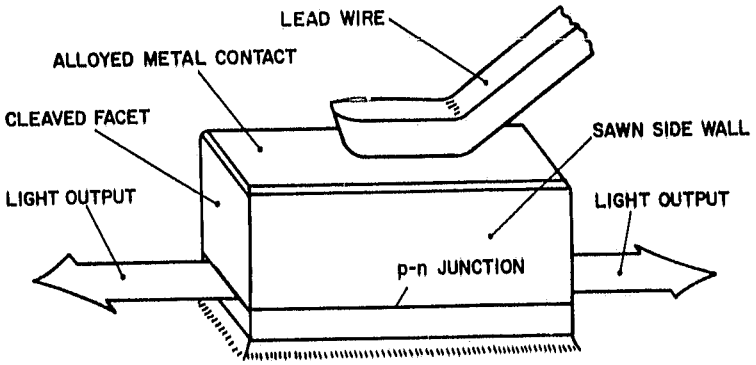

Figure 5-1. The semiconductor laser.

All semiconductor lasers have a threshold current density, at the junction, that must be exceeded before lasing action begins. Once lasing action begins, the increase in emitted optical power will be approximately proportional to the increase in current. This behavior results in the type of emission characteristic shown in Figure 5-2.

The beams emitted by semiconductor lasers are fairly broad, as shown in Figure 5-3. The beamwidth perpendicular to the junction, $\theta_{\perp}$, is typically 40°; the beamwidth parallel to the junction ($\theta_{||}$) is typically 10° in semiconductor lasers that employ some method to confine the lateral dimension of the active region.

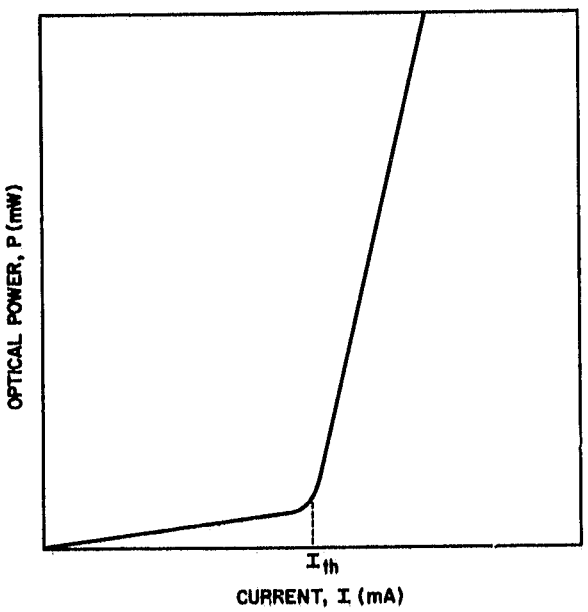

Figure 5-2. Emission characteristic of a semiconductor laser.

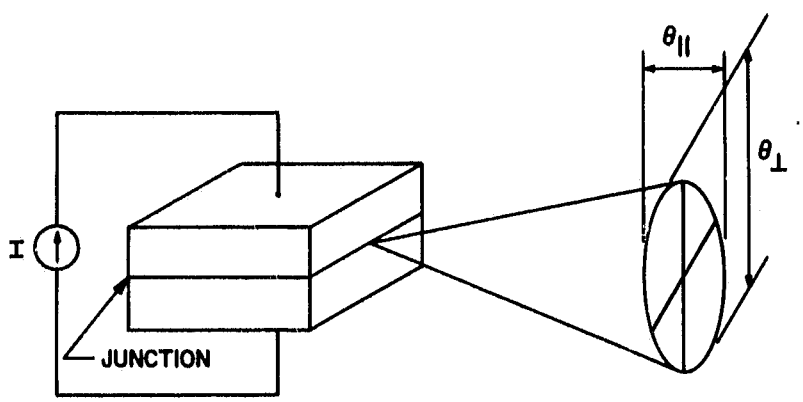

Figure 5-3. The beamwidths parallel to ($\theta_{||}$) and perpendicular to ($\theta_{\perp}$) the junction.

There are many problems faced by the semiconductor laser designer. Excessive temperature rise is a problem that can be avoided by reducing the threshold current and the optical losses. The threshold current, in turn, is reduced by somehow confining both the injected minority carriers and the optical wave to a narrow region around the p-n junction. There are limits to the amount of confinement that can be allowed, however. If the beam is too tightly confined, the total power generated will be small. Also, a very small emitting spot will lead to broad beams, in accordance with the laws of diffraction, and to a high power density, which may lead to facet damage.

The drive to reduce the threshold current while producing lasers with particular characteristics -- whether it be high pulse power, high cw power, long life, narrow beam, single mode operation, etc. -- has resulted in many different laser structures.

The first semiconductor lasers, shown in Figure 5-4(a), were made from one material, GaAs, and contained one junction, the interface between the n-type GaAs and the p-type GaAs. These lasers, termed homojunction lasers, had poor carrier and optical wave confinement and, as a result, the threshold currents were so high that room temperature cw operation could not be achieved. These lasers were, and still are, used in the low-duty-cycle pulse mode.

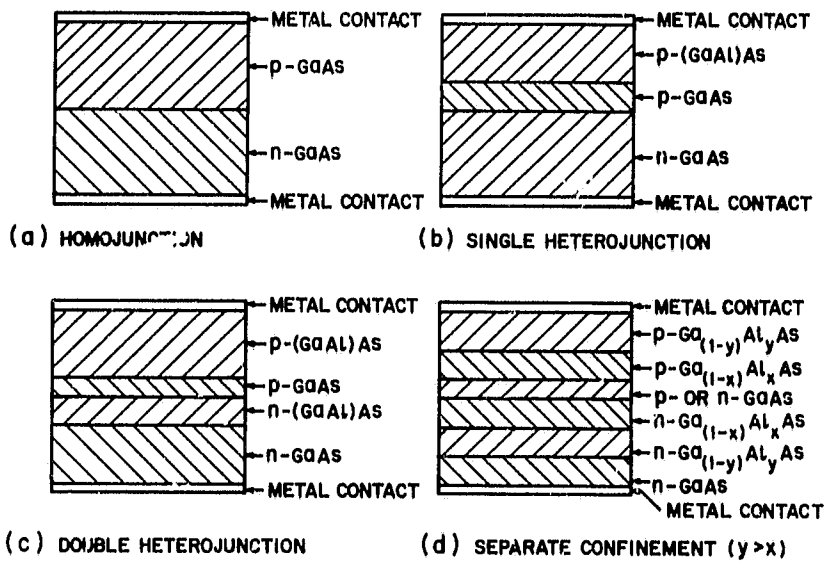

Figure 5-4. Semiconductor-laser structures.

The heterojunction laser was developed in response to the problems of the homojunction laser. The heterojunction laser has a threshold current density low enough to allow cw operation at room temperature. The threshold current density is reduced because the heterojunction tends to confine both the injected carriers and the optical wave to the p-n junction region.

The simplest heterojunction laser, the single-heterojunction laser, is shown in Figure 5-4(b). The (GaAl)As-GaAs junction acts to keep both the injected electrons from the n-type GaAs and the optical radiation from spreading away from the p-n junction. The double-heterojunction laser, shown in Figure 5-4(c), is more complex than the single-heterojunction laser but offers better performance.

There are applications that call for a laser structure that confines the injected carriers to a narrower region than that of the optical wave. One application is the design of high-power lasers. Spreading the light into as wide a region as possible reduces the optical power density at the facets, the limiting factor in some high-power lasers. A five-layer laser that accomplishes this separate confinement is shown in Figure 5-4(d).

So far we have discussed the different structures that have evolved in an attempt to confine the active region and the optical beam in a direction perpendicular to the junction. It is also necessary to confine the active region and the optical beam in the lateral dimension. This is done to reduce the threshold current, to produce narrow beamwidths in the direction parallel to the junction, and to avoid the generation of higher-order modes. One method of lateral confinement is the replacement of the sheet contact shown on the previous lasers with a stripe contact as shown in Figure 5-5.

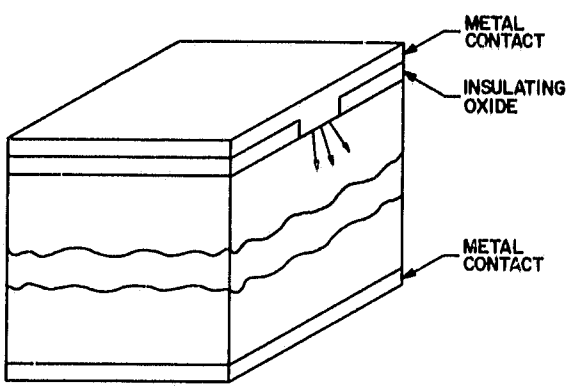

Figure 5-5. Stripe contact for lateral confinement.

5.2 Constricted Double Heterojunction-Large Optical Cavity (CDH-LOC) Laser

The highest power, single-mode, cw lasers available today are the CDH-LOC lasers developed at RCA Laboratories by D. Botez (refs. 33 and 34). The CDH-LOC-laser structure is shown in Figure 5-6. CDH-LOC lasers are currently capable of generating about 40 mW/facet; this value is expected to increase in the future (ref. 34). Figure 5-7 shows the output optical power as a function of drive current for representative CDH-LOC lasers of two different lengths. The beam pattern of the CDH-LOC laser is shown in Figure 5-8. The beam is a relatively narrow 6° x 25°.

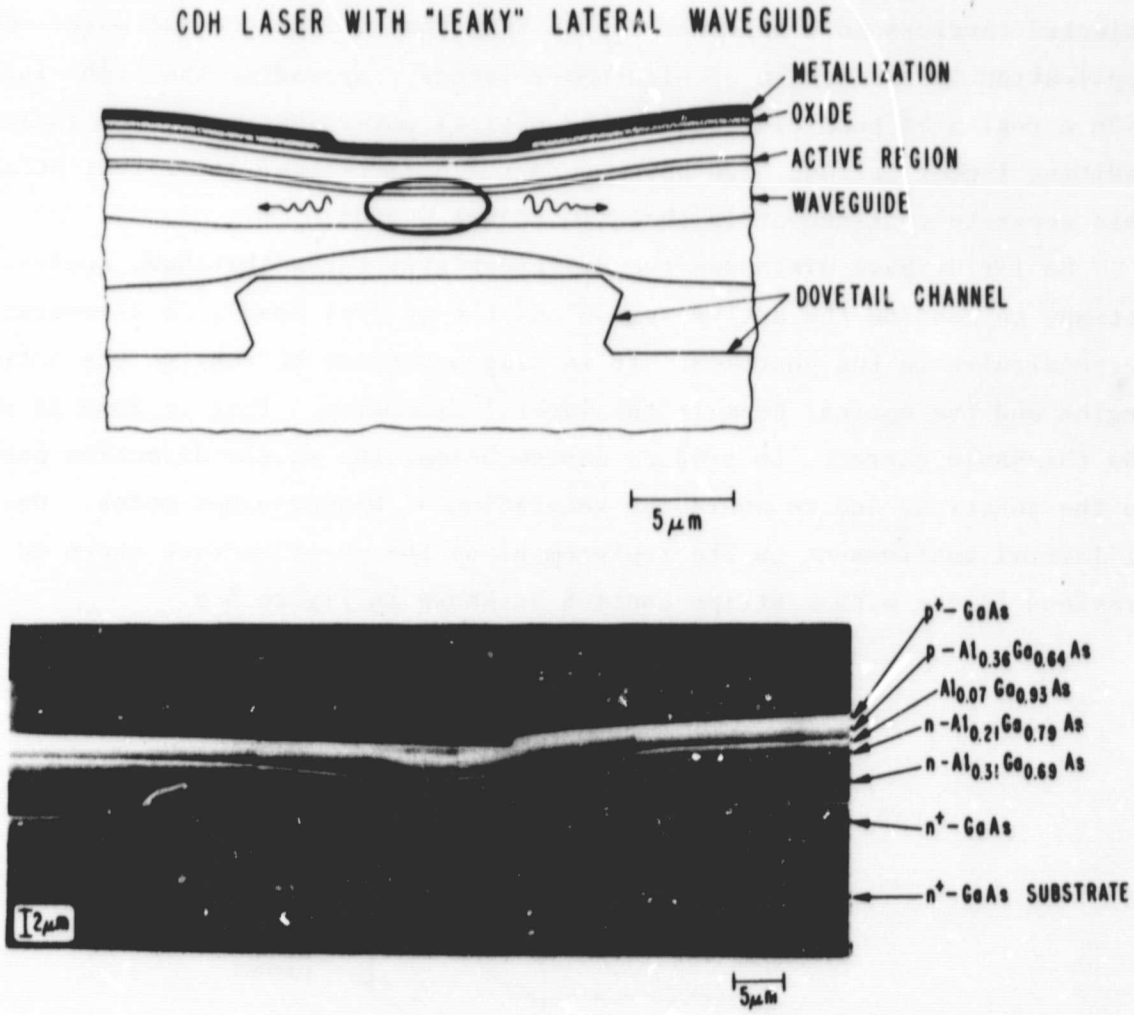

Figure 5-6. The CDH-LOC laser (after Botez; ref. 33).

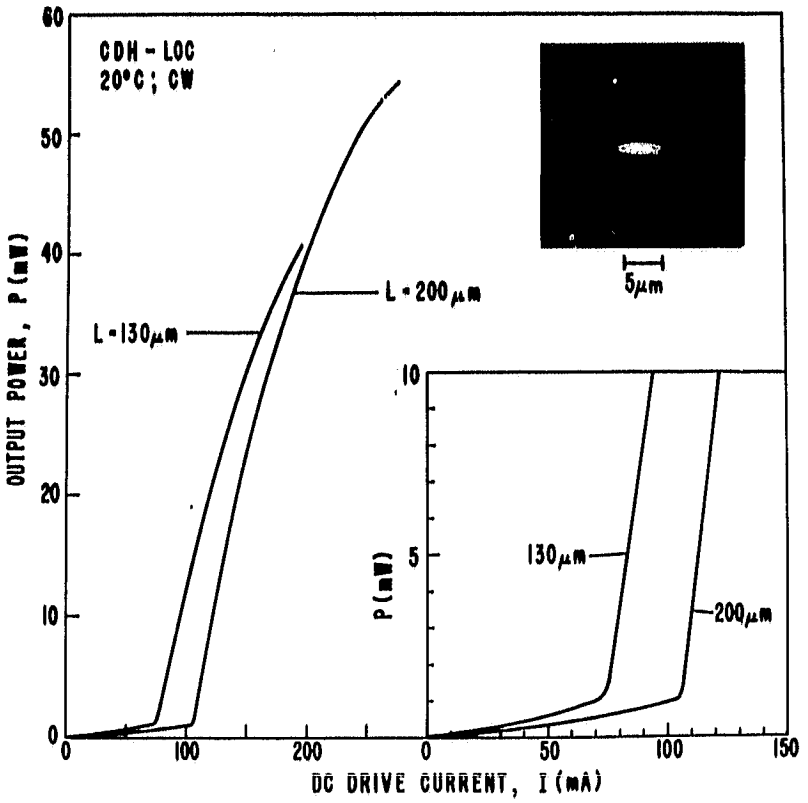

Figure 5-7. Performance characteristics of the CDH-LOC laser (after Botez; ref. 33).

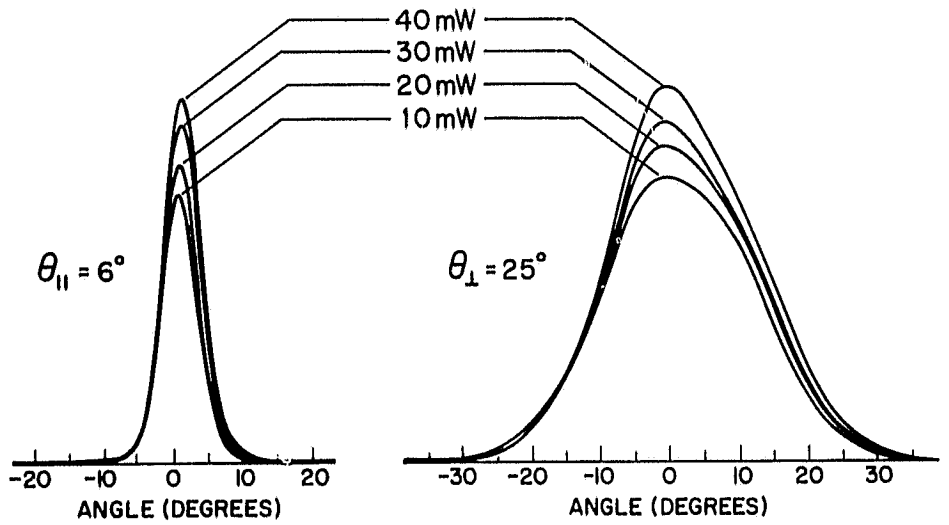

Figure 5-8. The far-field beam pattern of the CDH-LOC laser (after Botez; ref. 34).

The CDH-LOC laser emits its radiation in a single lateral and longitudinal mode. A single lateral mode implies that the beamshape is essentially Gaussian as shown in fig. 5-8. A single longitudinal mode implies that the emission is monochromatic. This is confirmed by the spectrum analyses displayed in Figure 5-9.

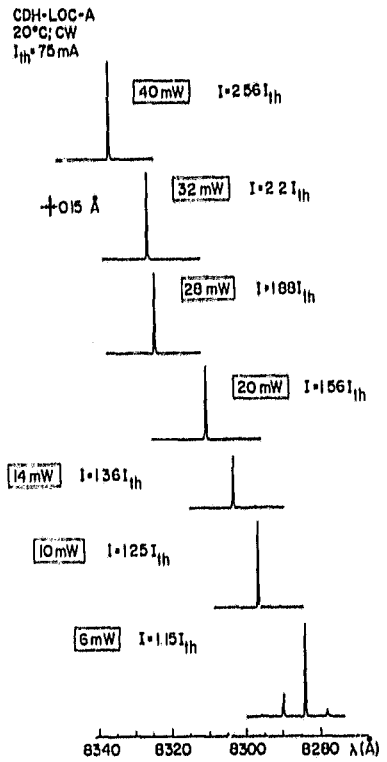

Figure 5-9. Emission spectra of the CDH-LOC laser (after Botez; ref. 33).

It is important that the lasers in the R&D sensor be reliable and have lifetimes exceeding 10,000 hours. Some life tests have been performed on the CDH-LOC lasers (ref. 35) and it appears that they can meet the reliability and lifetime requirements of this application. The results of a typical life test are shown in Figure 5-10. Two of the three lasers that were tested lasted at least 10,000 hours when operated at an initial peak output power of 40 mW at a 50% duty cycle. Figure 5-11 shows the change in threshold current experienced by one of the two lasers that survived the 10,000-hour test.

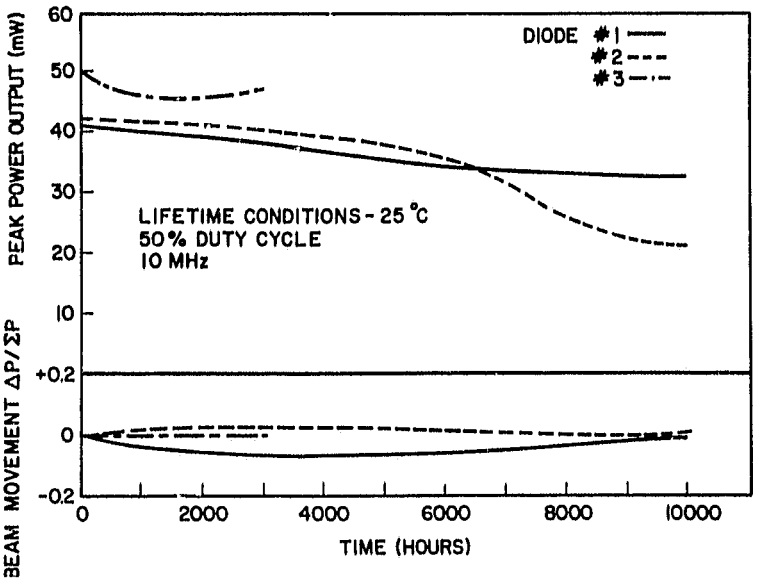

Figure 5-10. CDH-LOC laser lifetime-test results (after Ettenberg and Botez; ref. 35).

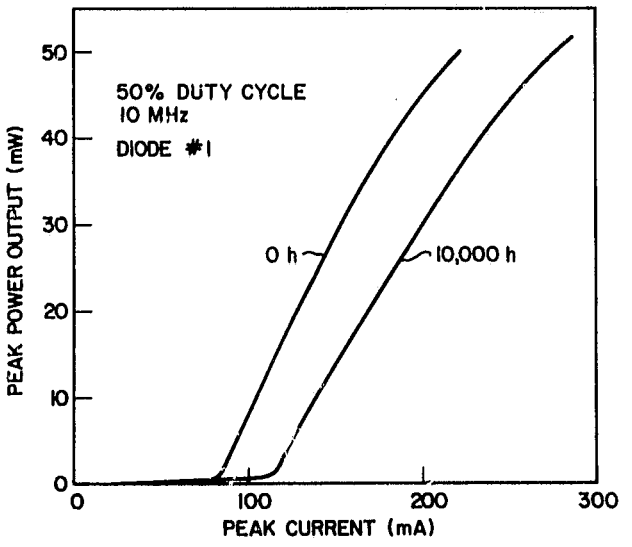

Figure 5-11. Threshold current increase in a CDH-LOC laser after 10,000 hours of operation (after Ettenberg and Botez; ref. 35).

In summary, we believe that the CDH-LOC laser is the best laser available today for the R&D sensor. The characteristics of this device are summarized below:

- Type: CDH-LOC
- Material: (GaAl)As
- Power: 40 mW
- Transverse Mode: TEM_{00}
- Beamwidth: 6° x 25°
- Wavelength: 830 nm
- Spectral Width: < 0.015 Å
- Lifetime: > 10^4 h
- Efficiency: > 10%

5.3 Semiconductor-Laser Transmitters

There are three primary considerations in the design of a semiconductor-laser transmitter for the R&D sensor. The first consideration is the method of modulation. Semiconductor lasers are normally directly modulated (ref. 36); the drive current is biased to the threshold level and then varied to produce an intensity variation proportional to the drive current variation. There may be some problems with this method of modulation if more than one laser is required, however, unless each laser has identical modulation characteristics.

The two other considerations are somewhat related. The first is that the power required from the transmitter is likely to exceed that available from one laser diode. The second is that the beamwidth of the transmitter output must be much smaller than that of a typical laser emitting into free space. These considerations are related because combining the outputs of several lasers becomes more difficult when narrow beams are required and, conversely, the generation of narrow beams from individual lasers may require that a considerable portion of the emitted power be discarded, necessitating the use of more lasers to achieve the required total power.

There are several methods that have been developed or proposed to combine the outputs of several lasers into one narrow beam. The following are four methods that we believe merit further investigation:

1. Use of a beam expander to collimate the output of a phase-locked monolithic-laser array.

2. Use of an external cavity to reduce the beamwidth of a phase-locked monolithic-laser array.
3. Use of an external cavity to force a multilateral mode laser with a very large optical cavity to operate in a single, narrow, lateral (TEM_{00}) mode.
4. Use of an external cavity to stabilize the longitudinal modes of several lasers (that is, to select a precise operating frequency) whose outputs are combined by wavelength multiplexing in a diffraction grating.

Methods 1 and 2 require the use of a phase-locked monolithic laser array. Phase-locked laser arrays are in the research stage at this time, but should become available within several years. RCA has developed 300-mw cw nonphased-locked monolithic laser arrays containing 10 lasers fabricated 150 μm apart. Figure 5-12 shows the measured intensity profile from such an array while Figure 5-13 shows the total power output as a function of drive current. These arrays are not suitable as is, but are an indication of what might be expected in several years.

Method 1 relies on a collimator, such as those shown in Figure 5-14, to reduce the divergence of the array beam. Since the array beam would probably not be spherical, cylindrical lenses would have to be employed. Spatial filtering might have to be used at some point in the optics, and the effect of this plus practical limits on the diameter of the lenses could result in considerable power lost from the beam.

The next three methods depend on external cavities (refs. 37-39) for mode stabilization and reduction of divergence. When semiconductor lasers are placed in optical cavities, the properties of the resulting combination is dominated by the characteristics of the relatively large cavity. The large size of the cavity also enables the placement of filters, stops, switches, etc., within the optical feedback path where they can influence the resulting emissions. A typical external cavity is shown in Figure 5-15.

Method 2 relies on an external cavity to reduce the beamwidth of a phase-locked laser array. Experience suggests that an external cavity can reduce the beamwidth of a laser to near the diffraction limit of the cavity aperture.

Figure 5-12. The intensity pattern from a 10-laser array (after Botez; ref 34).

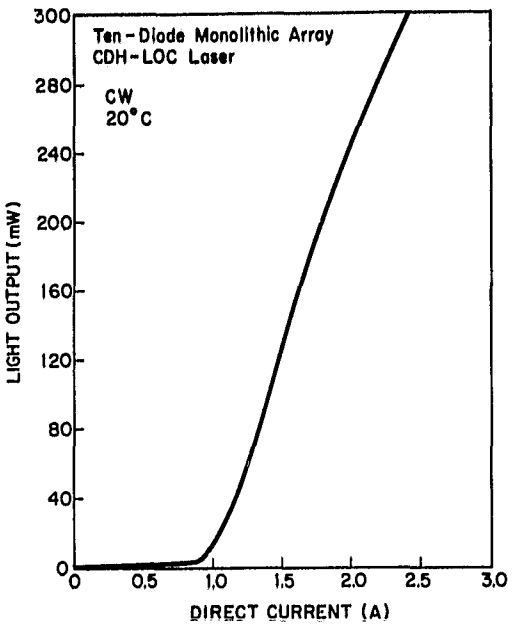

Figure 5-13. The output power from a 10-laser array (after Botez; ıef. 34).

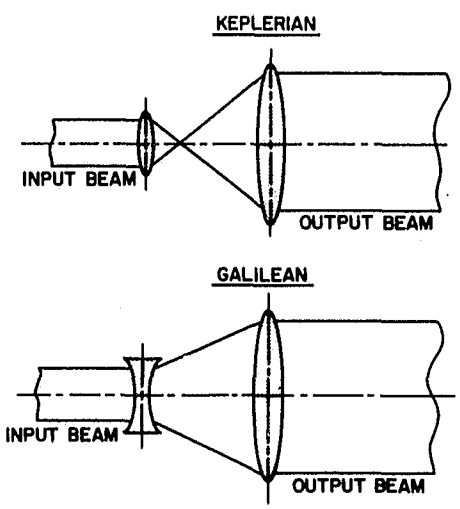

Figure 5-14. Two types of collimators.

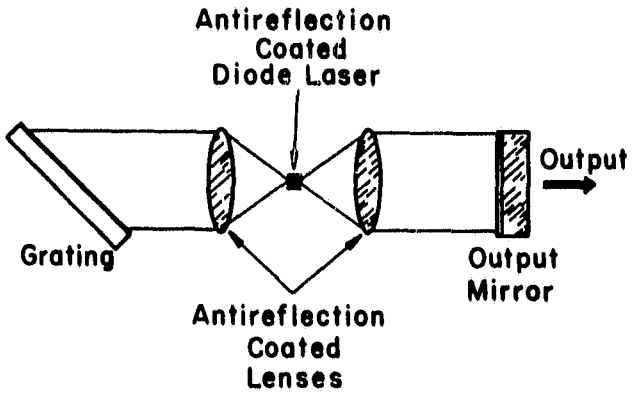

Figure 5-15. An external-cavity-controlled semiconductor laser.

Method 3 relies on an external cavity to control the lateral mode structure of a very large active area laser. All the lasers produced to date have some means of restricting the size of the active region. One of the reasons for this is that as the active region increases in size, higher order modes, TEM_{01}, TEM_{10}, TEM_{11}, etc. begin to appear. In most applications the emission must be in the TEM_{00} mode.

An external cavity might be used to force a large-active-area laser that would normally operate in several modes to emit exclusively in the TEM_{00} mode. This could be accomplished by placing stops within the cavity arranged to provide attenuation for the higher-order modes. Since the power output of a laser increases as the active region does, this is a possible method of obtaining high-power narrow beams from a single laser.

Method 4 relies on an external cavity to stabilize the operating frequency and reduce the beamwidth of several conventional lasers. The resulting outputs are then multiplexed at a diffraction grating. Since each output is at a different wavelength, the intensities add without interference. This process is depicted in Figure 5-16.

In summary, there appear to be several methods to obtain narrow beams of higher power than is presently available from a single semiconductor laser. Since the laser transmitter is one of the key elements in the R&D sensor we believe that a more detailed investigation into the feasibility of each of these methods should be undertaken as soon as possible.

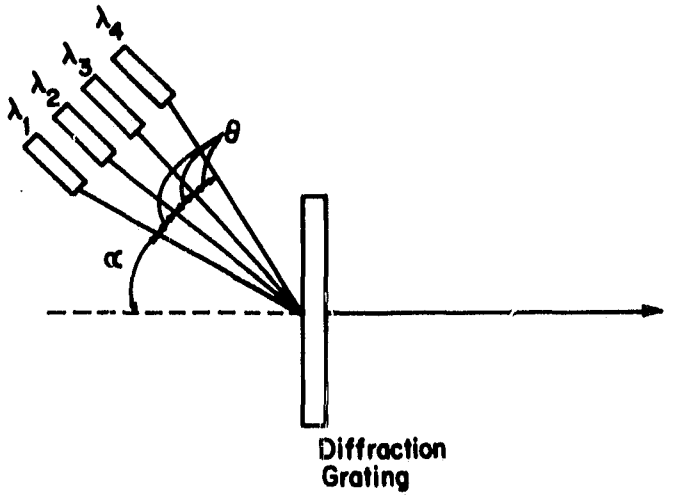

Figure 5-16. Wavelength multiplexing the output of several lasers.

5.4 Beamsteerers (ref. 40)

A beamsteerer is required to direct the narrow beam from the transmitter to any point within the fov. Some of the considerations involved in the selection of a beamsteerer are:

- Speed
- Random Access Time
- Range
- Resolution
- Precision and Accuracy

The beamsteerer for the R&D sensor must be able to move the beam quickly over the entire fov when the initial search for the target takes place. Once the rendezvous has been completed and docking begins, the beamsteerer must be able to direct the beam quickly from reflector to reflector. Near the end of the docking maneuver the reflectors will be at the extremes of the fov. A beamsteerer that can perform both these functions must have both high speed and low-random-access time. High-inertia mechanisms, such as the various types of rotating-mirror scanners, are not suitable for use in the R&D sensor beamsteerer because they have almost no random-access capability.

The types of low-inertia deflectors that might be suitable for the R&D sensor beamsteerer are:

- Acousto-optic
- Electro-optic
- Galvanometer
- Piezoelectric

We can determine which of these deflectors are suitable by considering the aperture (which is directly related to resolution) and deflection-range requirements imposed by our application. First, with regard to deflection range, note that it is not necessary that the deflector be able to deflect a beam over the 500-mrad fov by itself. This is because a deflection magnifier (reversed beam expander) can be used to increase the deflection angle (ref. 41). However, as shown in Figure 5-17, the deflection magnifier will also reduce the beam diameter and increase the divergence by the same factor that it increases the deflection angle.

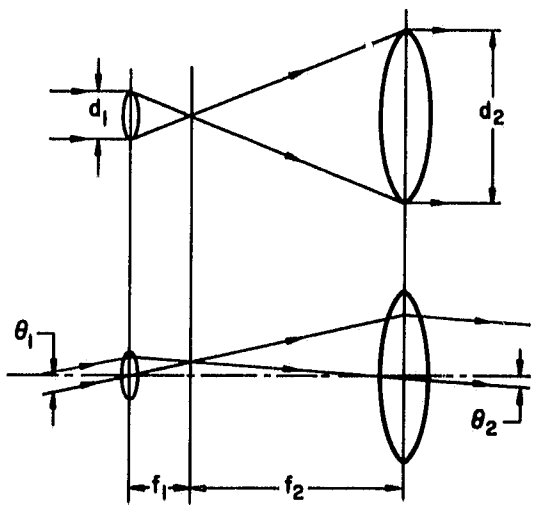

$$\left.\begin{aligned} d_1 \cdot f_2 &= d_2 \cdot f_1 \\ \theta_1 \cdot f_1 &= \theta_2 \cdot f_2 \end{aligned}\right\} \; d_1 \cdot \theta_1 = d_2 \cdot \theta_2$$

Figure 5-17. The effect of a deflection magnifier.

A reasonable value for the (constant) product of the transmitter beam's diameter and divergence (at the source) is 4×10^{-6} m-mrad. In other words, it should be possible to obtain either a 2-mm wide beam having 2-mrad divergence or a 20-mm wide beam having 0.2-mrad divergence from the transmitter. Since a 2-mm, 2-mrad beam is about what we wish to finally transmit, we see that the beam deflector must have an aperture, A_d, equal to

$$A_d = D_b \left(\frac{\theta_{fov}}{\theta_d} \right) \tag{5-1}$$

where A_d = deflector aperture
θ_d = deflector angular range
θ_{fov} = total required fov (500 mrad)
D_b = final beam diameter (2mm)

The criteria developed above can be used to evaluate the four types of low-inertia deflectors. The acousto-optic and electro-optic deflectors have small ranges, less than 20 mrad. Therefore, in accordance with Eq. (5-1), the aperture would have to be fairly large: 50 mm for θ_s = 20 mrad, θ_{fov} = 500 mrad, and D_b = 2 mm. Acousto-optic or electro-optic deflectors with apertures this large are simply not available. Therefore, only the galvanometer and piezoelectric deflectors are feasible.

The galvanometer deflector (ref. 42, 43) is shown in Figure 5-18. This device is capable of deflecting a 2-mm wide beam over a 500-mrad fov and would therefore not require a deflection magnifier after it. The random-access time of the galvanometer may, however, be marginal. Also, since the galvanometer contains sliding surfaces, its lifetime and reliability may not be adequate.

The piezoelectric deflector (refs 44, 45) is shown in Figure 5-19. This device has a limited scan range, perhaps 40 mrad at most, but can easily handle a 20-mm wide beam (that is, it can support a 20-mm mirror). Therefore, with the use of a deflection magnifier, a 2-mm wide beam can be steered over a 500-mrad fov. Figure 5-20 shows the form such a combination would take. Only one beamsteerer assembly is shown in the figure; two would be required in practice.

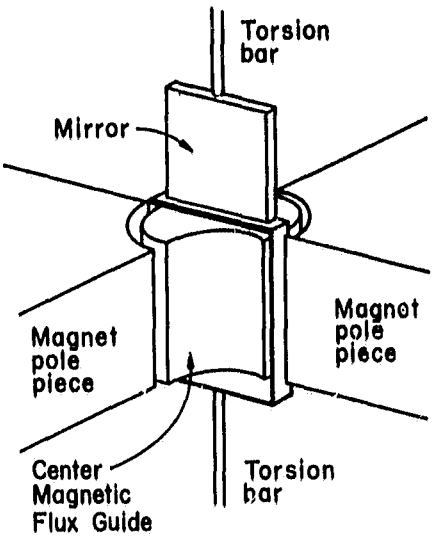

Figure 5-18. The galvanometer deflector.

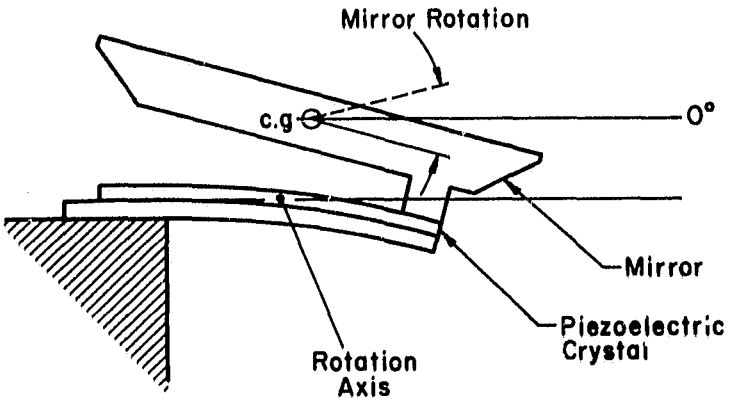

Figure 5-19. A piezoelectric deflector.

5.5 Reflectors (refs. 46, 47)

Reflectors are required on the target vehicle both to increase the strength of the returned signal and to give the sensor distinct points of known positions to track. Cube-corner (or corner-cube) reflectors, as shown in Figure 5-21, would be used.

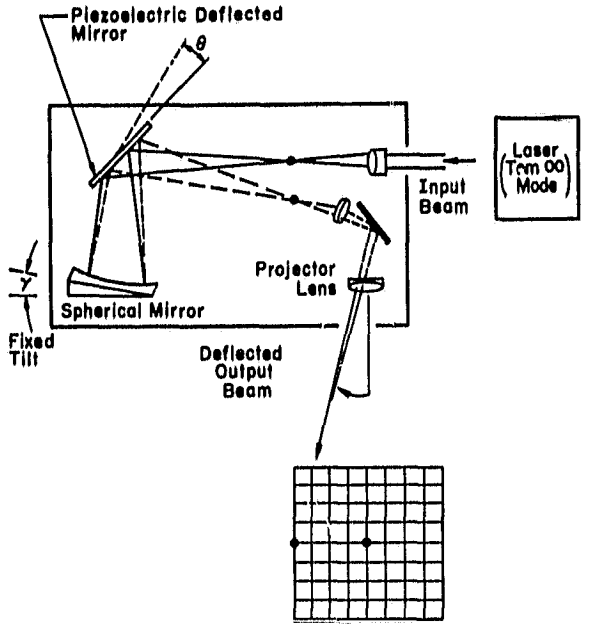

Figure 5-20. A piezoelectric-deflector-based beamsteerer.

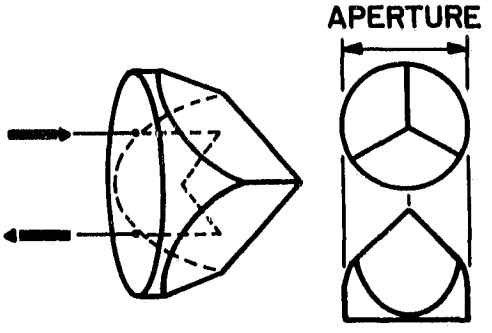

Figure 5-21. The cube-corner reflector.

An infinitely large cube-corner reflector of perfect construction would reflect all radiation incident from a $\pi/2$ steradian fov back in the direction it came from, with reversed polarization, as shown in Figure 5-22. The finite

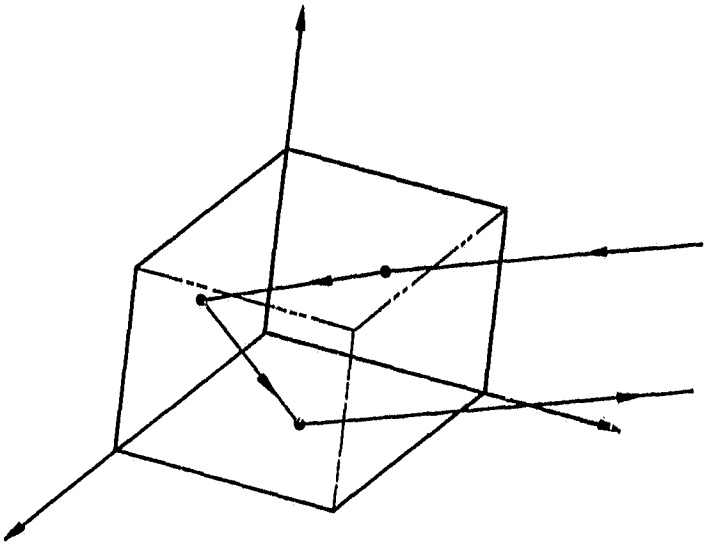

Figure 5-22. Reflection by a cube-corner reflector.

size of practical reflectors causes the effective aperture to shrink toward zero as the angle of incidence approaches 90° to the normal axis, as shown in Figure 5-23.

The reflected beam from the reflector will have a finite divergence, θ_f, attributable to three sources. That is,

$$\theta_f = \theta_i + \theta_d + \theta_a$$

where θ_i = divergence of the intercepted beam

θ_d = divergence due to diffraction

θ_a = divergence due to manufacturing imperfections

The divergence due to the intercepted beam is negligible for small retro-reflectors and moderate ranges, as shown in Figure 5-24. The divergence due to diffraction is unavoidable and is given by

$$\theta_d = \frac{\lambda}{D_f}$$

where λ = wavelength of radiation

D_f = reflector aperture diameter

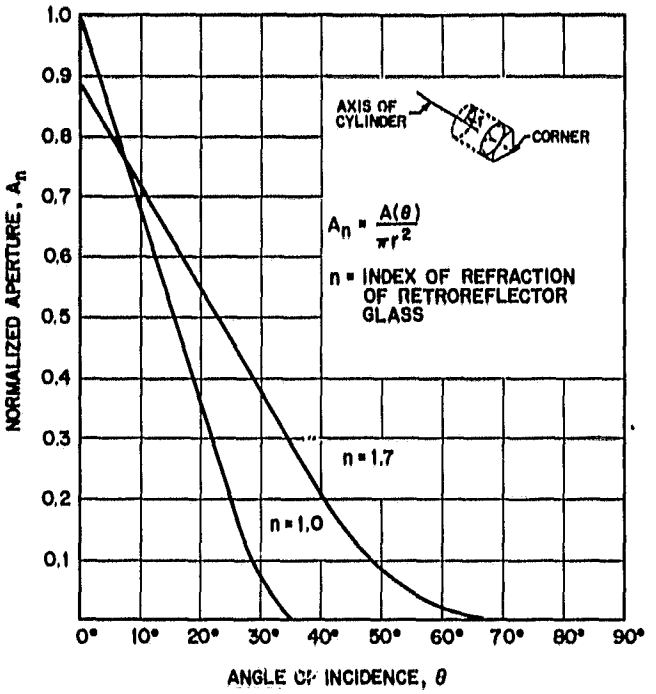

Figure 5-23. The effective aperture of a circular cube-corner reflector as a function of incident angle.

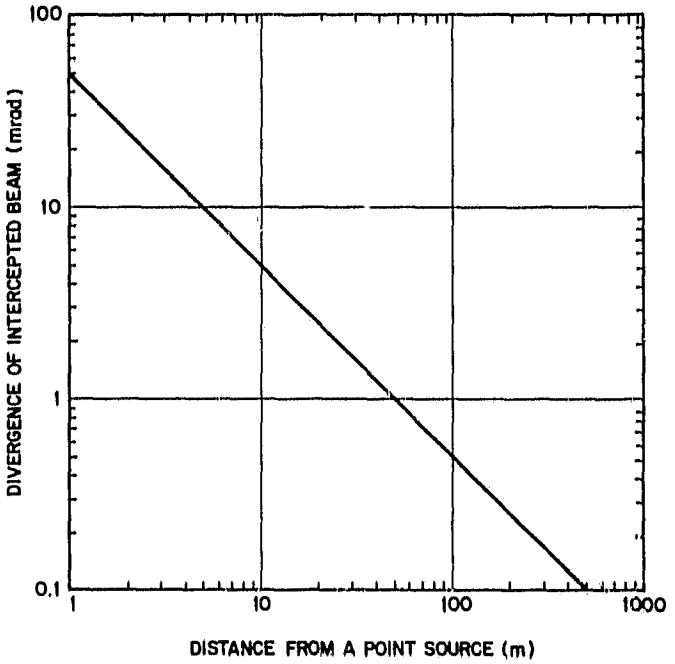

Figure 5-24. Divergence of the beam intercepted on-axis by a 50-mm-aperture cube-corner reflector.

The divergence due to manufacturing imperfections is generally quite small. We assume, in the analysis to follow, that the divergence of the beam from the reflector is twice the diffraction limit. This is a conservative estimate for all but the closest ranges where signal strength is not a problem anyway. Figure 5-25 shows the beam divergence from a circular cube-corner reflector as a function of aperture diameter for λ = 830 nm.

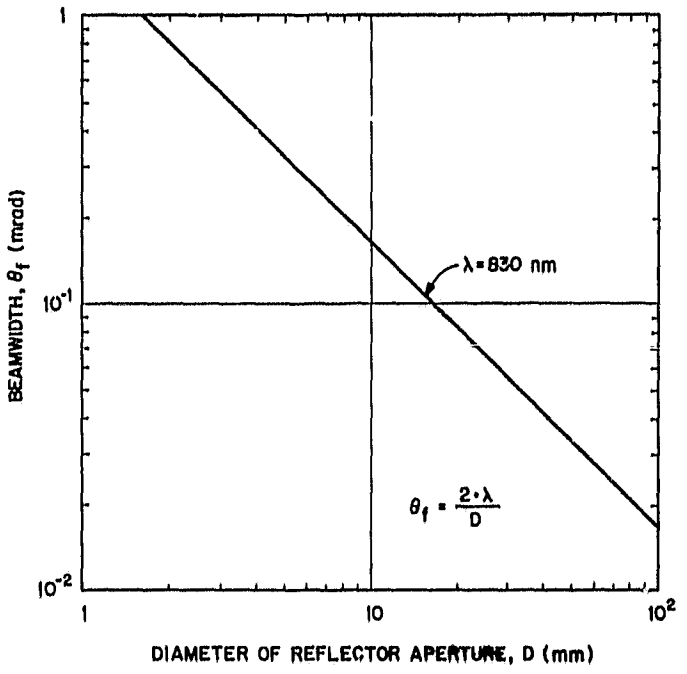

Figure 5-25. Divergence of the reflected beam from a circular cube-corner reflector.

The increase in return signal obtained by using a reflector is quite large. The peak radiance due to the reflection of a plane wave of irradiance E W/m^2 from an isotropically reflecting target of area A_f is I_i W/sr where:

$$I_i = \frac{E\ A_f}{4\pi} \qquad (5\text{-}2)$$

The radiance due to reflection from a circular cube-corner reflector of the same aperture area A_f is I_f W/sr where:*

$$I_f = \frac{E\ A_f}{(\pi/4)\theta_B^{\ 2}} \tag{5-3}$$

$$= \frac{E\ A_f}{(\pi/4)(4\theta_b/\pi)^2} \tag{5-4}$$

$$= \frac{E\ A_f}{(4/\pi)(2\lambda/D_f)^2} \tag{5-5}$$

$$= \frac{E\ A_f^{\ 2}}{4\ \lambda^2} \tag{5-6}$$

The gain of the cube-corner reflector over the isotropic reflector is, therefore,

$$G = \frac{I_f}{I_d} = \frac{A_f}{16\pi\ \lambda^2} \tag{5-7}$$

G is 5.7×10^{-7} for λ = 830 nm and D_f = 50 mm; a considerable improvement.

---

*θ_B is a fictitious beamwidth that is equal to the total beam power divided by peak intensity; that is,

$$\frac{\pi}{4}\ \theta_B^{\ 2} = \frac{P}{I_{pk}}$$

For the diffraction pattern resulting from a uniformly illuminated circular aperture,

$$\theta_B = \frac{4}{\pi}\ \theta_b$$

where θ_b is the beamwidth between half-intensity points.

5.6 Telescopes

The receiver telescope gathers the light reflected from the target and forms an image of the fov on the image dissector's photocathode. There are two basic types of telescopes: the refractive, constructed of lenses, and the reflective, constructed of mirrors. Examples of each are shown in Figure 5-26. Generally, the determining factor in the choice of telescope type is the aperture size. Refractive telescopes are preferred for small apertures; reflective telescopes are preferred for large apertures because large-aperture refractive telescopes are bulky and expensive.

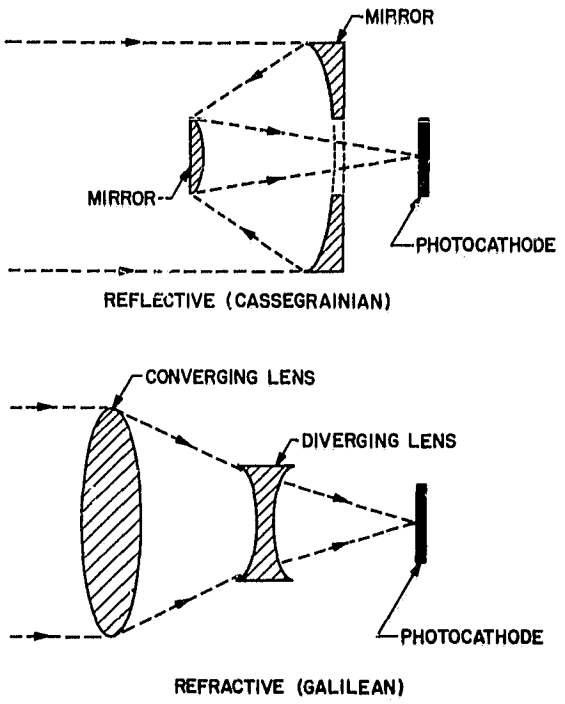

Figure 5-26. The two basic types of receiver telescopes.

The R&D-sensor-receiver aperture would be relatively small, 50-100 mm, which would dictate the use of a refractive telescope. The simple lens shown in Figure 5-26 would not be adequate, however. A practical lens would look more like the one in Figure 5-27.

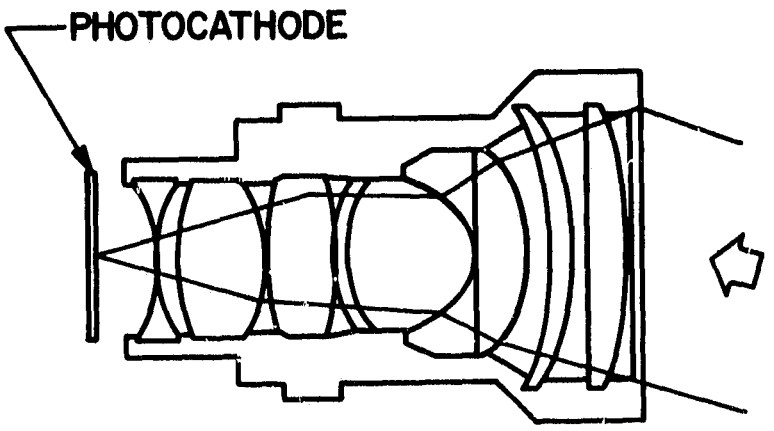

Figure 5-27. A practical receiver lens.

The use of a complex, multielement lens gives the designer additional parameters to vary in his quest for a receiver objective that meets the aperture, fov, detector size, and maximum distortion requirements. However, there is one fundamental limit that applies to all aplanatic lenses (those free from spherical aberration and coma). It is (ref. 48)

$$\frac{\theta_{fov} D_a}{2D_d} \leq \sin \theta_d \qquad (5\text{-}8)$$

The various quantities are depicted in Figure 5-28.

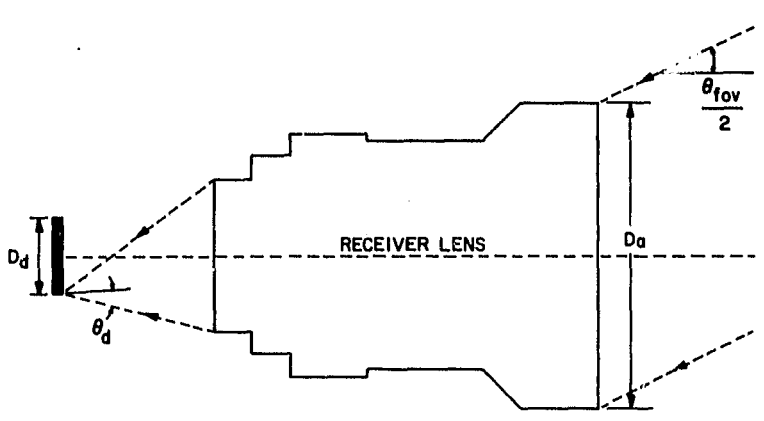

Figure 5-28. Parameters that determine the minimum receiver aperture.

The maximum possible value of sin θ_d is 1, however, a limit of 0.5 is more realistic, particularly when aberrations must be small. If we assume that sin $\theta_d \leq 0.5$ and that the detector (photocathode) diameter is 25 mm then the relationship between the lens aperture, D_a, and the fov, θ_{fov}, becomes

$$\theta_{fov} D_a \leq 25 \text{ mm} \tag{5-9}$$

This relationship is shown in Figure 5-29. We can see that, for θ_{fov} = 500 mrad and D_d = 25 mm, the minimum allowable lens aperture is 50 mm.

The illumination at the detector will be lower for off-axis image points, even if there is no vignetting (ref. 49). The cause of this loss of illumination is illustrated in Figure 5-30.

For small values of ϕ, $\phi' = \phi \cos^2\theta$, and the solid angle subtended by the exit pupil from point b, Ω_b, is

$$\Omega_b = \Omega_a \cos^3 \theta \tag{5-10}$$

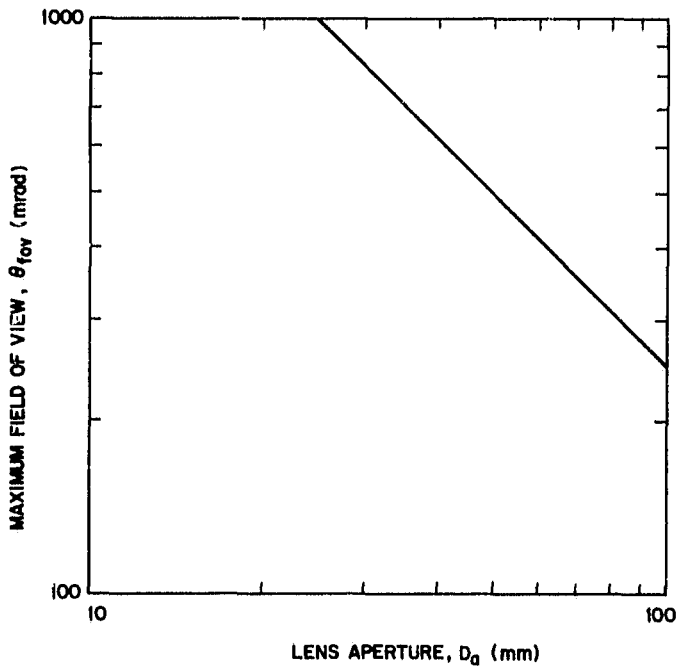

Figure 5-29. The maximum fov, θ_{fov}, for a lens aperture, D_a, assuming a 25-mm-diameter detector.

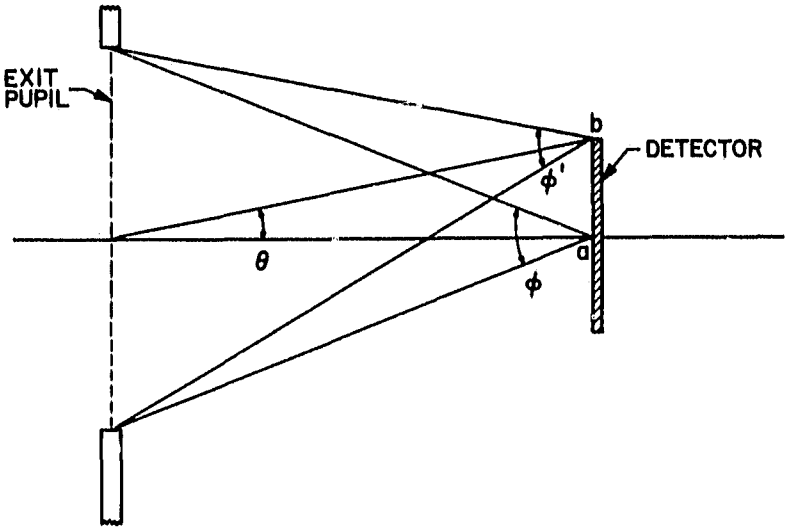

Figure 5-30. Off-axis imaging.

where Ω_a is the angle subtended by the exit pupil from point a. The radiation striking point b is spread over an area 1/cos θ times that of the radiation striking point a. Therefore, the illumination at point b, I_b, is

$$I_b = I_a \cos^4 \theta \qquad (5\text{-}11)$$

where I_a is the illumination at point a. This relationship is shown in Figure 5-31. The loss in illumination is considerable for θ greater than about 20°.

5.7 Optical Filters

An optical filter is used to eliminate as much background radiation as possible. The emission from the semiconductor-laser transmitter would have a spectral width much less than 1 nm; therefore, a very narrowband filter could be used. There are only two types of optical filters that have very narrow bandwidths (less than 10 nm): the interference filter (ref. 50) and the birefringent filter (refs. 51-53).

Modern interference filters are constructed of alternating layers of high and low index-of-refraction dielectrics as shown in Figure 5-32. Interference filters are thin, efficient, economical, and can have extremely narrow bandwidths. However, they do have one drawback: their passband shifts with the angle of incidence.

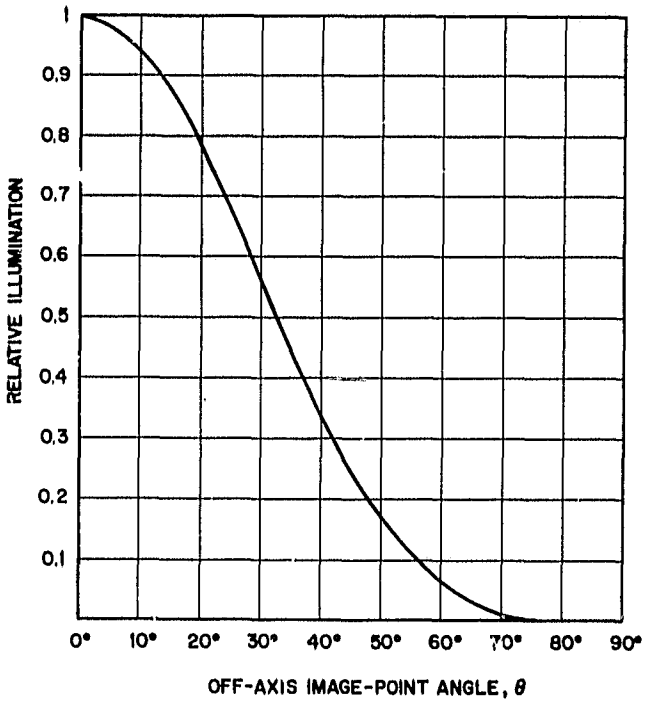

Figure 5-31. Loss of illumination for off-axis image points.

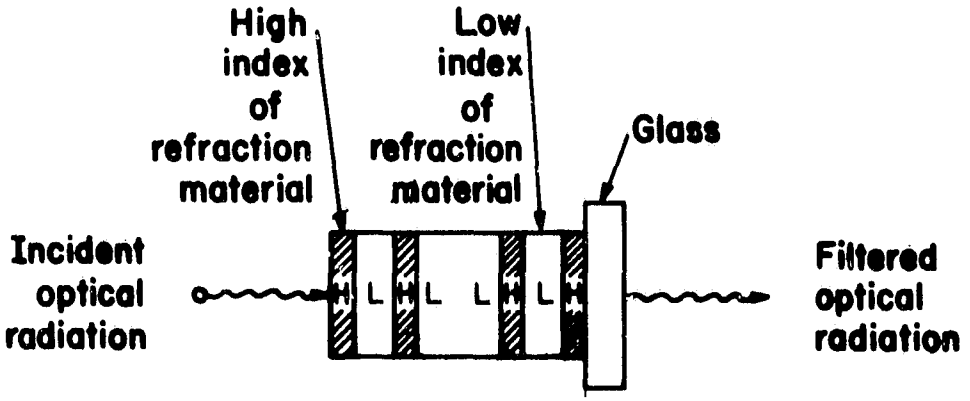

Figure 5-32. The interference filter.

The shift in center wavelength for a collimated beam incident at an angle θ can be approximated by

$$\frac{\Delta\lambda}{\lambda_0} \cong \frac{n - (n^2 - \sin^2 \theta)^{1/2}}{n} \qquad (5\text{-}12)$$

where θ = angle of incidence

$\Delta\lambda$ = shift in center wavelength = $\lambda_0 - \lambda_\theta$

λ_θ = center wavelength for beam incident at θ

λ_0 = center wavelength for beam incident at 0°

n = effective index of refraction

This relationship is shown in Figure 5-33.

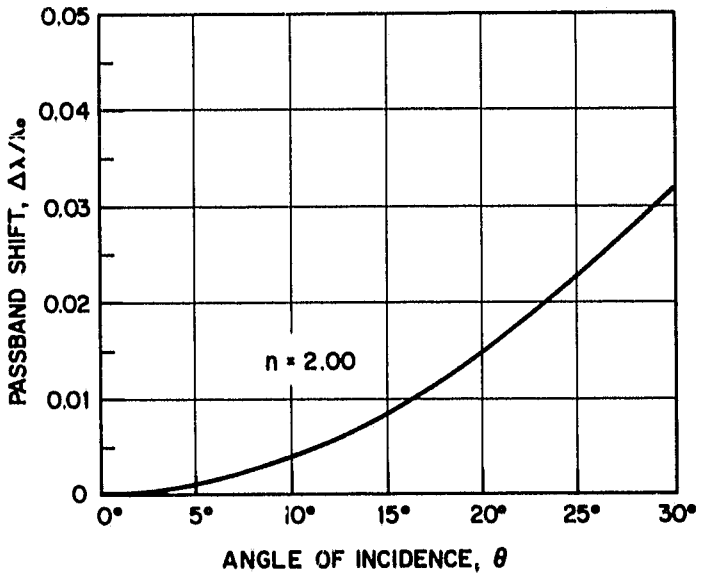

Figure 5-33. The passband shift of an interference filter with n = 2.00 for small angles of incidence.

An interference filter for a sensor with a 500-mrad fov (30°) would have a maximum incident angle of 250 mrad (15°) which would result in $\Delta\lambda$ = 7 nm for λ_0 = 830 nm and n = 2.00. Therefore, a filter having approximately a 10-nm-wide passband would be required, even though the bandwidth of the received signal is

much less than 1 nm. This is the reason that we have considered another type of filter -- the birefringent filter -- for the R&D sensor.

The birefringent filter, also called the polarization interference filter, is constructed of alternating layers of polarizers and birefringent crystals, as shown in Figure 5-34. These filters are used to filter polarized light to bandwidths as narrow as several angstroms. The most important characteristic of birefringent filters, from our point of view, is that they can be designed with wide fovs. Birefringent filters are, however, bulkier and lossier than interference filters. There has been little experience with this type of filter for applications such as ours. While we cannot recommend the birefringent filter over the interference filter at this point, we do believe it merits further investigation.

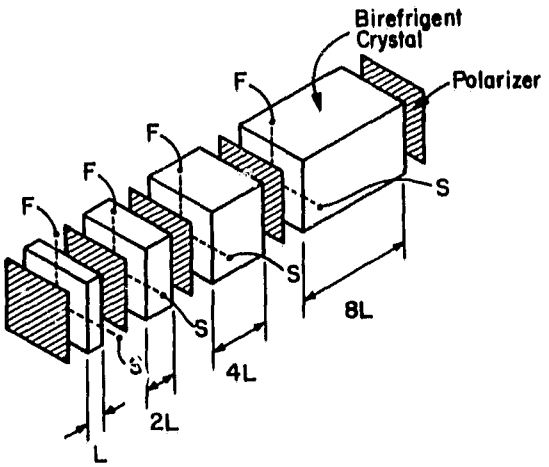

Figure 5-34. The birefringent filter.

5.8 Image Dissector (ref. 54)

The image dissector, shown in Figure 5-35, is a nonstorage imaging tube. In operation the fov is focused onto the photocathode by a lens. Electrons emitted from the photocathode are then focused onto the plate by the focusing coils. The electrons that impinge on the aperture in the plate enter the photomultiplier where they become the output signal. The deflection coils determine which spot on the photocathode emits the electrons that eventually

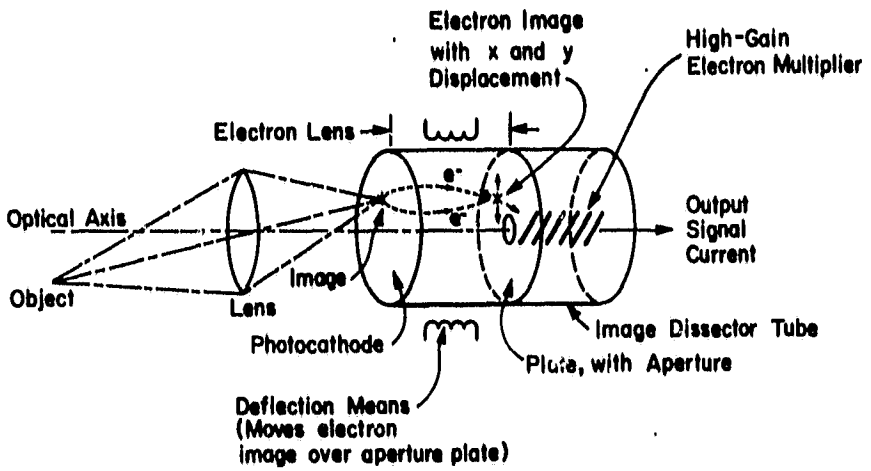

Figure 5-35. The image dissector.

become the output signal. In this way, a small portion of the total scene (fov) can be observed. The major elements of the image dissector are the:

- Photocathode
- Deflection mechanism
- Aperture
- Photomultiplier

The photocathode is the most important part of the image dissector. The key parameters of the photocathode are the

- Material
- Size
- Sensitivity
- Power density limit

Conventional photocathode materials have low sensitivity in the spectral range around 830 nm, as shown in Figure 5-36. GaAs, a material with much higher sensitivity (see Figure 5-37), is currently being developed into a practical photocathode by several organizations (refs. 55-57). We assume that an image dissector with a GaAs photocathode, in whatever diameter we find necessary, will be available or can be developed for the R&D sensor. The sensitivities of GaAs and several standard photocathodes at 830 nm are compared in Table 5-1.

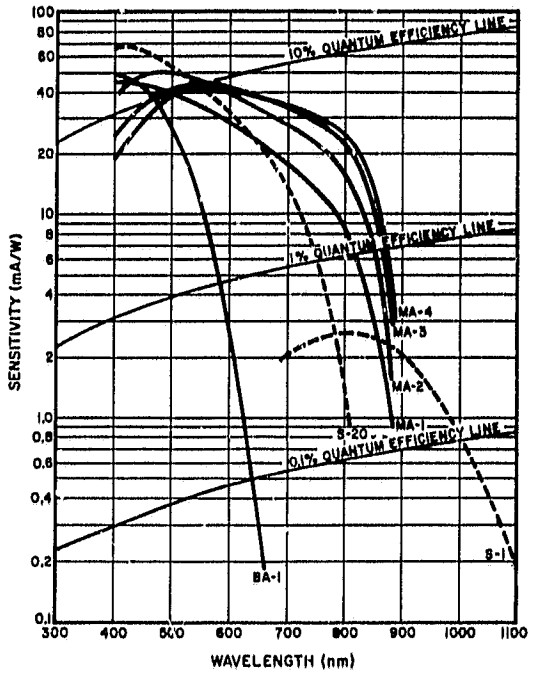

Figure 5-36. Conventional photocathode-material sensitivity.

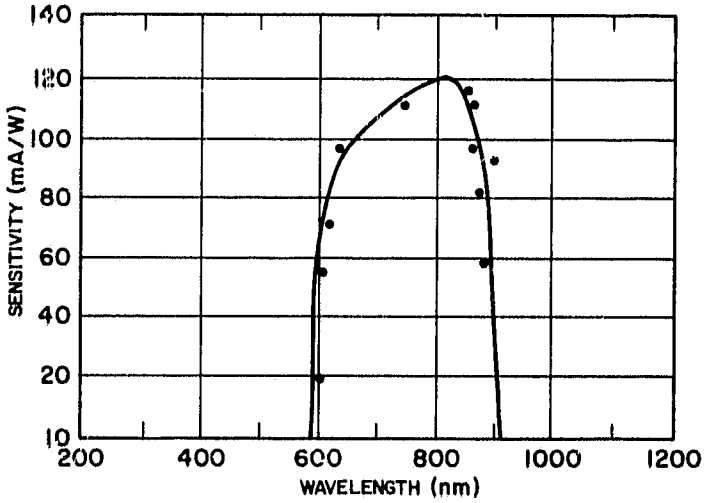

Figure 5-37. GaAs photocathode sensitivity.

TABLE 5-1. PHOTOCATHODE SENSITIVITIES AT 830 nm

Photocathode	Sensitivity (mA/W)
S1	2.5
MA-1	5
MA-2	10
MA-3	15
MA-4	20
GaAs	100

Photocathodes can be damaged by excessive currents due to high optical-power densities (ref. 58). The nature of the problem is not fully understood but we can establish some practical limits. Published specifications for commercial image dissectors set the current limit at approximately 10 $\mu A/cm^2$ averaged over the entire photocathode surface. When the incident optical power is concentrated onto one small portion of the photocathode the peak current density can be considerably higher than 10 $\mu A/cm^2$, perhaps as high as 100 $\mu A/cm^2$. We have assumed a limit of 20 $\mu A/cm^2$ in our analysis.

Of course, what we really want to know is the level of optical power that the photocathode can withstand. In normal operation, the worst case will occur at very close ranges when the reflectors will return almost all the transmitted power into one resolution cell. The power density in one resolution cell is

$$\rho = \frac{P_r}{A_c} \tag{5-13}$$

where P_r = total received power

A_c = area of one resolution cell

Since it is necessary that

$$\rho \leq \frac{J_{max}}{D} \tag{5-14}$$

where J_{max} = maximum allowed current density = 20 $\mu A/cm^2$

D = photocathode sensitivity

P_r must be less than

$$P_{r,max} = \frac{J_{max} A_c}{D} \tag{5-15}$$

The area of one resolution cell is

$$A_c = A_p \left(\frac{\theta_b}{\theta_{fov}}\right)^2 \tag{5-16}$$

where A_p is the area of the photocathode. Therefore,

$$P_{r,max} = \left(\frac{J_{max}\, A_p}{D}\right) \left(\frac{\theta_b}{\theta_{fov}}\right)^2 \tag{5-17}$$

The maximum allowable received power, $P_{r,max}$, for D = 100 mA/W, J_{max} = 20 $\mu A/cm^2$, and D_p = 25 mm is shown in Figure 5-38 as a function of beam concentration, θ_{fov}/θ_b. The maximum allowed received power for θ_{fov} = 500 mrad and θ_b = 2 mrad is 16 nW.

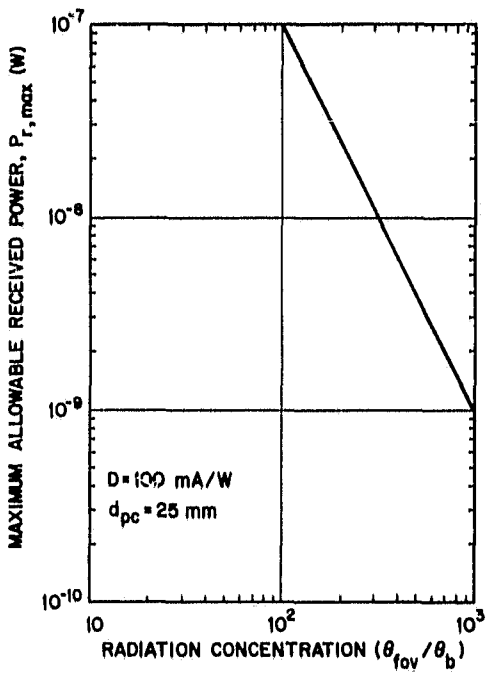

Figure 5-38. Radiation tolerance of the image-dissector photocathode.

The deflection mechanism may be either magnetic or electric. Magnetic deflection is more accurate than electric; all modern image dissectors are

equipped with magnetic deflection coils. The aperture will be circular and will have the same diameter as the photocathode resolution cell. The aperture diameter for a 25-mm photocathode, a 2-mrad beamwidth, and a 500-mrad fov is 100 μm.

Conventional photomultiplier structures such as the "box and grid" or the "venetian blind" are employed in most image dissectors. They are suitable for bandwidths up to 100 MHz. There are various types of wide bandwidth photomultipliers that have been developed or proposed in the past (refs. 59, 60). These would be necessary if a subcarrier modulation system were to be employed; however the standard photomultipliers are adequate for the modulation scheme we have selected.

6. PERFORMANCE ANALYSIS

In Section 4 we considered the form the R&D sensor should take. In Section 5 we discussed the optical components involved. In Section 6 we examine the capability of a representative system.

We do not claim that the design described in the following section is an optimum one. Nor do we attempt to perform an exhaustive analysis. Our objective is simply to show that a system of this type can perform the functions of an R&D sensor.

6.1 Representative System

The design of a representative R&D sensor is described in Table 6-1 and shown in Figure 6-1. The sensor begins operation by searching the fov around the designated target position for the target. The transmitter beam is directed in a spiral scan, beginning at the designated point and ending at the limits of the fov. The receiver beam is directed, at all times, in the same direction as the transmitter beam.

The transmitter signal is only modulated by the 15-MHz tone when operating in the search mode. If the beam hits a target within the maximum range, the return signal will cause the output of the bandpass filter and envelope detector in the detection channel to exceed the threshold and the comparator output will be asserted.

Once the target has been detected, all the ranging tones are imposed on the carrier. The phase shift of each carrier is determined by a phase detector. The transmitted and received ranging tones are heterodyned down to a low frequency prior to the phase measurement.

In an actual system the frequencies of all the ranging tones and local oscillator signals would be generated from one master clock by frequency synthesis so that they were all harmonically related and coherent with one another. It is unlikely that the ranging tones could be precisely 15 MHz, 150 kHz, and 1.5 kHz under such circumstances. However, for our purposes, nothing is gained by determining an exact set of frequencies that are properly related and within several hertz of those assumed, so we will continue to use the values mentioned above.

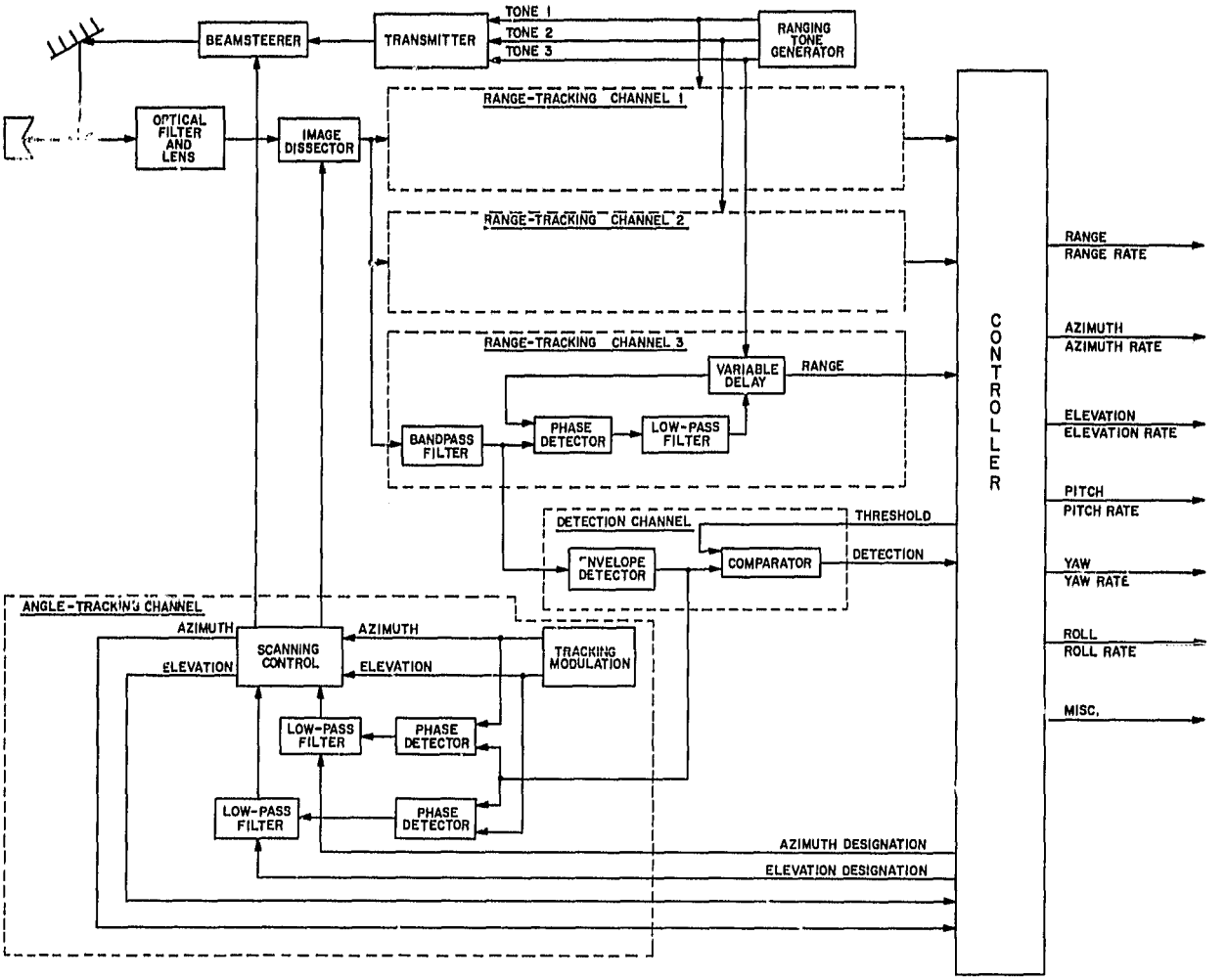

Figure 6-1. The R&D sensor.

Once the target has been detected, angle tracking begins. The sensor beam is conically scanned around the target position. The scanning process modulates the return signal from the target. If the target is located at the center of the scan, as assumed, the modulation, which is extracted from the envelope of the 15-MHz tone, has no average value or phase shift. If the target has moved off-center, the average value of the envelope and the phase shift indicate the direction in which the beam must be moved to once again put the target in the scan center. Since the target is kept in the center of the beam scan in this way, the target position can be determined from the average

C-2

TABLE 6-1 REPRESENTATIVE R&D SENSOR DESIGN

- SYSTEM
  - Fov: 500 mrad
  - Beamwidth: 830 nm
  - Transmitted Power: 1 W
  - Search Scan: Spiral, 20% overlap
  - Track Scan: Conical
  - Modulation: cw/IM (3 sinusoidal tones): 15 MHz, 150 kHz, 1.5 kHz
  - Background Radiation: Earth in beam
- TRANSMITTER
  - Type: Semiconductor laser
  - Beamwidth: 0.2 mrad (2 cm diameter)
  - Power Out: 1 W
  - Wavelength: 830 nm
  - Modulation: Direct
- BEAMSTEERER
  - Type: Piezoelectric
  - fov: 500 mrad
  - Scan Angle Magnification: 10
- REFLECTORS
  - Type: Cube Corner
  - Number: 3
  - Diameter: 50 mm
  - Deviation: 40 mrad (1/ mrad = diffraction limit)
- OPTICAL FILTER
  - Type: Interference
  - Center Wavelength: 825 nm
  - Bandwidth: 10 nm
- TELESCOPE
  - Type: Compound-element lens
  - Aperture: 50 mm

TABLE 6-1 REPRESENTATIVE R&D SENSOR DESIGN (Continued)

- PHOTODETECTOR
  - Type: Image Dissector
  - Photocathode Material: GaAs
  - Photocathode Diameter: 25 mm
  - Photocathode Sensitivity: 100 mA/W @ 830 nm
  - Deflection Mechanism: Magnetic
  - Aperture: 50 μm
  - Photomultiplier Gain: 10^{6}
  - Dark Current: 10^{-10} A
- DETECTION CHANNEL
  - Bandpass-Filter Bandwidth: 2 kHz
  - Low-pass-Filter Bandwidth: 20 Hz
- RANGE-TRACKING CHANNEL
  - Bandpass-Filter Bandwidth: 2 kHz
  - Low-pass-Filter Bandwidth: 20 Hz
- ANGLE-TRACKING CHANNEL
  - Bandpass-Filter Bandwidth: 2 kHz
  - Low-pass-Filter Bandwidth: 20 Hz

voltages on the piezoelectric deflectors or the average currents in the image-dissector deflection coils.

When a docking maneuver is performed, the sensor must measure the range and angle of each reflector, in turn, before moving on to the next one. About five measurements per reflector per second would be required.

The controller is basically a digital computer and it performs five major functions:

- Runs the sensor
- Filters (smooths) the measurements
- Calculates pitch, yaw and roll
- Calculates all rates
- Records the present and previous states of each target

6.2 Range Equation (ref. 61)

The first step in evaluating the performance of the R&D sensor is to determine the receiver power as a function of transmitted power, range, and any other relevant parameters. Referring to Figure 6-2 we see that the power density at the reflector is

$$\rho_f = \frac{P_t}{R^2 \, \Omega_t} \tag{6-1}$$

where P_t = transmitted power

R = range

Ω_t = transmitter solid-angle beamwidth

The total power, P_f, intercepted by the reflector is

$$P_f = \rho_f \, A_f \tag{6-2}$$

where A_f = reflector aperture.

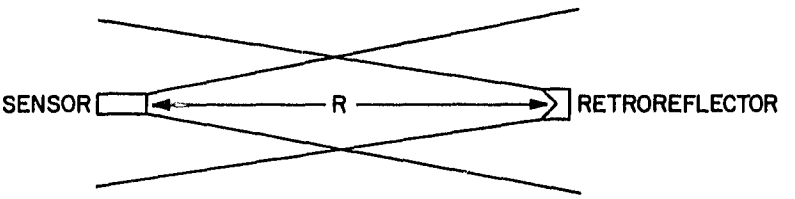

Figure 6-2. The power returned to the sensor is primarily determined by the sensor and reflector beamwidths and apertures.

The power intercepted by the reflector is returned to the sensor and produces a power density at the sensor receiver of

$$\rho_r = \frac{P_f}{R^2 \, \Omega_f} \tag{6-3}$$

where Ω_f is the reflector solid-angle beamwidth. The total power intercepted by the sensor is

$$P_r = A_r \rho_r \tag{6-4}$$

where A_r is the receiver aperture. Combining Eqs. (6-1) through (6-4) we obtain the relationship between P_r and P_r:

$$P_r = P_t \left(\frac{A_r}{R^2\Omega_t}\right)\left(\frac{A_f}{R^2\Omega_f}\right)\left(\frac{1}{L}\right) \tag{6-5}$$

where the factor L has been added to account for losses.

Equation (6-5) is only valid when the reflector aperture is equal to or smaller than the transmitter-beam cross section and the receiver aperture is equal to or smaller than the reflector-beam cross section. This will be the case if

$$\frac{A_f}{R^2\ \Omega_t} \leq 1 \tag{6-6}$$

and

$$\frac{A_r}{R^2\ \Omega_f} \leq 1 \tag{6-7}$$

If the reflector aperture exceeds the transmitter beamwidth then $A_f/R^2\ \Omega_t$ should be replaced by 1 in Eq. (6-5); if the receiver aperture exceeds the reflector beamwidth then $A_r/R^2\ \Omega_f$ should be replaced by 1. In the limiting case, when both quantities are equal to 1, $P_r = P_t$, neglecting losses. This case is illustrated in Figure 6-3.

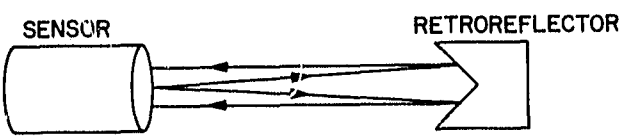

Figure 6-3. $P_r = P_t$ at very short ranges.

If we assume that

$$P_t = 1 \text{ W}$$

$$A_r = (\pi/4)\ (0.05)^2 \text{ m}^2$$

$$\Omega_t = (\pi/4)\ (0.002)^2 \text{ sr}$$

$$A_f = (\pi/4)\ (0.05)^2 \text{ m}^2$$

$$\Omega_f = (\pi/4)\ (0.0004)^2 \text{ sr}$$

$$L = 4$$

then Eq. (6-5) becomes

$$P_r = 2.4\text{x}10^8 \left(\frac{P_t}{R^4}\right) \tag{6-8}$$

The relationship between P_r and R, given by Eq. (6-8), is shown in Figure 6-4. Note that the received power level reaches the damage threshold of the image dissector at $1.1\text{x}10^4$ m. At shorter ranges the received power must be kept at or below this level by attenuating the transmitted beam.

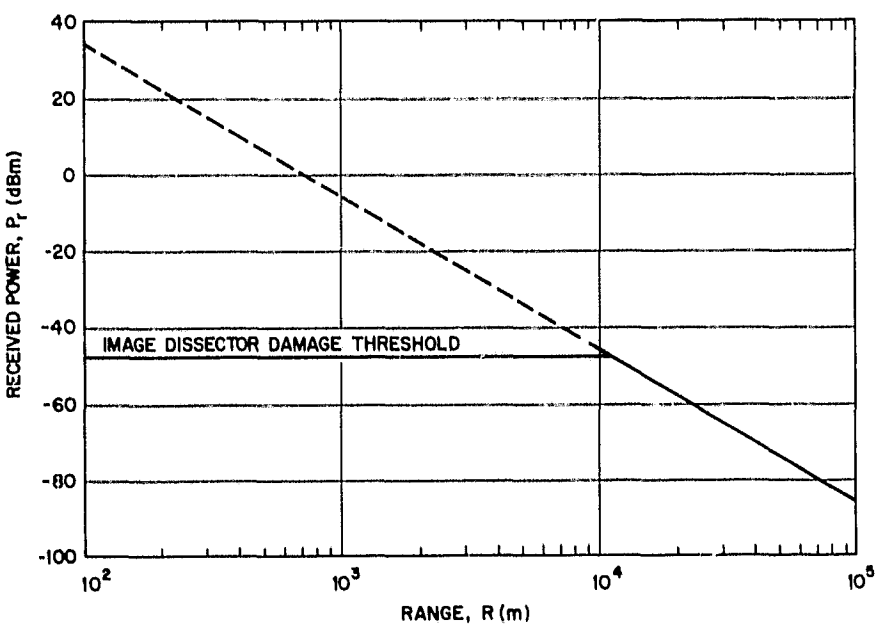

Figure 6-4. Received power as a function of target range.

6.3 Signal-to-Noise Ratio (ref. 62)

The returned signal from the target can be represented as

$$P_r(t) = \frac{1}{2}\,[1+A_m\cos\,(\omega_m t+\phi)]\;A_c^{\,2}\,\cos^2\,\omega_c t \qquad (6\text{-}9)$$

where $P_r(t)$ = receiver power

P_c = peak carrier power

ω_c = carrier frequency

A_m = modulation amplitude

ω_m = modulation frequency

ϕ = arbitrary phase shift

This power is converted into a proportional current by the photocathode:

$$i_p = \frac{D\,A_c^{\,2}}{4}\,[1 + A_m\cos\,(\omega_m t + \phi)] \qquad (6\text{-}10)$$

where D is the photocathode sensitivity. We prefer to express Eq. (6-10) in terms of carrier power since this is the specified transmitter parameter. If the transmitter were average-power limited then we should express the equation in terms of the average receiver power, which is

$$P_{c,av} = \frac{A_c^{\,2}}{4} \qquad (6\text{-}11)$$

However, if the transmitter were peak-power limited then we should express Eq. (6-10) in terms of the peak received power, which is

$$P_{c,pk} = \frac{A_c^{\,2}}{2} \qquad (6\text{-}12)$$

Note that when we say peak power we mean the peak of the power averaged over many optical carrier cycles. The peak optical power, which cannot be measured and is of no significance, is

$$P_{c,pk,opt} = A_c^{\,2} \qquad (6\text{-}13)$$

We will assume, in the following developments, that the transmitter is peak-power limited and therefore, since we will use $P_{c,pk}$ exclusively, we will drop the pk subscript and simply refer to this power as P_c.

The rms value of the photocathode current, described by Eq. (6-10), can therefore be expressed as

$$I_p = \frac{D\ P_c}{2\sqrt{2}} \tag{6-14}$$

I_p passes through the photomultiplier, of gain G, and the electrical bandpass filter, which does not affect it, to the load resistor R_L where it delivers a total power

$$P_s = G^2\ I_p^{\ 2}\ R_L \tag{6-15}$$

$$P_s = \frac{G^2\ D^2\ P_c^{\ 2}\ R_L}{8} \tag{6-16}$$

There are four sources of noise in the receiver: carrier quantum noise, background-radiation quantum noise, dark-current shot noise, and thermal noise due to R_L. Each noise has a constant spectral density. The spectral densities of the first three are proportional to the average value of the currents that give rise to them:

$$\Phi_c = \frac{G^2\ q\ D\ P_c}{2} \tag{6-17}$$

$$\Phi_b = G^2\ q\ D\ P_b \tag{6-18}$$

$$\Phi_d = G^2\ q\ I_d \tag{6-19}$$

The variances of the resulting noise currents are the products of the spectral densities and the bandwidth, B_e, of the electrical bandpass filter. The noise powers dissipated in R_L are, therefore,

$$P_{nc} = \frac{G^2\ q\ D\ P_c\ B_e\ R_L}{2} \tag{6-20}$$

$$P_{nb} = G^2\ q\ D\ P_b\ B_e\ R_L \tag{6-21}$$

and

$$P_{nd} = G^2 \, q \, I_d \, B_e \, R_L \tag{6-22}$$

The thermal noise, P_{nt}, due to the resistor is

$$P_{nt} = 2 \, K \, T \, B_e \tag{6-23}$$

where K = Boltzmann's constant (1.28×10^{-23} J/K)

T = temperature, K

The signal-to-noise ratio, S/N, is determined by the ratio of P_s, from Eq. (6-16), and P_n, where

$$P_n = P_{nc} + P_{nb} + P_{nd} + P_{nt} \tag{6-24}$$

It so happens that, assuming a photomultiplier with high gain and low dark current, P_{nt} and P_{nd} are insignificant compared to P_{nc} and P_{nb} for the signal and background levels the R&D sensor will encounter. Therefore, the S/N is

$$S/N = \frac{D \, P_c^{\,2}}{16 \, q \, (P_c/2 + P_b) \, B_e} \tag{6-25}$$

6.4 Detection

The first performance measure we will determine for the representative R&D sensor is the probability of detecting a target within its beam. This probability is a function of the S/N that was derived in the previous section.

We assume that the beam is traveling at a rate of 2 rad/s, which allows a 1-ms dwell time for a motionless target. During detection, only the 15-MHz modulation tone is transmitted. The output of a 2-kHz bandpass filter centered at 15 MHz is envelope-detected and compared to a threshold selected to keep false alarms to an acceptable level. If the output of the envelope detector is exceeded, the output of the comparator is asserted and the sensor goes into a tracking mode.

An assembly of reflectors, such as we described earlier, may be a poorly behaved target. The cross section may vary with angle but, more importantly, interference phenomena may take place. These considerations warrant future analysis. For the present we make the simple assumption that the target looks like one 50-mm-aperture reflector.

The background radiation due to the Earth is required before we can calculate the S/N. From Eq. (4-5),

$$P_b = \frac{B_o \, \theta_b^{\,2} \, W_e \, A_r}{4}$$

with B_o = 10 nm

θ_b = 2 mrad

$W_e = 5 \times 10^{-3}$ W/cm^2 μm

A_r = 50 mm

we find that $P_b = 9.8 \times 10^{-10}$ W. Now, from Eq. (6-25),

$$S/N = \frac{D \, P_c^{\,2}}{16 \, q \, (P_c/2 + P_b) \, B_e}$$

with D = 100 mA/W

$P_c = 4 \times 10^{-11}$ W (from Figure 6-4)

$P_b = 9.8 \times 10^{-10}$ W

B_e = 2 kHz

$q = 1.6 \times 10^{-19}$

we find that S/N = 15 dB

Figure 6-5 shows that, for a false alarm probability less than 10^{-6}, the resulting detection probability is about 99.8%. This should be adequate.

6.5 Range Tracking

Once a target has been detected, the sensor begins to track it in range and angle. Range is determined from the phase shifts on the three modulation tones. We assume that all three tones are transmitted simultaneously, although this is not absolutely necessary. The result is that the S/N of each tone is 1/3 of what it would be if only one tone were transmitted.

The low-pass filter in the range tracking loop need not have a very wide bandwidth; 20 Hz is probably more than adequate. We will assume 20 Hz in the analysis that follows. Once the sensor begins the docking maneuver, a wider bandwidth will become necessary because the sensor will have to accurately

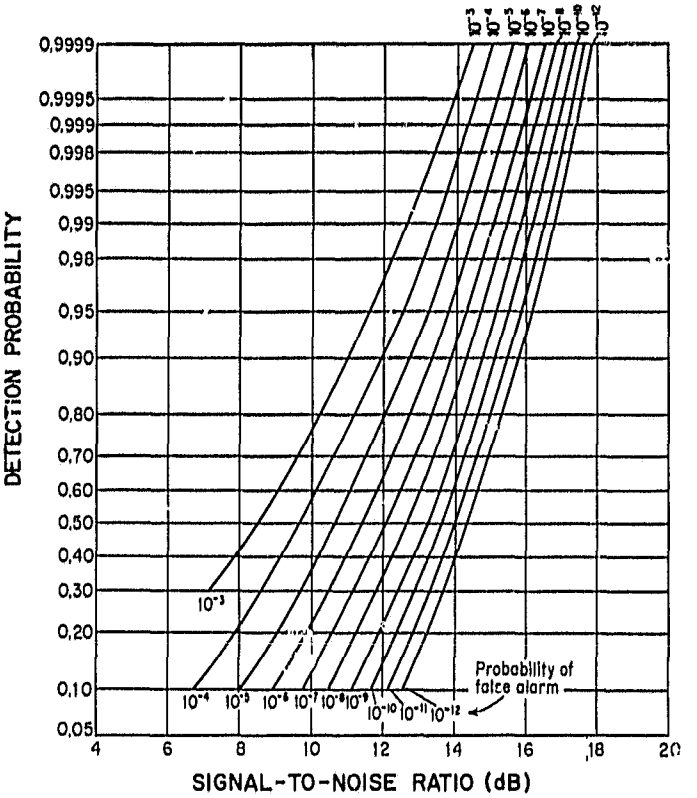

Figure 6-5. Detection probability as a function of S/N and false alarm probability.

track several targets sequentially. There are various ways to approach this problem. They are not discussed here because close-in range accuracy is not considered a problem; the S/N is very high at docking ranges.

The S/N in each tracking loop is given by a modified version of Eq. (6-25):

$$S/N = \frac{D\ P_c^2}{48\ q\ (P_c/2 + P_b)\ B_e} \qquad (6\text{-}26)$$

The S/N is plotted in Figure 6-6 for

D = 100 mA/W

P_c = see fig. 6-4

$P_b = 9.8 \times 10^{-10}$ W

$B_e = 20$ Hz

$q = 1.6 \times 10^{-19}$ C

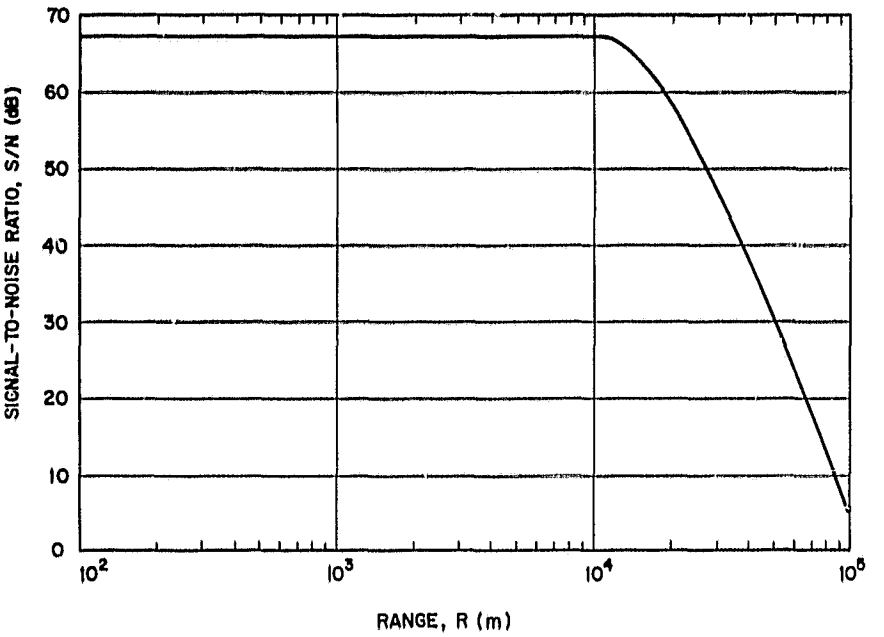

Figure 6-6. S/N in the range-tracking loops.

The resulting range error is, from Eq. (4-5)

$$\sigma_{\hat{R}} = \frac{\lambda_m}{4\pi \sqrt{S/N}} \tag{6-27}$$

The range error due to the 15-MHz tone is shown in Figure 6-7.

6.6 Angle Tracking (ref. 63)

The angle error for conical-scan angle tracking, is approximately

$$\sigma_\theta \cong \frac{\theta_b}{\sqrt{S/N}} \tag{6-28}$$

where S/N is the effective S/N in the angle-tracking loops. If we assume that the noise bandwidth of the angle tracking loop is also 20 Hz, then the angle

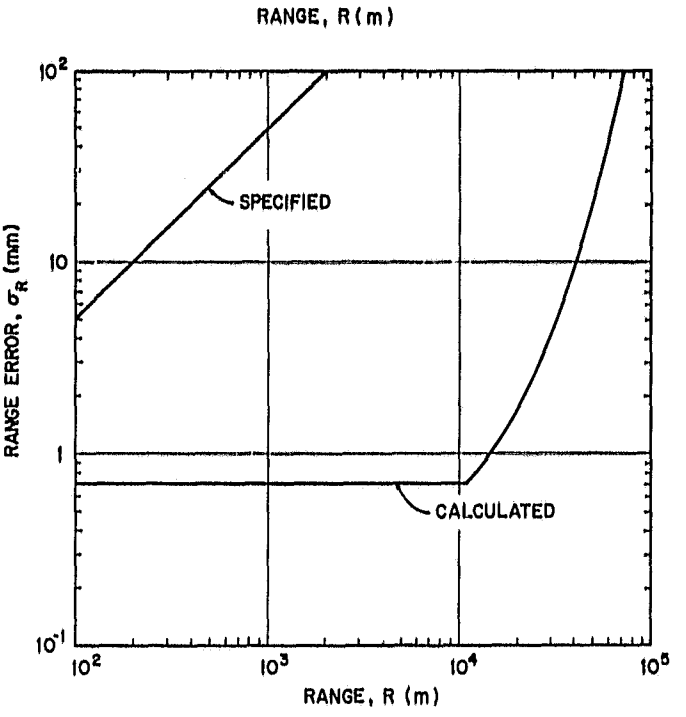

Figure 6-7. Range error as a function of range.

error can be determined from Eq. (6-28) and Fig. 6-6. The result is shown in Figure 6-8.

6.7 Search Pattern (ref. 64)

The sensor acquires a target by searching the area around the target's estimated position. The probability distribution of the target's angular position will be Gaussian with a mean equal to the estimated position and a standard deviation that depends on the quality of the initial estimate. The best type of search scan for a target whose location probability is as described above is the spiral scan.

We have selected a spiral scan with a 20% overlap, as shown in Figure 6-9, for the R&D sensor. The spiral scan operates at a constant tangential angular velocity, ψ_t, where

$$\psi_t = \theta(t)\ \dot{\phi}(t) \qquad (6\text{-}29)$$

ψ_t, in turn, is the beamwidth, θ_b, divided by the dwell time:

$$\psi_t = \frac{\theta_b}{t_d} \tag{6-30}$$

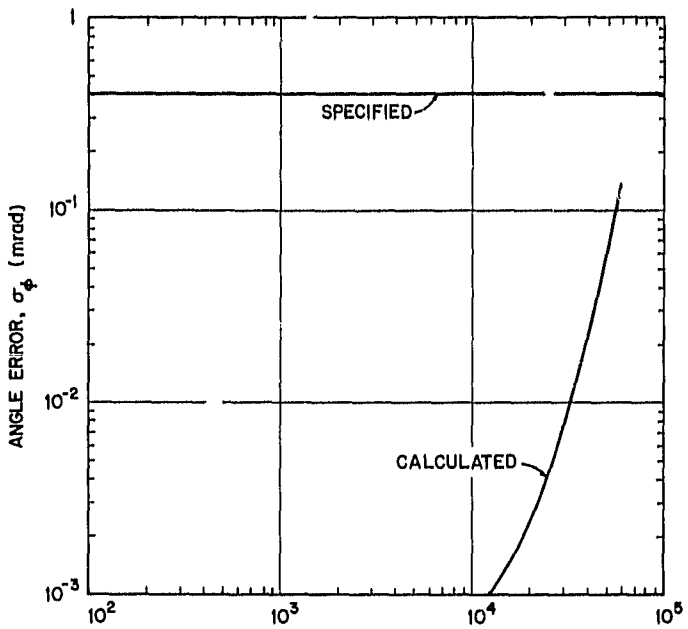

Figure 6-8. Angle error as a function of range.

The total number of revolutions the beam makes in scanning an area of angular radius θ_m is n where

$$n = \frac{(\theta_m - \theta_b/2)}{(\theta_m - \theta_o)} \tag{6-31}$$

In the following paragraphs we attempt to answer the following questions:

- How long does it take to search a given area?
- What is the maximum angular velocity a target may have if it is to be acquired by the sensor?

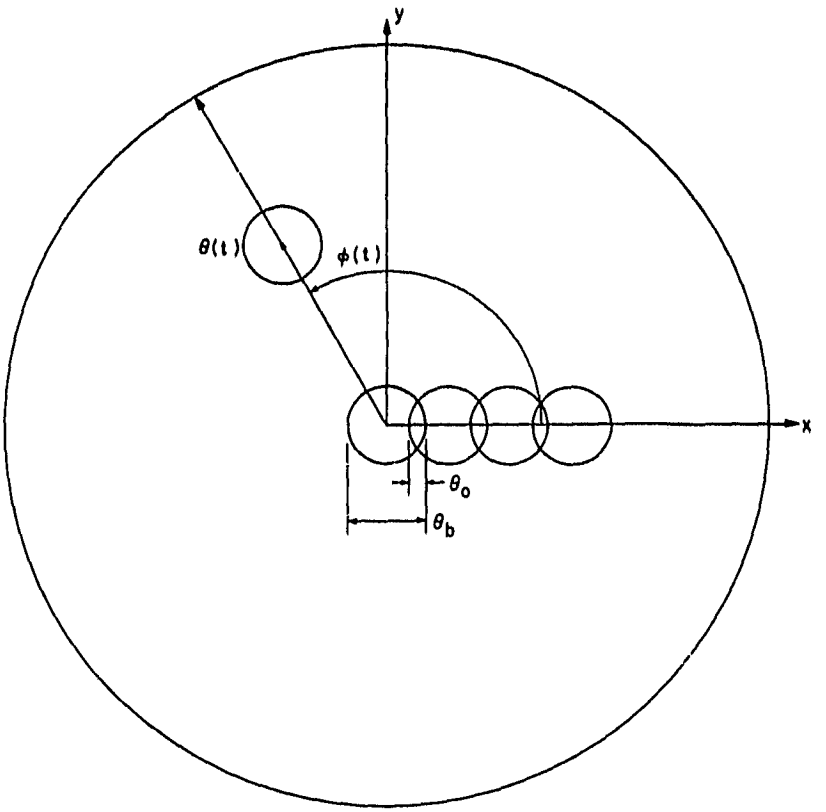

Figure 6-9. The spiral scan.

- What is the probability that a target will be acquired, given its initial probability distribution of angular position and velocity?

The answer to the first question begins by noting that each time the scan makes one revolution, the beam position extends outward one beam position minus the overlap. That is,

$$\theta(t) = \frac{\phi(t)}{2\pi} (\theta_b - \theta_o) \qquad (6\text{-}32)$$

where θ_b = beamwidth

θ_o = beam overlap

$\phi(t)$ = see fig. 6-9

$\theta(t)$ = see fig. 6-9

We can substitute Eq. (6-32) into Eq. (6-29) to obtain

$$\psi_t = \frac{\phi(t)}{2\pi} (\theta_b - \theta_o) \dot{\phi}(t) \tag{6-33}$$

which can be integrated with the result

$$\psi_t \int_o^{T_s} dt = \frac{(\theta_b - \theta_o)}{2\pi} \int_o^{2\pi n} \phi \, d\phi \tag{6-34}$$

where T_s = total search time

n = number of revolutions

Carrying out the indicated integrations and substituting for ψ_t and n by using Eqs. (6-30) and (6-31), respectively, we arrive at a final expression for T_s:

$$T_s = \frac{\pi \, t_d \, (\theta_m - \theta_b/2)^2}{\theta_b \, (\theta_b - \theta_o)} \tag{6-35}$$

which can be approximated as

$$T_s = \frac{\pi \, t_d \, \theta_m^{\,2}}{\theta_b^{\,2}(1 - \theta_o/\theta_b)} \tag{6-36}$$

This expression is more informative when put in a normalized form which expresses the search time in units of dwell time and the total angular radiis of the search area in units of beamwidth:

$$\frac{T_s}{t_d} = \frac{\pi \, (2 \, \theta_m/\theta_b)^2}{4 \, (1 - \theta_o/\theta_b)} \tag{6-37}$$

This relationship is shown in Figure 6-10 for $\theta_o/\theta_b = 0.2$.

We will now determine the limit to the target's angular velocity required to ensure successful acquisition. This limit will be a function of the target's initial position; the further the target is from the starting point the lower the angular velocity limit. We assume that the target travels radially outward along the X-axis at constant angular velocity, ω_T. The position of the target at time t is then

$$\theta_T(t) = \theta_i + \omega_T \, t \tag{6-38}$$

where θ_i = initial target position

$\theta_T(t)$ = target position at time t

ω_T = constant angular velocity of target

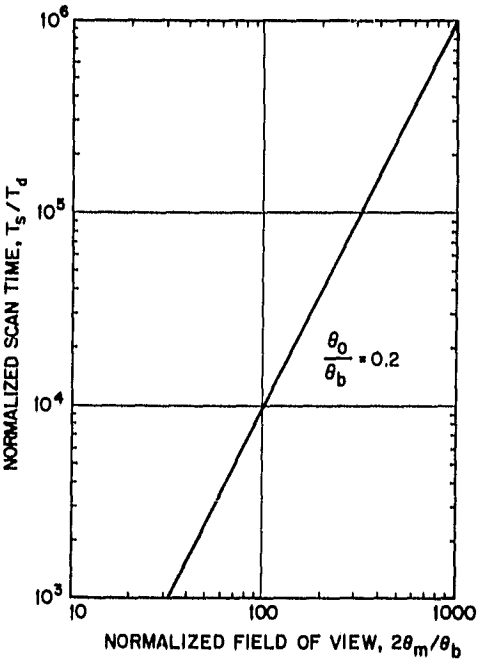

Figure 6-10. Total search time for the spiral scan.

The target-angular-velocity limit will be determined algebraically in a moment. Considerable insight into the form the solution should take, however, is possible by first using some simple graphical constructions.

First, we require the beam position, $\theta(t)$, as a function of time. This can be obtained simply by noting, first, that Eq. (6-36) can be rewritten as

$$\frac{T_s}{\theta_m^2} = \text{constant}$$

and, second, that the equation remains valid if we substitute t for T_s and $\theta(t)$ for θ_m. Therefore,

$$\frac{t}{\theta^2(t)} = \frac{T_s}{\theta_m^2} \qquad (6\text{-}39)$$

or

$$\frac{\theta(t)}{\theta_m} = \sqrt{\frac{t}{T_s}} \qquad (6\text{-}40)$$

This relationship is shown in Figure 6-11.

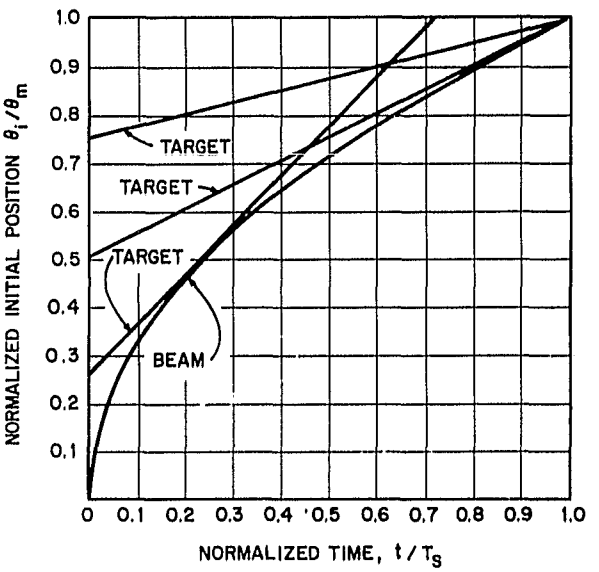

Figure 6-11. Target and beam positions as a function of time for various initial target positions.

Now we can graphically determine the maximum constant angular-target velocity corresponding to any initial position. To do this we draw the steepest straight line that starts at the initial position, θ_i, on the Y axis and touches the beam curve at one point. When the starting position is near the center of the search area the target motion line will be tangent to the beam curve. At some initial position (actually $\theta_i = \theta_m/2$), the point at which the

two curves are tangent falls exactly at θ_m. For further starting positions the tangent point would occur at an angle $\theta > \theta_m$; therefore, the highest allowable angular target velocity becomes the slope of the line that runs from the initial target position, θ_i, to the point (T_s,θ_m).

We are now ready to determine, algebraically, the maximum allowable target angular velocity. The first step is to determine an expression for the position at which the target and the beam coincide. From Eqs. (6-39) and (6-40) we see that when $\theta_T(t) = \theta(t)$

$$\theta_m \sqrt{\frac{t}{T_s}} = \theta_i + \omega_T\, t \tag{6-41}$$

or

$$\omega_T^2\, t^2 + (2\,\theta_i\,\omega_T - \theta_m^2/T_s)\, t + \theta_i^2 = 0 \tag{6-42}$$

If we symbolize Eq. (6-42) as

$$a\, t^2 + b\, t + c = 0 \tag{6-43}$$

then the tangent line is that one for which

$$b^2 - 4\, a\, c = 0 \tag{6-44}$$

or

$$\omega_T = \frac{\theta_m^2}{4\,\theta_i\, T_s} \tag{6-45}$$

The time at which the target and beam coincide is t_c where

$$t_c = \frac{-b}{2a} \tag{6-46}$$

or

$$t_c = 4 \left(\frac{\theta_i}{\theta_m}\right)^2 T_s \tag{6-47}$$

The corresponding position is, from Eq. (6-39),

$$\theta_c = 2\,\theta_i \tag{6-48}$$

The limit for θ_T given in Eq. (6-45) will hold as long as

$$\theta_i \leq \theta_m/2 \tag{6-49}$$

If $\theta_i \geq \theta_m/2$, the velocity limit will be

$$\omega_T = \frac{(\theta_m - \theta_i)}{T_s} \tag{6-50}$$

In this case the target and beam positions, but not velocities, will coincide at the scan area boundary.

The target velocity limits can be expressed in a normalized form:

$$\frac{\omega_T}{(\theta_m/T_s)} = \frac{1}{4\ (\theta_i/\theta_m)} \qquad \text{for } (\theta_i/\theta_m) \leq \frac{1}{2} \tag{6-51}$$

$$\frac{\omega_T}{(\theta_m/T_s)} = 1 - (\theta_i/\theta_m) \qquad \text{for } (\theta_i/\theta_m) \geq \frac{1}{2} \tag{6-52}$$

These limits are shown in Figure 6-12.

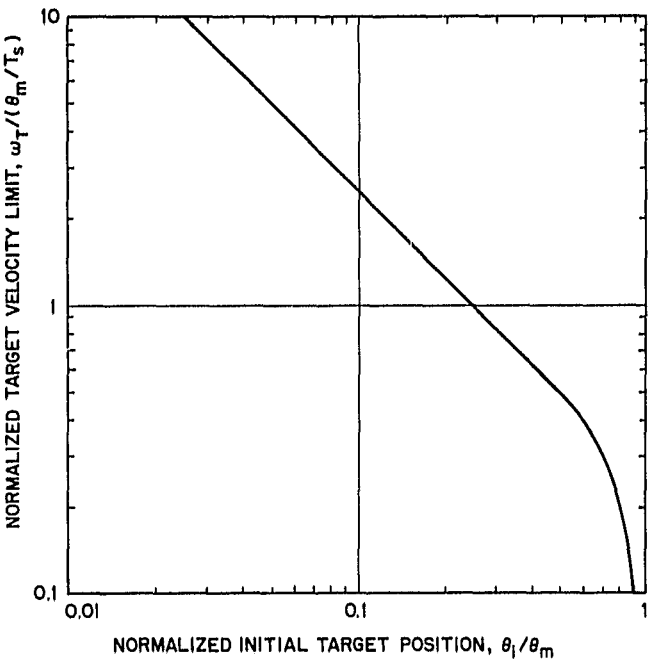

Figure 6-12. Normalized target angular-velocity limit to ensure acquisition.

For the system we described in Section 6.1, $2\ \theta_m/\theta_b = 250$ and, therefore, from fig. 6-10, $T_s/t_d = 6\text{x}10^4$. A 1-ms-dwell time yields a total scan time of

60 s. The actual (not normalized) target velocity limit is shown in Figure 6-13 for θ_m = 250 mrad and T_s = 60 s.

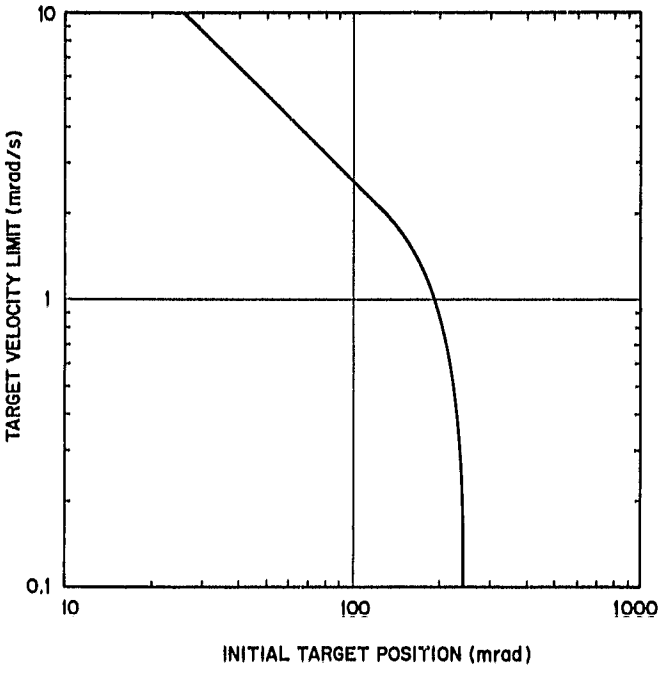

Figure 6-13. Target angular velocity limit for θ_m = 250 mrad and T_s = 60 s.

6.8 Summary

In Section 6 we have taken a quick look at how the type of R&D sensor we have selected would perform. A representative system was postulated and its capability for detection and tracking examined. From figs. 6-7 and 6-8 we see that the range and angle accuracy requirements specified in Table 3-1 are met.

The acquisition performance is a more difficult matter to evaluate. In Table 3-1 we specify an acquisition limit of 20 mrad/s. From fig. 6-13 we see that a target traveling at 20 mrad/s will only be acquired if the scan starts within 13 mrad of the target. The problem, of course, is that we are trying to scan a relatively large fov with a narrow beam.

The matter of acquisition can be put in some perspective if we look at what tangential linear velocities are required to result in a 20-mrad/s-angular

velocity at different ranges. This relationship is shown in Figure 6-14. We see that a velocity of 1000 m/s is required to generate an angular velocity of 20 mrad/s at a range of 50 km/s. This is a far greater velocity than can be expected.

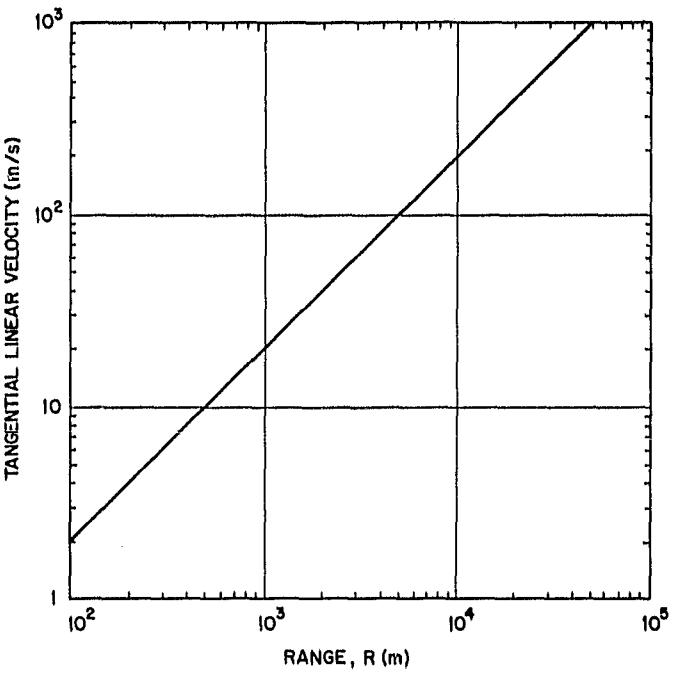

Figure 6-14. Tangential linear velocity corresponding to an angular velocity of 20 mrad/s.

Another way to view the acquisition performance is to plot the tangential-velocity limit versus initial position for several different ranges, as in Figure 6-15. From it we see that the tangential linear velocity limit increases as the range does.

In the light of the previous considerations, we believe that specifying one fixed angular velocity limit, 20 m/s in this case, for all ranges is probably unrealistic. A specification in better conformance with actual target behavior would allow an angular velocity limit that decreases with increasing range. In this case, we believe that an R&D sensor of the type we have selected could meet target acquisition specifications.

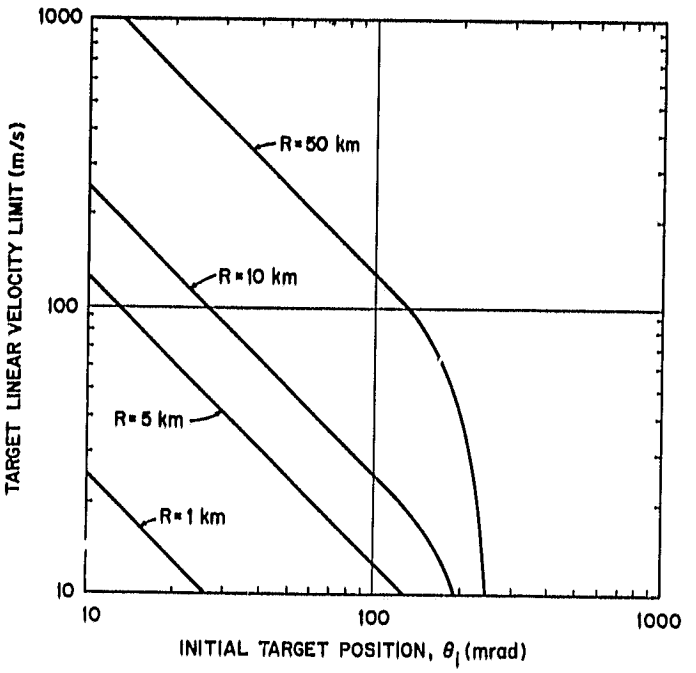

Figure 6-15. Linear velocity limit for the R&D sensor when θ_m = 250 mrad, θ_b = 2 mrad, θ_o/θ_b = 0.2, and T_s = 60 s.

7. CONCLUSIONS AND RECOMMENDATIONS

We have concluded that an R&D sensor that can support the Earth-orbital operations of future space vehicles, such as the Shuttle, TMS, and OTV, should be an optical radar with the following major characteristics:

- Semiconductor-laser transmitter
- Piezoelectric beamsteerer
- Image-dissector receiver
- cw IM ranging modulation

This conclusion is based on the following assumptions:

- The sensor should be physically compatible with the shuttle, TMS, and OTV.
- The target vehicle should be required to carry no more than passive aids (reflectors).
- Attitude is determined from range and angle measurements to three (or more) reflectors.
- Both soft and hard docking must be supported.
- The sensor must operate with the Earth in its fov.
- The sensor must provide its own source of illumination, it cannot depend on third parties, such as the Sun.
- The maximum operating range will be reduced from that required in the past due to better navigational systems.

Rendezvous and docking and the design of sensors to support them are complex subjects. Our brief examination of these matters has probably raised as many questions as it has answered. We recommend that the following matters be investigated in greater detail in follow-on studies:

- The data required for rendezvous and docking should be re-examined in greater detail. Particularly critical are the maximum range and the range-rate and angle-rate accuracy requirements.
- The development of a 1-W laser transmitter will be a difficult task. Some consideration should be given to it as soon as possible.
- The feasibility of using birefringent filters should be explored.
- The development of a space-qualified image dissector with a GaAs photocathode should be considered.

- The representative system described in Section 6 was just that; some thought should be given to the parameters of an optimum system.
- A more detailed performance analysis is required. The effect of lens aberrations on angle accuracy must be taken into account.

The items above will require a good deal of effort to complete. Once they and any subsequent questions that arise have been resolved, the detailed design and development of an R&D sensor should proceed. One fact is certain: regardless of its final form, a new R&D sensor is required to support future Earth-orbital operations.

REFERENCES

1. United States Civilian Space Programs 1958-1978 (U.S. Government Printing Office, Washington, DC, 1981), pp. 344-444.
2. W. C. Curtis and L. B. Wooten, "Lunar Excursion Module Rendezvous Radar and Transponder," RCA Engineer 11(5), 34-38 (1966).
3. L. M. Carrier and W. S. Pope, "An Overview of the Space Shuttle Orbiter Communication and Tracking System," IEEE Trans. Commun. COM-26(11), 1494-1506 (1978).
4. R. H. Cager et al., "Orbiter Ku-Band Integrated Radar and Communications Subsystem," IEEE Trans. Commun. COM-26(11), 1604-1619 (1978).
5. C. L. Weber et al., "Space Shuttle Proximity Operation Sensor Study," NASA-CR-151634, Feb. 1978.
6. T. P. Dixon et al., "A Laser Guidance System for Rendezvous and Docking," Navigation 13(3), 231-245 (1966).
7. T. Flom, "Spaceborne Laser Radar," Appl. Opt. 11(2), 291-299 (1972).
8. L. Cardone et al., "Optical Guidance System (OGS) for Rendezvous and Docking," Final Report prepared under NASA Contract No. NAS8-20717, July 1969.
9. T. Flom et al., "Design of a Scanning Laser Radar for Spaceborne Applications, Phase 3," NASA-CR-121014, Oct. 1971.
10. T. Flom et al., "Construction and Testing of a Scanning Laser Radar (SLR, Phase 2)," NASA-CR-123530, Dec. 1971.
11. C. L. Wyman, "An Advanced Laser Tracking Technique for Future Space Guidance Systems," J. Spacecraft 7(4), 504-507 (1970).
12. C. L. Wyman, "Test Performance of an Experimental Laser Radar for Rendezvous and Docking," J. Spacecraft 5(4), 430-344 (1968).
13. W. X. Culpepper, "Optical Docking Sensor Design Report," MSC/TCSD Document 21-189, Dec. 1969.
14. C. L. Laurence, "Phase Comparison Optical Docking System Error Analysis," MSC/TCSD Document 1B2014, May 1971.
15. W. X. Culpepper, "Error Analysis of the MSC Stadiametric Docking Tracking System Concept," TCSD Document 1007, Aug. 1971.
16. V. P. Legostaycu and B. V. Roushenbakh, "Automatic Rendezvous in Space," Foreign Technol. Div. Document No. FTD-HT-23-1346-68, 1968.

17. D. Chiarappa, "Analysis and Design of Space Vehicle Flight Control Systems. Volume VIII: Rendezvous and Tracking," NASA-CR-827, July 1967.
18. R. S. Dunning, "The Orbital Mechanics of Flight Mechanics," NASA-SP-325, 1973.
19. A. A. Lebedev and V. B. Isokolov, "Rendezvous in Orbit," Foreign Technol. Div. Document No. FTD-MT-24-26-71, Aug. 1971.
20. General Motors Corp., "Introduction to Orbital Mechanics and Rendezvous Techniques," Final Report prepared under NASA Contract NAS9-497, Nov. 1969.
21. W. T. Thomson, Introduction to Space Dynamics (Wiley, New York, 1961), pp. 29-100.
22. M. H. Kaplan, Modern Spacecraft Dynamics and Control (Wiley, New York, 1976), pp. 24-115.
23. Martin Marietta, "Space Tug Docking Study. Volume 2: Study Results," NASA-CR-a44240, Mar. 1976.
24. J. Wohl, "Space Tug Automatic Docking Control Study," NASA-CR-120578, Oct. 1974.
25. E. P. Blanchard et al., "Space Shuttle Vehicle Automatic Docking Study," NASA-CR-115248, Oct. 1971.
26. W. K. Pratt, Laser Communication Systems (Wiley, New York, 1969), pp. 6-8.
27. Ibid., pp. 111-127.
28. M. Ross et al., "Space Optical Communications with the Nd:YAG Laser," Proc. IEEE 66(3), 319-344 (1978).
29. J. H. McElroy, "CO_2 Laser Communication Systems for Near-Earth Space Applications," Proc. IEEE 65(2), 221 ^51 (1977).
30. M. I. Skolnik, Introduction to Radar Systems (McGraw-Hill, New York, 1980), pp. 95-98.
31. J. H. Lowry, "Electromagnetic Guidance Study," NASA-CR-865, Sept. 1967, pp. 49-52.
32. G. H. B. Thompson, Physics of Semiconductor Laser Devices (Wiley, New York, 1980), pp. 132-162.
33. D. Botez, "CW High-Power Single-Mode Operation of Constricted Double-Heterojunction AlGaAs Lasers with a Large Optical Cavity," Appl. Phys. Lett. 36(3), 190-192 (1980).
34. D. Botez, D. J. Chanin, and M. Ettenberg, "High-Power Single-Mode AlGaAs Laser Diodes," Proc. SPIE, Conf. Paper 321-13, Los Angeles, CA, Jan. 25-28, 1982.

35. M. Ettenberg and D. Botez, "High-Power Diode Lasers for Optical Recording with Operating Lifetimes in Excess of 10,000 Hours," Electron. Lett. 18(4) pp. 153-155 (Feb. 1982).
36. T. L. Paoli and J. E. Ripper, "Direct Modulation of Semiconductor Lasers," Proc. IEEE 58(10), 1457-1465 (1970).
37. R. P. Salathé, "Diode Lasers Coupled to External Resonators," Appl. Phys. 20(1), 1-28 (1979).
38. M. W. Fleming and A. Moorodian, "Spectral Characteristics of External-Cavity Controlled Semiconductor Lasers," IEEE J. Quantum Electron. QE-17(1), 44-59 (1981).
39. E. M. Phillip-Rutz and H. D. Edmonds, "Diffraction Limited GaAs Laser with External Resonator," Applied Optics 8(9), 1859-1865 (1969).
40. M. Ross, ed., Laser Applications Vol. 2 (Academic Press, New York, 1974), pp. 53-160.
41. Ibid., p. 17.
42. P. Brosens, "Scanning Accuracy of the Moving-Iron Galvanometer Scanner," Optical Eng. 15(2), 95-98 (1976).
43. J. Montagu, "A Practical Approach to Low Inertia Scanner Selection," in Laser Scanning Components and Techniques, SPIE 84, 42-46 (1976).
44. V. J. Fowler, "Investigation of Electro-Optical Techniques for Controlling the Direction of a Laser Beam," NASA-CR-68895, Mar. 1965.
45. J. F. Stephany and I. P. Gates, "Bimorph Optical Beam Deflectors," Appl. Opt. 15(2), 307-308 (1976).
46. G. T. Ruck et al., Radar Cross Section Handbook, Vol. 2 (Plenum Press, New York, 1970), pp. 588-601.
47. RCA, Electro-Optics Handbook, 1974, pp. 217-224.
48. W. J. Smith, Modern Optical Engineering (McGraw-Hill, New York, 1966), pp. 231-232.
49. Ibid., pp. 132-133.
50. W. L. Wolfe and G. J. Zissis, eds., The Infrared Handbook (United States Government Printing Office, Washington, DC, 1978), pp. 7-103 to 7-114.
51. Ibid., pp. 7-11 to 7-118.
52. J. W. Evans, "Solc Birefringent Filter," J. Optical Soc. Am. 48(3), 142-145 (1958).
53. J. W. Evans, "The Birefringent Filter," J. Optical Soc. Am. 39(3), 229-242 (1949).

54. "A Survey of Image Dissector Performance Characteristics," ITT Electro-Optic Products Div., TN-112, 1/70.
55. "GaAs Photocathode Aids Sight at Night," Electron. 54, 68-69 (Nov. 30, 1981).
56. J. R. Howorth et al., "Exploring the Limits of Performance of Third Generation Image Intensifiers," Vacuum 30(11/12), 551-555 (1981).
57. J. C. Richard and E. Roaux, "Low Light Level Imaging Tube with GaAs Photocathode," Vacuum 30(11/12), 549-550 (1981).
58. R. A. Smith, "Image Dissector Photocathode Solar Damage Test Program," NASA-CR-151657, Oct. 1977.
59. L. K. Anderson and B. J. McMurtry, "High-Speed Photodetectors," Proc. IEEE 54(10), 1335-1349 (1966).
60. M. B. Fisher, "A Scannable Detector of Microwave-Modulated Light," IEEE J. Quantum Electron. QE-1(4), 37-42 (1965).
61. C. G. Bachman, Laser Radar Systems and Techniques (Artech House, Dedham, MA, 1979), pp. 9-11.
62. Ref. 26, pp. 178-183.
63. D. K. Barton, Radar System Analysis (Prentice-Hall, Englewood Cliffs, NJ, 1964), pp. 263-286.
64. Axiomatix, "Study to Investigate and Evaluate Means of Optimizing the Radar Function for the Space Shuttle," NASA-CR-147842, July 1976, Appendix M.

APPENDIX

SPACE MISSIONS REQUIRING ADVANCED MULTIPURPOSE RENDEZVOUS TRACKING SYSTEMS 1986 - 1995

J. PRESTON LAYTON

PREPARED FOR MICROWAVE TECHNOLOGY CENTER
RCA LABORATORIES
PRINCETON, N. J.

DECEMBER 1981

J. PRESTON LAYTON
CONSULTANT
60 PENN-LYLE ROAD
PRINCETON JUNCTION, N.J.
08550 USA
(609) 799-3094

SPACE MISSIONS REQUIRING ADVANCED MULTIPURPOSE RENDEZVOUS TRACKING SYSTEMS 1986 - 1995

INTRODUCTION

At the beginning of the space shuttle era it is necessary to consider in some detail the various mission operations that will result from its flights in the decade after it becomes fully operational. The orbital needs of spacecraft, vehicles, platforms, stations and various large structures will require that advanced components and subsystems be identified and receive timely development so the full capabilities offered by the shuttle orbiter can be realized without undue delay.

It is becoming increasingly clear that the orbiter will need to interface with many kinds of craft under a wide variety of conditions to properly perform its orbital services both near and remote. A large number of these services will require special systems with many free-flyers of varying capabilities including long term orbit dwellers. It is also clear that the most significant missions will require a high degree of autonomy incorporating sophisticated rendezvous and docking capabilities.

The space shuttle transportation system will itself evolve in the period from 1986 to 1995 in a way that will be characterized not only by the major vehicle elements but also by the detailed operational influences of a large number of devices and other elements that must be brought to a state of readiness and proven capability before the overall

system can become really functional and economic. This will necessitate analytical, research and technology work that anticipates requirements and also tracks the operational experience.

The arena for focused space activity in the decade from the mid-1980s to the mid-1990s includes primarily the volume of space from the low earth orbits (LEO) with various inclinations of the shuttle orbiter to geostationary orbit (GSO) and beyond to several times GSO altitude as provided by a variety of propulsion systems, stages and vehicles. As the mission traffic increases during this decade the need for routine rendezvous, stationkeeping and docking will be increasingly felt.

While it is not possible to predict missions or capabilities in detail with any accuracy until the thrust of space activities in the 1986-95 decade is better defined, it is even more difficult to foresee the levels of activity individually or in the overall especially on a world-wide basis. On the other hand, it is possible to identify highly likely mission concepts and the spacecraft, vehicles and capabilities needed to carry them out. One identifiable capability of basic importance is an advanced multipurpose rendezvous tracking system including its sensors, electronics and other hardware as well as the software necessary for interfacing with other systems such as propulsion, guidance and control, et al. A careful consideration of a number of significant missions with their typical spacecraft, vehicles, and accompanying operational capabilities should be helpful in determining the essential and desirable characteristics of advanced multipurpose rendezvous tracking systems.

SPACE MISSIONS REQUIRING RENDEZVOUS, STATIONKEEPING AND DOCKING 1986-1995

Some classes of space missions in the 1986-1995 time period that will surely require rendezvous, stationkeeping and docking systems are listed in Table 1. Civil and military mission categories are listed that are similar in their fundamental characteristics while others are peculiar to each of these two major categories.

Civil communications satellites are expected to increase in size and sophistication to handle growing voice, TV (network and cable) and data traffic. Direct broadcast-voice and TV, public service and teleconferencing are relatively new services that are expected to have very substantial growth during this period.

A communications satellites of increasing size and complexity will, in general, need to be serviced, repaired or have components replaced during a typical lifetime and the entire satellite may need to be retrieved and replaced at end of life. Some traffic will surely be handled from large, multifunction spacecraft or platforms that will require rendezvous and docking in geostationary orbit by automated and, possibly, at a later time manned vehicles.

A typical multifunction communications space platform concept of the early 1990s is shown in Figure 1.[1]* Crowding in geostationary (i.e., geosynchronous equatorial) orbit by increasing numbers of civil communications spacecraft for a wide variety of rapidly growing domestic and international services will strengthen the trend to large hybrid and multifunction satellites. Operational and economic considerations may

---

*Superscript Arabic numbers in parenthesis indicate references listed at the back of the text.

Table 1

Classes of Space Missions Requiring Rendezvous Docking 1986-1995
-As of November 1981

CIVIL MISSIONS

Applications Satellites and Platforms

- Communications
- Environmental, including Meterological
- Surface Observation - Land and Ocean
- Navigation
- Space Experiments and Tests
- Space Manufacture and Processing

Science Satellites

- Solar Observatories
- Space Telescopes

Solar System Exploration Spacecraft

- Orbiters
- Landers and Rovers
- Sample Return Spacecraft

MILITARY MISSIONS

Information Systems

- Communications, Command and Control
- Meteorological
- Navigation
- Observation

Surveillance Systems

Inspectors/Interceptors

Space Weapons

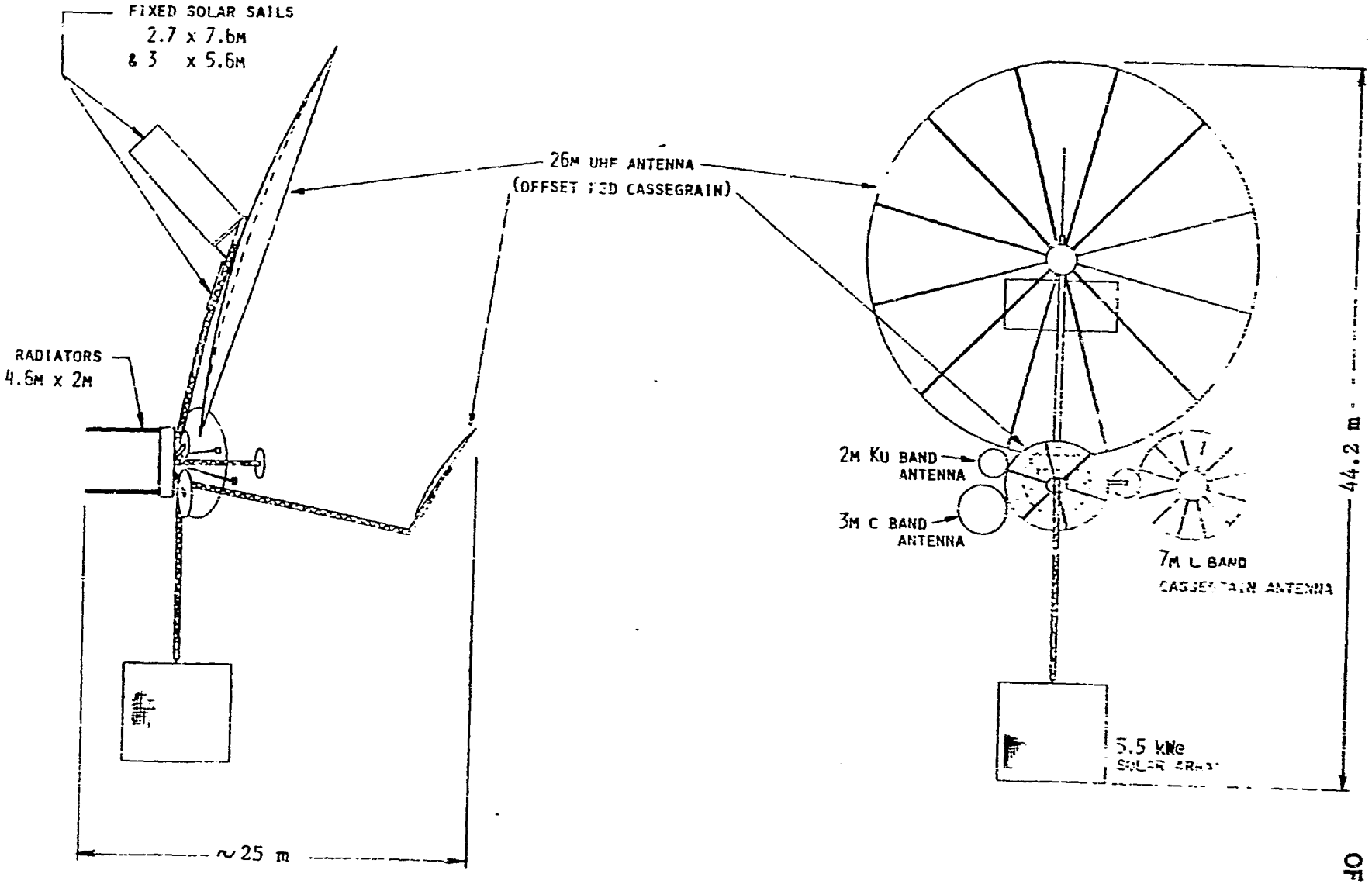

Figure 1 Typical Multifunction Communications Space Platform of late 1980s

lead to spacecraft clusters or platforms. Although much routine military traffic is handled commercially, the necessity for secure military communications will demand a dedicated system of survivable satellites for use during hostilities and these will probably also require servicing in orbit and ultimate retrieval.

Civilian environmental, surface (including oceanic) observation and navigation missions may be integrated into multipurpose spacecraft or platforms incorporating some communication payloads. This may be especially true if operational considerations or the economies of scale are proven.

If space experiments and tests, including prototype space manufacture and processing use free-flying spacecraft and platforms, they will require rendezvous and docking systems as a primary consideration in their design.

Science satellites are growing in complexity, size and consequently in cost. As the operational communities utilizing observatories and telescopes begin to depend on these instruments in the late 1980s, the necessity for servicing including replacement and upgrading of various elements will be required on both a planned and emergency basis. The space telescope, which has involved a substantial investment and is scheduled for placement in orbit by the shuttle in 1985, will undoubtedly be a focus for servicing and updating of its elements during the late 1980s. Minimization of operational costs will also be a primary consideration for this and other observatories, as well as military surveillance spacecraft.

Although it appears at present that substantial solar system exploration will be deferred until the late 1990s at the earliest, it is not too soon to consider the requirements for the very complex and demanding system capabilities that will characterize the next generation of missions. Although the advanced orbiter missions will involve rendezvous stationkeeping and perhaps docking with non-cooperating and passive targets, the later landers, rovers and sample return missions that are expected to characterize solar system exploration around the end of the century will need the full gamut of automated, multipurpose rendezvous tracking systems. An early (late 1980s) unmanned science and applications platform (SASP) concept is shown at rendezvous with a shuttle orbiter in Figure 2.[2] Table 2 presents a list of candidate mission payloads for such a free-flying platform. Regular rendezvous would be needed to provide for man-tended supervision and monitoring of the payloads on such a platform as well as the servicing and growth of its capabilities. A manned platform that would involve both scheduled and emergency rendezvous could evolve from the SASP in the 1990s.

Military missions will be dominated by the need to provide an effective and survivable communications, command and control architecture utilizing systems that meet the requirements of an established military space doctrine with life cycle costs a primary consideration. The entire question of secure and dependable military communications, in particular during a period of hostilities, must be dealt with in terms that are satisfactory to the multitude of users. This will call for capabilities throughout geocentric space in all frequency bands which will grow in size and complexity especially as additional information capabilities

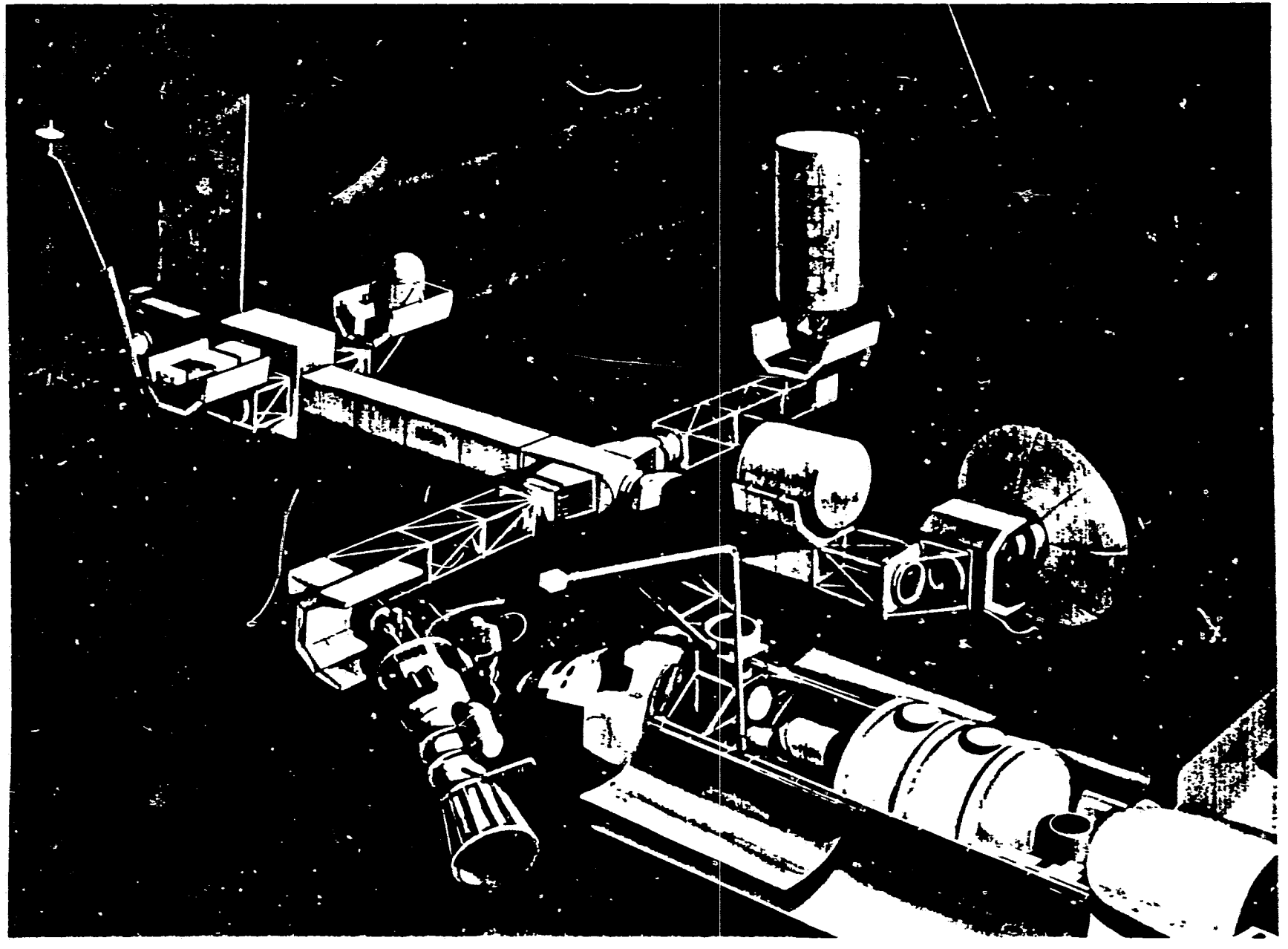

Figure 2 Shuttle Orbiter at Rendezvous with a Typical Unmanned Science and Applications Platform (SASP) of Early 1990s

Table 2

Candidate Mission Payloads for Science and Applications Platforms

Astronomy

Shuttle Infrared Telescope (SIRTF)

Very Long Baseline Interferometry (VLBI)

Starlab

Solar Physics

Solar Optical Telescope (SOT)

High Energy Astrophysics

Elemental Composition and Energy Spectra of Cosmic Ray Nuclei (SCRN)

Transition Radiation and Ionization Colorimeter Telescope (TRIC)

Super Conducting Magnetic Spectrometer

Heavy Nuclei Explorer (HNE)

Large Cosmic Ray Detector

Large Area Modular Array (LAMAR)

High Resolution Spectrometer

Materials Science

Electrophoresis Operations in Space (EOS)

Solidification Experiment System (SES)

Materials Experiment Assembly (MEA)

Space Plasma Physics

Space Experiments with Particle Accelerators (SEPAC)

Wave Injection in Space (WISP)

Environmental Observations

Ocean Wave Direction of Spectrometer

Advanced Limb Sounder

Land Observing Radar

Active Cavity Radiometer

Solar Ultraviolet Irradiance Monitor

Advanced Microwave Sounder

including meteorology, navigation, observation and certain intelligence functions are integrated based on present trends. The platforms that will result will certainly require sophisticated automated rendezvous, docking and teleoperator capabilities as well as such vehicles and modules shown in Figure 3. The requirement for rendezvous, docking and other teleoperator functions is identified in the figure. Much analysis, research and technology work as well as space demonstration testing will be needed to accomplish these functions on an operational basis in the decade of the 1990s.

Surveillance systems in the shuttle era will certainly grow to respond to the capabilities offered by the orbiter and its services both near and remote. Advanced multipurpose rendezvous tracking system characteristics will need to be heavily influenced by the requirement to provide a variety of services to these vital spacecraft.

Spacecraft inspectors and interceptors will by definition require rendezvous, stationkeeping and presumably "docking" capabilities. Since they will necessarily possess a very substantial propulsion capability, regular servicing and maintenance will be required.

The large number of possible space weapon concepts under consideration, which undoubtedly will not be sorted out and development undertaken until late in the period, can be influenced by the projected characteristics of various advanced multipurpose rendezvous tracking systems. Such weapons need to be studied on a broad parametric basis with a wide variety of subsystem technologies before choices are made. These choices are important because they can, and should, influence the evolutionary direction of the rendezvous, stationkeeping and docking systems.

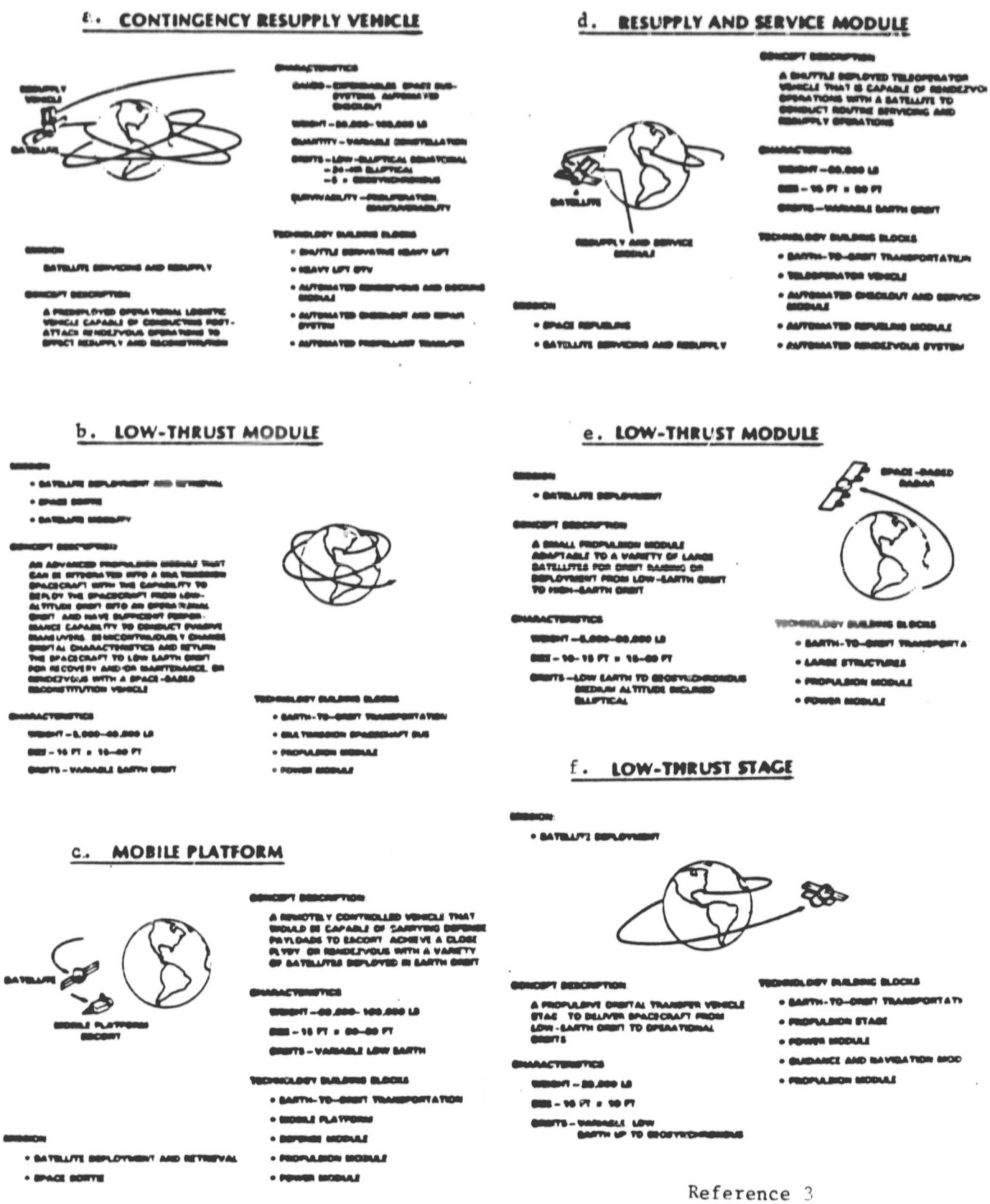

Reference 3

Figure 3 Potential Military Space Systems Applications - 1990s

SELECTED SPACECRAFT, VEHICLES AND OTHER CONCEPTS UTILIZING ADVANCED MULTI-PURPOSE RENDEZVOUS TRACKING SYSTEMS

The space missions discussed above will be performed utilizing a multitude of spacecraft, vehicles and other concepts, including platforms, stations, and bases that cannot yet be clearly defined; however, a number of concepts either exist or are sufficiently well conceived so their needs for rendezvous, stationkeeping and docking capabilities can be identified in a general way. Table 3 lists selected concepts that are representative and credible based on recent studies and projections of the United States Space Program. Needless to say, all of these concepts will not be developed but an overall synthesis of their operational requirements should provide an acceptable basis for defining the need for advanced multipurpose rendezvous tracking systems in the 1986-1995 time period. A few of the most significant spacecraft, vehicles and other concepts are discussed in the paragraphs that follow.

The shuttle orbiter is equipped with a radar docking system, shown in Figure 4,[4] with both automatic and manual capabilities, although final docking will usually be performed manually. The shuttle orbiter will perform as both an interceptor and target and requires a system with capabilities to perform rendezvous, stationkeeping and docking with the wide variety of spacecraft, vehicles, platforms, etc. listed in Table 3. Shuttle services near the orbiter will require interaction with a miscellany of spacecraft, and other objects, units and small systems such as a space suited astronaut in the Extravehiclular Mobility Unit (EMU) tethered or untethered or riding in the Manned Maneuvering Unit (MMU).

Table 3

List of Selected Spacecraft, Vehicles and Other Concepts Requiring Advanced Multipurpose Rendezvous Tracking Systems - 1986 to 1995

Shuttle Orbiter

Orbital Transfer Vehicles (OTV)

- Wide Body Centaur
- Advanced Chemical Rocket OTV
  - High Thrust
  - Low Thrust
- Electric Rocket OTV and Propulsion Stages
  - Solar
  - Nuclear

Extravehicular Mobility Unit (EMU)

Manned Maneuvering Unit (MMU)

Small Payload Maneuvering System (SPMS)

Teleoperator Maneuvering Systems (TMS)

Typical Low Earth Orbit (LEO) Spacecraft (S/C)

Long Duration Experiment Facility (LDEF)

Typical LEO Space Platforms

Science and Applications Space Platforms

- Unmanned (SASP)
- Manned (SAMSP)

Space Operations Center (SOC)

Various Geostationary Orbit (GSO) S/C

Typical GSO Platforms, Stations and Bases

Solar System Exploration S/C

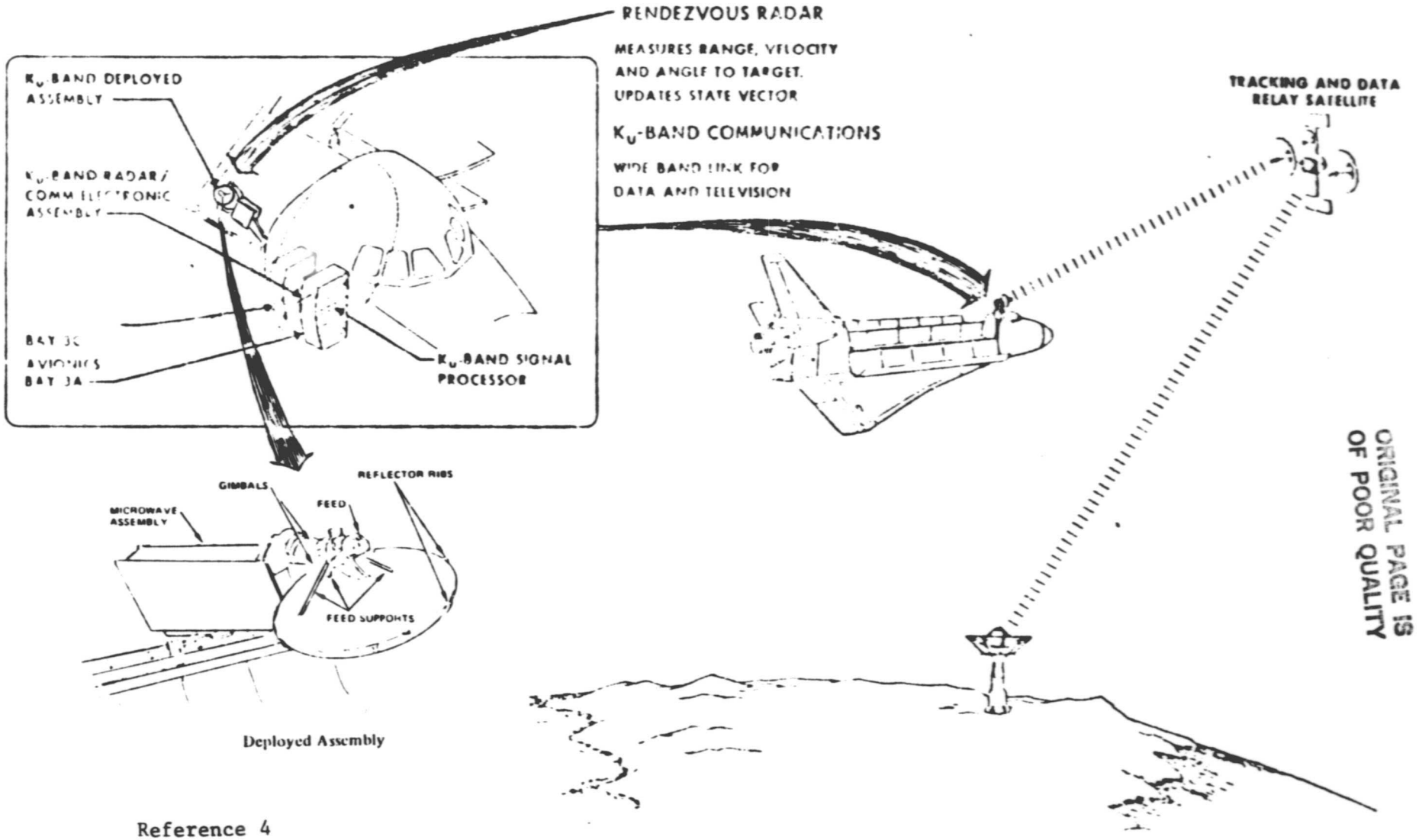

Reference 4

Figure 4 Shuttle Orbiter K_u-Band Radar/Communications System

The Small Payload Maneuvering System (SPMS) should perform a wide variety of automated services near the orbiter, although it has somewhat limited range and other capabilities.

The Orbital Transfer Vehicles (OTVs) will need a fully capable advanced multipurpose rendezvous tracking system to permit them to intercept orbiters, spacecraft or platforms throughout geocentric space and to stationkeep or dock with precision. A concept for an initial version of chemical rocket OTV is shown in Figure 5.[5] OTVs in a number of evolutionary versions during the 1986-95 period will be the workhorse vehicles for space operations between LEO and GSO and beyond. They will probably develop interchangeable cargo, personnel and teleoperator front ends depending on specific mission assignments and will probably be entirely space-based by the end of the period.

Teleoperator maneuvering systems (TMS) will operate as an interceptor near and remote from an orbiter or space station on which it is based with transport over major distances provided by the OTVs or other propulsion stages. TMS must maneuver with considerable precision and be very versatile in the services provided. A recent TMS system concept is diagrammed in Figure 6,[6] general arrangement views of the teleoperator concept are presented in Figure 7 and pictorial views of the teleoperator are shown in Figures 8 and 9. Prospective TMS evolution in the performance of various application services is diagrammed pictorially in Figure 10.[7] The development of TMS capabilities during this time period needs to be studied in

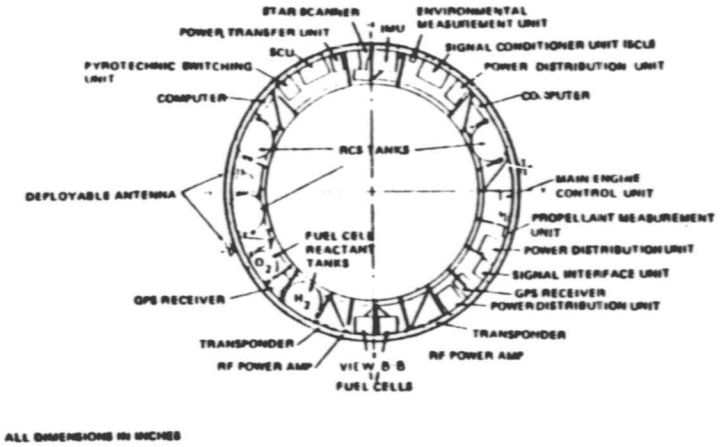

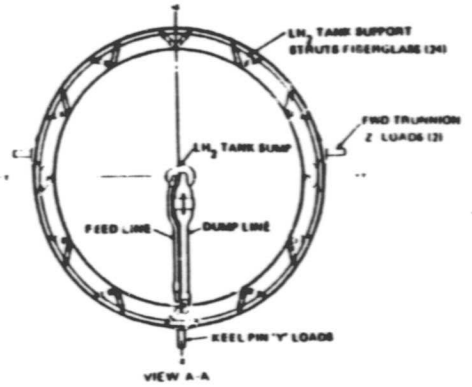

Reference 5

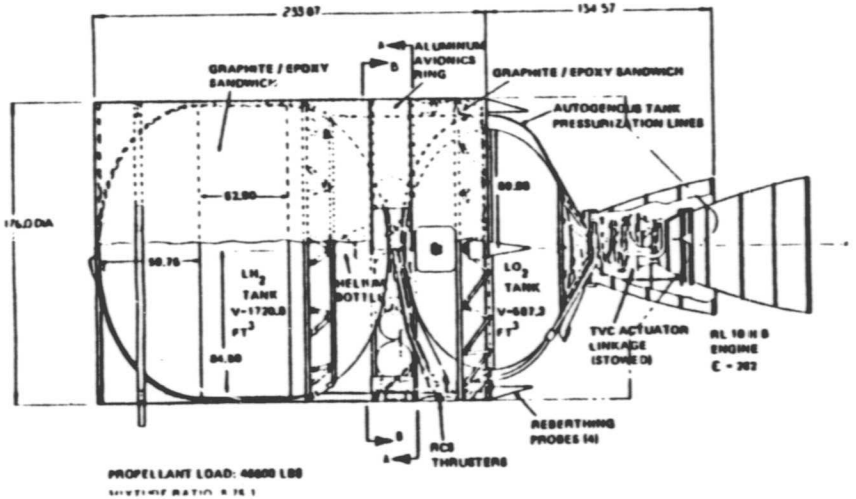

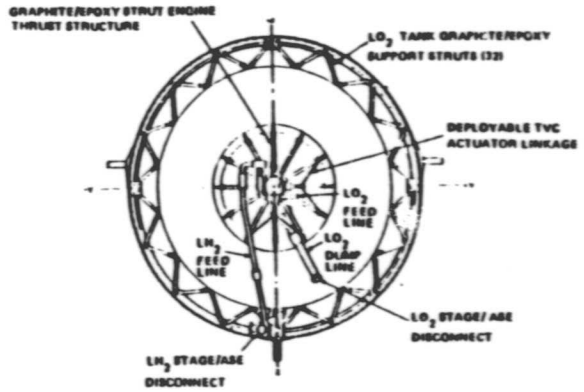

Figure 5 Initial Orbital Transfer Vehicle (after Boeing)

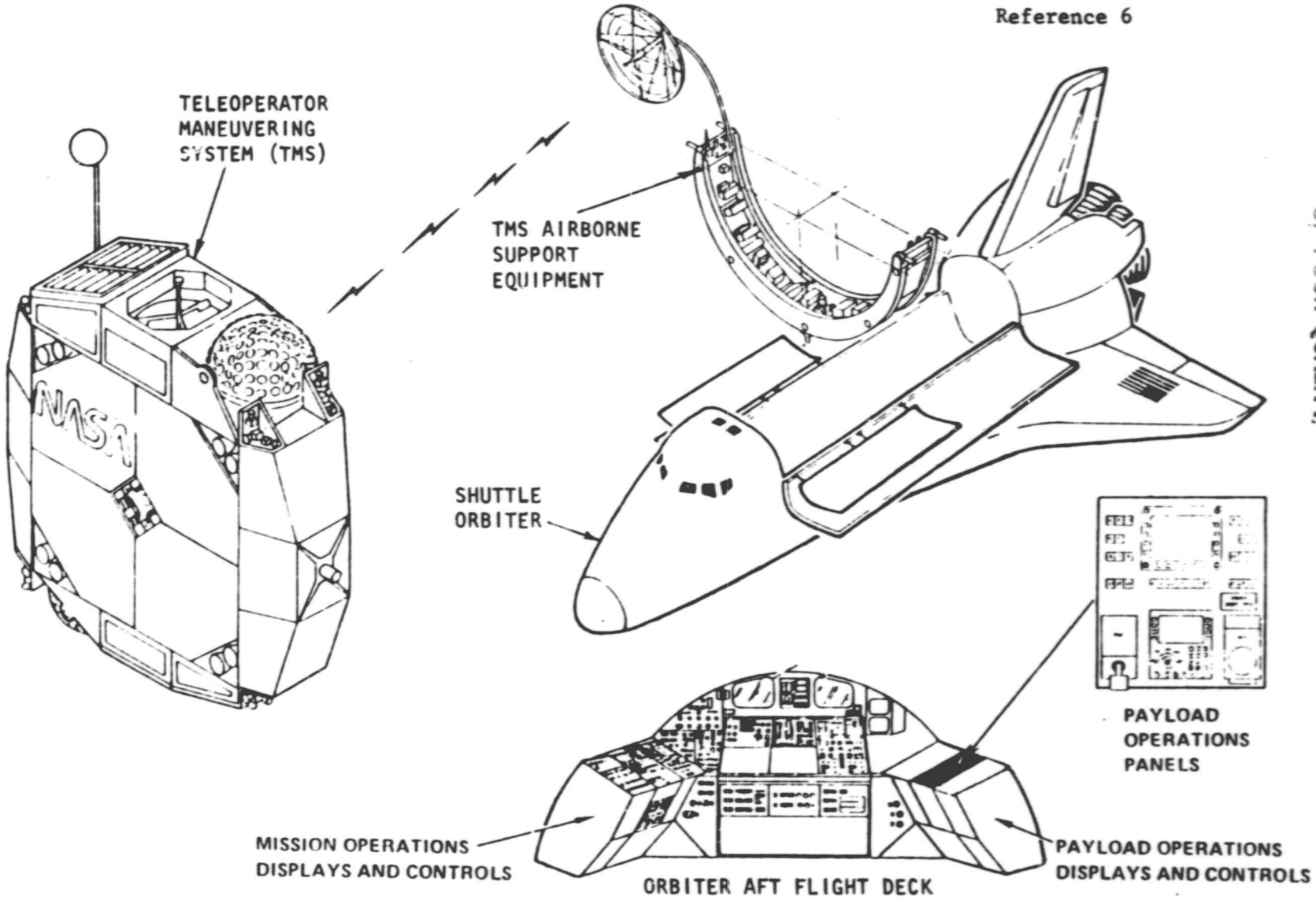

Figure 6 Teleoperator Maneuvering System (TMS) Concept

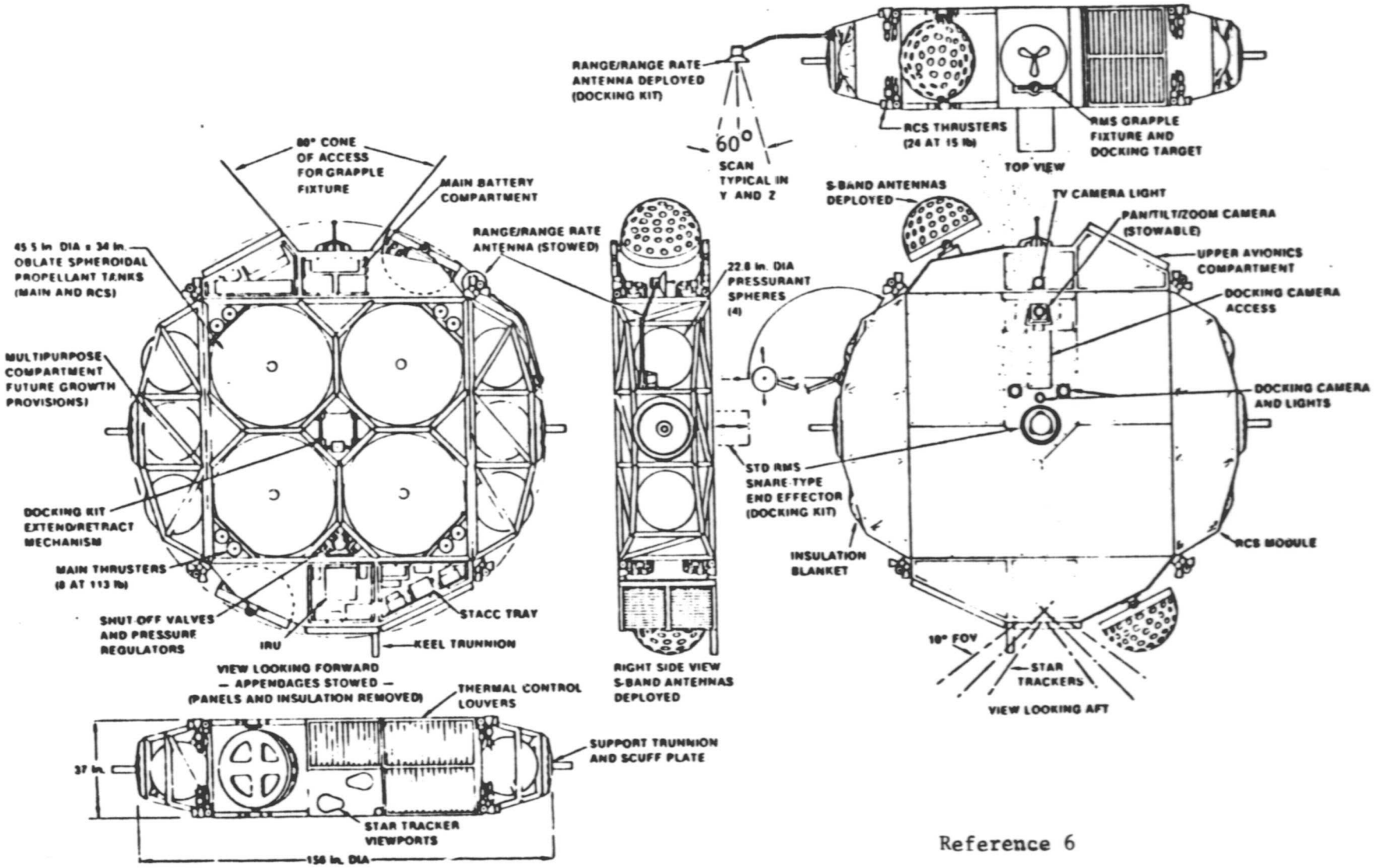

Reference 6

Figure 7 General Arrangement Views of a Teleoperator Maneuvering System (TMS) Concept

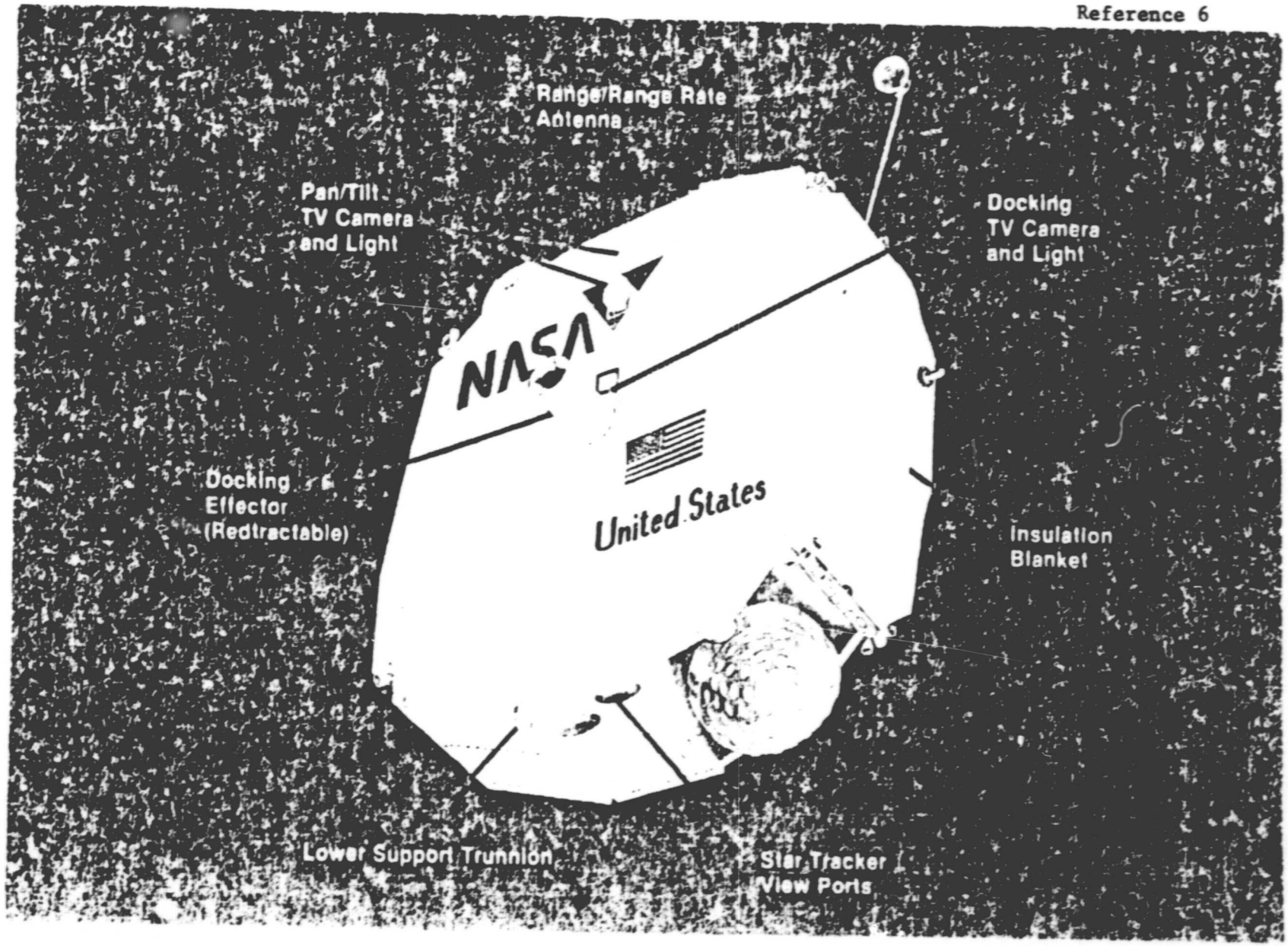

Figure 8 Teleoperator Maneuvering System (TMS) Concept Configuration - Front View

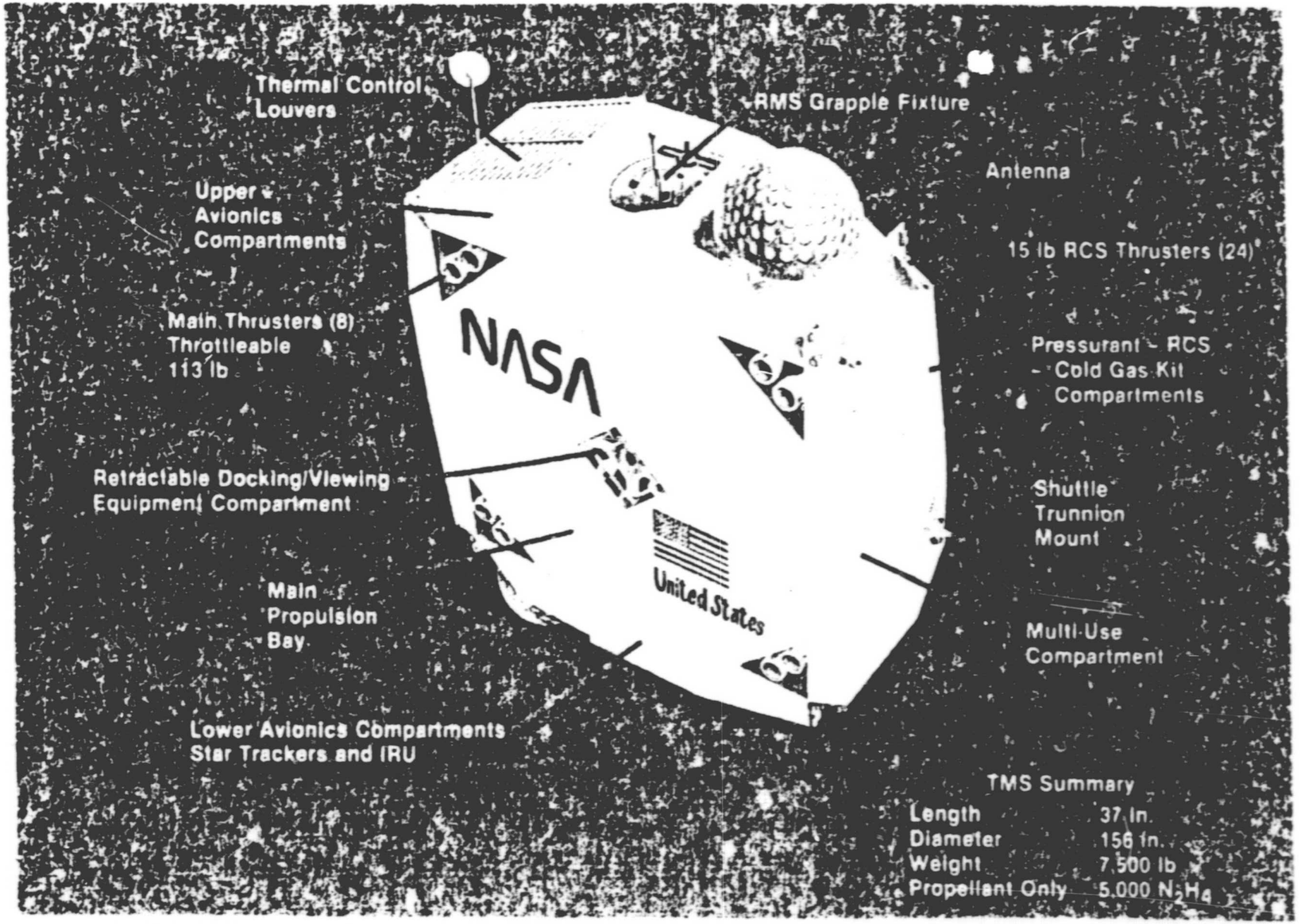

Figure 9 Teleoperator Maneuvering System (TMS) Concept Configuration - Rear View

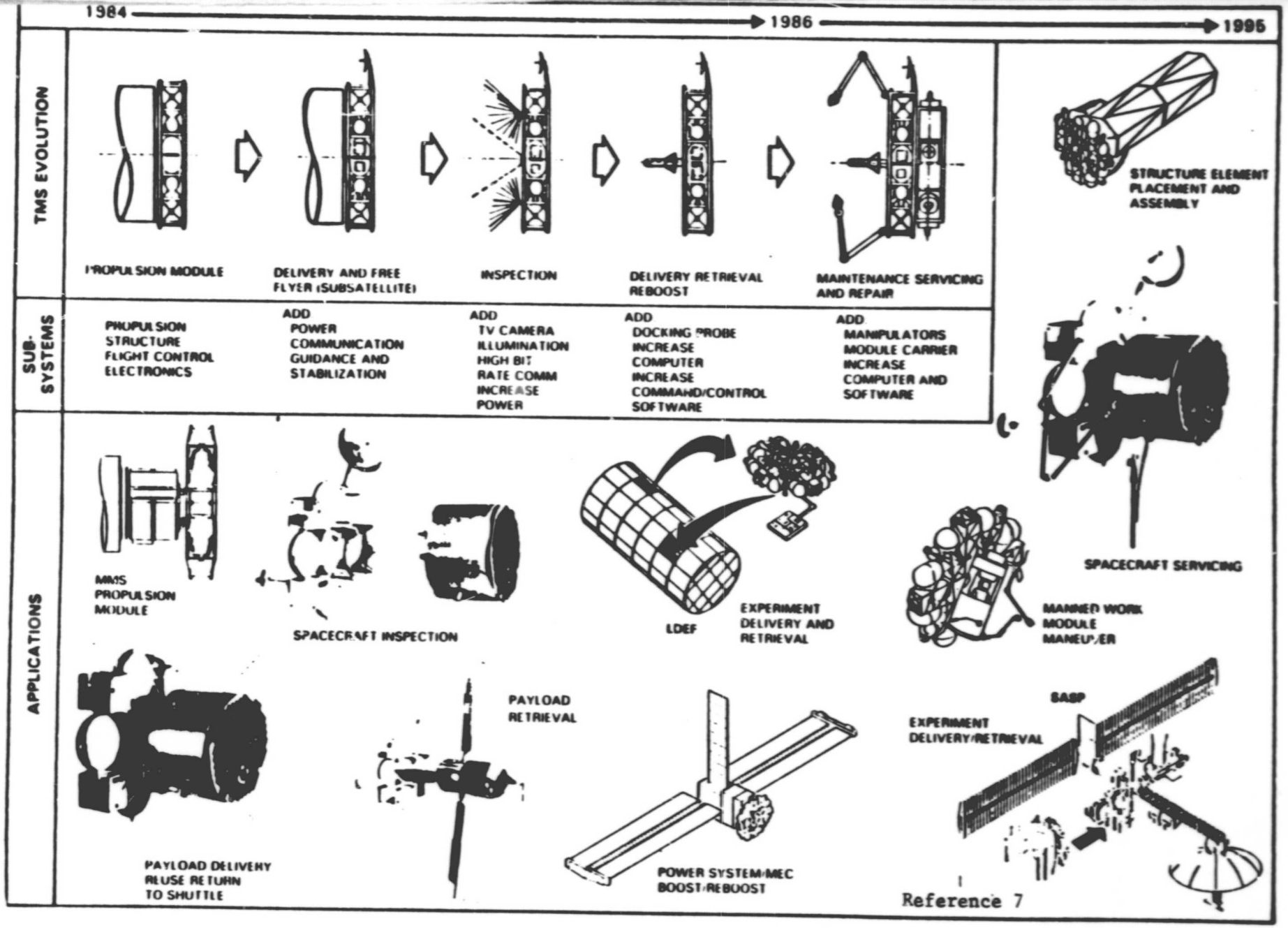

Figure 10 A Prospective Teleoperator Maneuvering System (TMS) Evolution

considerable detail so that all interacting systems operating requirements and characteristics are properly related. A typical TMS retrieval mission scenario is diagrammed in Figure 11, range/range rate sensor requirements are listed in Table 4 and communications links are sketched in Figure 12.

A Space Operations Center (SOC) is expected to be a primary place of focus for operating in orbit by the mid-1990s. A recent concept is shown in Figure 13 with the SOC approach and objectives listed in Table 5.[8] The SOC will provide for a permanent manned presence in LEO and a way station to GSO and beyond. It will also serve as a staging point for return to the Earth's surface. A very wide variety of objectives can be met at the SOC in addition to freeing the orbiter for the transport duties for which it was primarily designed. Basing for OTVs and TMSs is seen as the SOC's most important function.

Figure 14 shows a geostationary communications platform also projected for the mid-1990s with large deployable antennas.[9] The internal detail of its service module that would be used to provide expendable supplies and docked to the platform core structure by a teleoperator maneuvering system is delineated in Figure 15.

Solar system exploration spacecraft will have a wide variety of requirements some of which will be unique, e.g., rendezvous with an asteroid, but many will be provided for by the geocentric mission requirements, such as the return to Earth orbit by a Sample Return Spacecraft. Even here some special requirements may be anticipated in the probable use of aerobraking maneuvers to reduce the incoming heliocentric to geocentric orbital velocities. This technique will probably prove to be advantageous for return to a SOC from cis-lunar space and geostationary orbit.

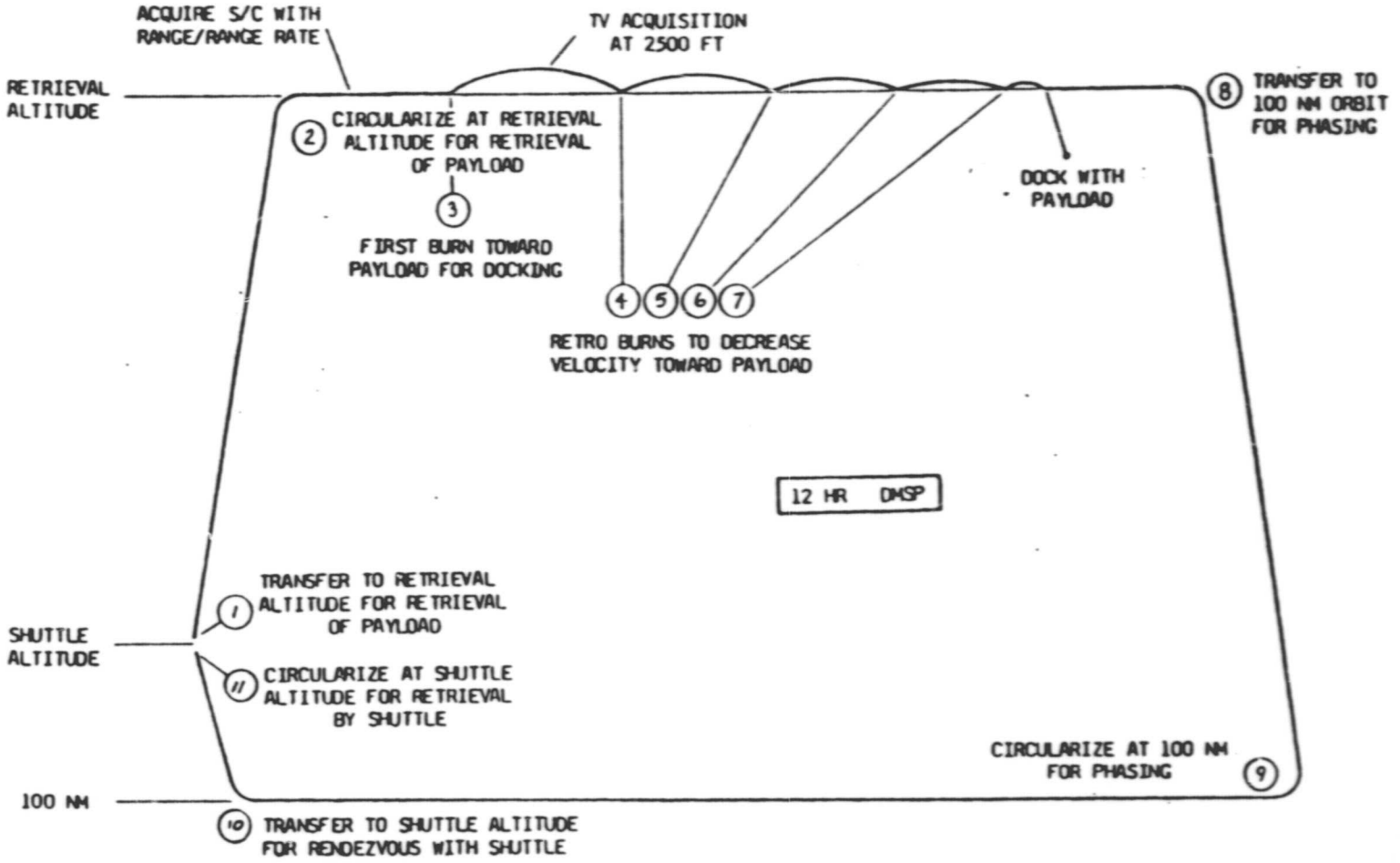

Reference 6

Figure 11 Typical Teleoperator Maneuvering Systems (TMS) Retrieval Mission Scenario

Table 4 Reference 6

Teleoperator Maneuvering System (TMS) Range/Range Rate Sensor Requirements

Range	0 ft to 10 nmi
Range Accuracy	± (20 ft + 2% of range) @ 100 ft to 10 nmi range ± 6 in or 1% of range @ 0 to 100 ft range
Range Rate	0 to 100 ft/sec
Range Rate Accuracy	5% of range rate @ 10 ft to 20 NM range ± 0.1 ft/sec @ 0 to 10 ft range
Field of View or Scan Area	60^{o} included conical angle
Angle Accuracy	TBD
Mass	Goal 50 lbm or less
Volume	Goal 1 ft^3 or less
Target Aids	To be defined by sensor supplier
Redundancy	Function redundancy required (degradation in back-up mode to be defined by sensor supplier)

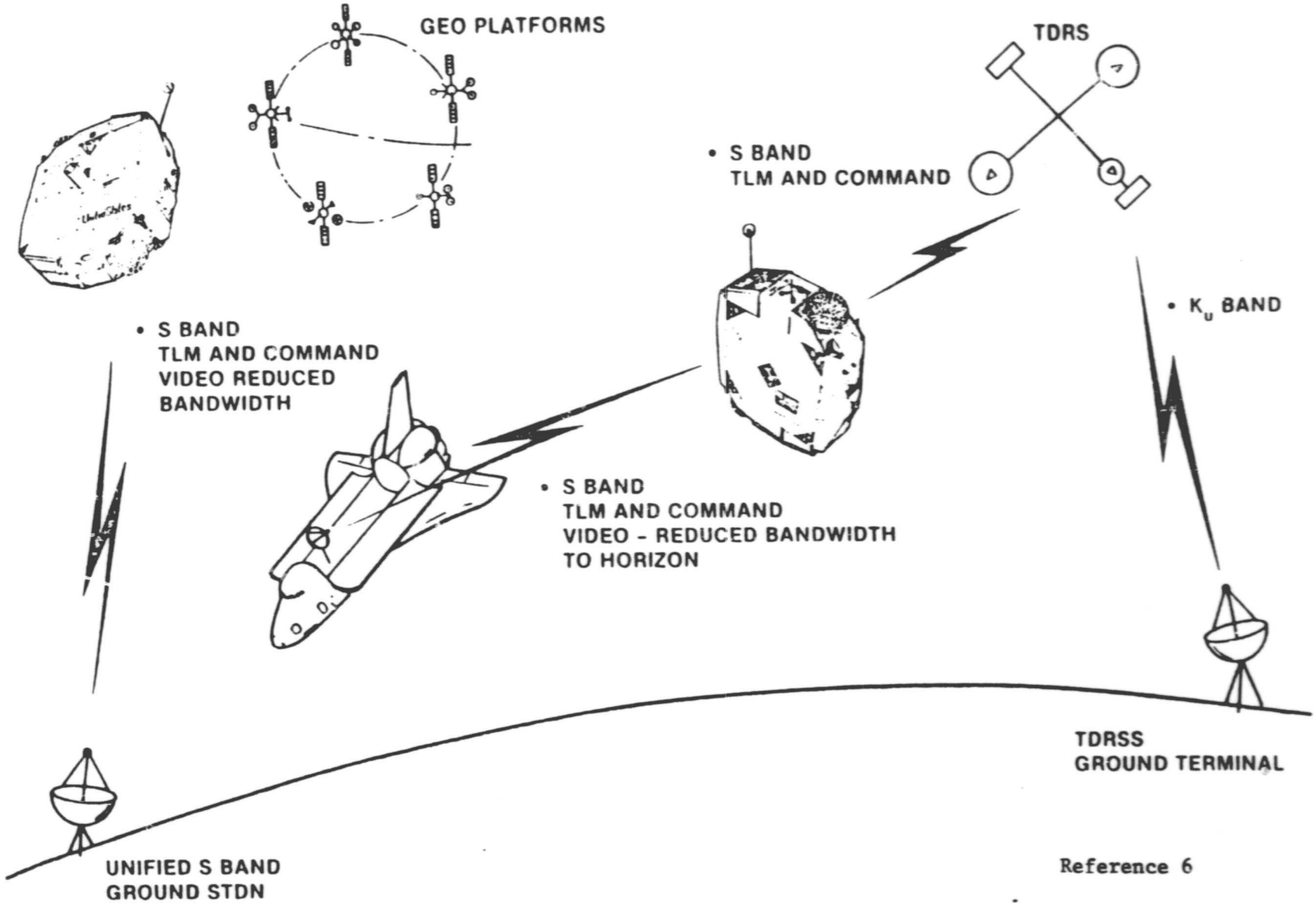

Figure 12 Teleoperator Maneuvering System (TMS) Communication Links

ORIGINAL PAGE
BLACK AND WHITE PHOTOGRAPH

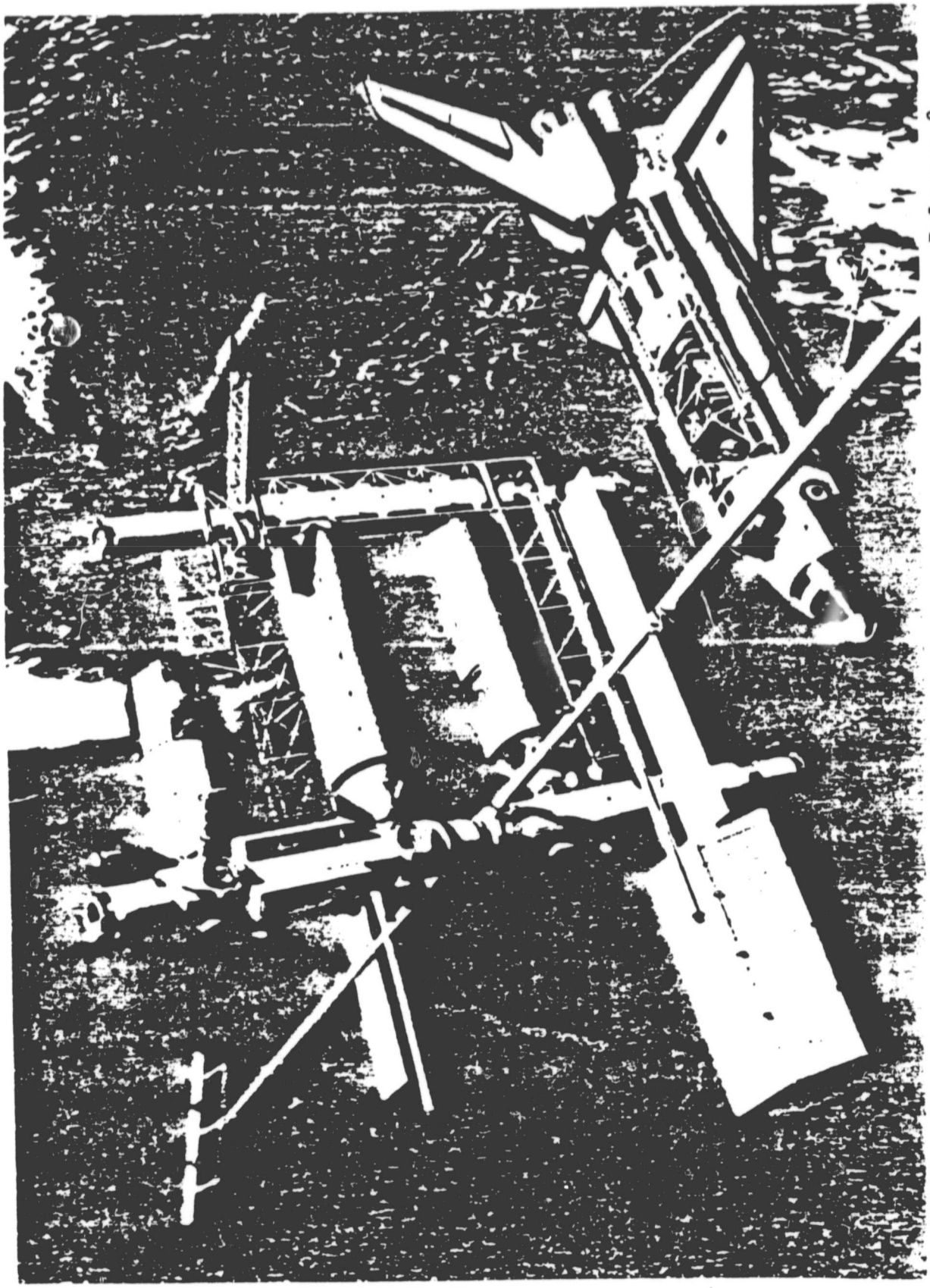

Reference 8

Figure 13 Space Operations Center (SOC) with Docking Orbiter in Mid-1990s

Table 5 **Reference 8**

Space Operations Center (SOC) Approach and Objectives

APPROACH

- Shuttle-serviced permanent manned facility in low Earth orbit
  - 4 to 8 person crew
  - 90 day resupply
  - Dual path, redundant design
  - Partially closed life support system
- Transfer extended time-line missions from shuttle to permanent facility

OBJECTIVES

- Satellite and platform servicing
  - Placement and retrieval
  - Maintenance and repair
  - Staging for platform payloads
- Staging for high energy missions
  - Propellant storage and transfer
  - Space based OTV's
  - System assembly and check out
  - Staging base for geo servicing
- Assembly and construction of large structures
- Establish permanent occupancy in space for manned operations

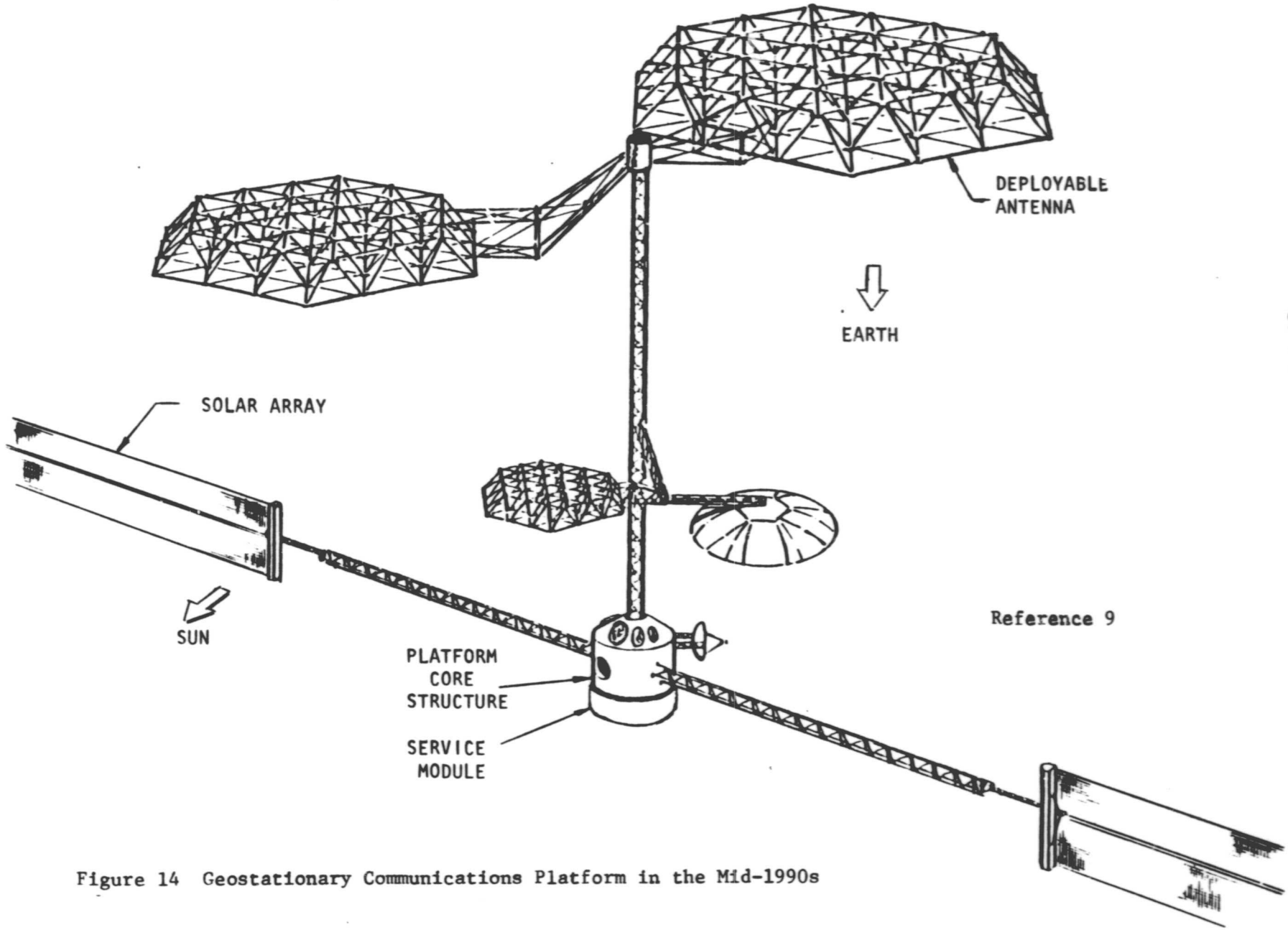

Reference 9

Figure 14 Geostationary Communications Platform in the Mid-1990s

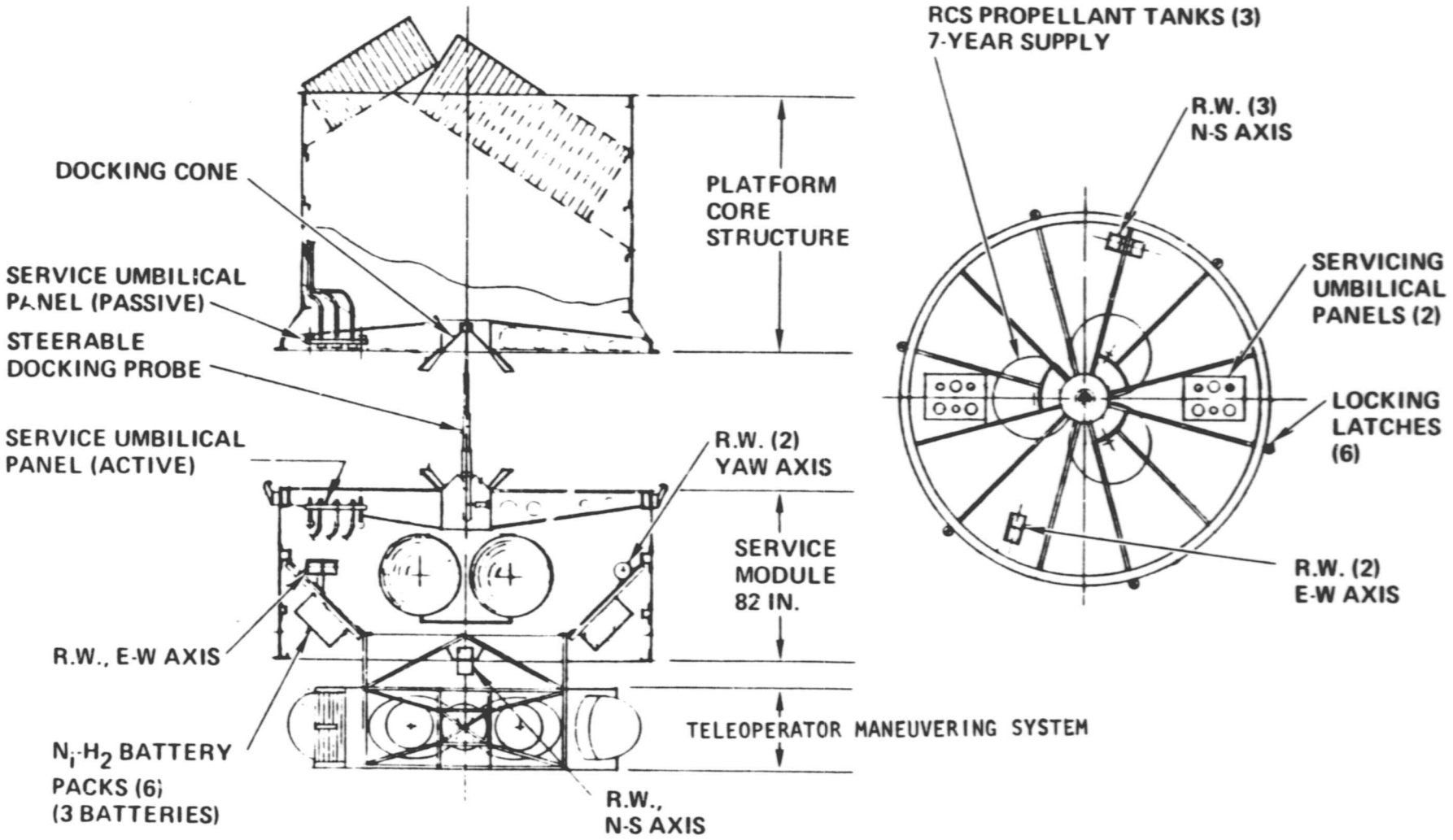

Reference 9

Figure 15 Geostationary Communications Platform Service Module

TYPICAL CHARACTERISTICS OF SELECTED SPACECRAFT, VEHICLES AND OTHER CONCEPTS

The characteristics of selected spacecraft, vehicles and other concepts that are related to advanced multipurpose rendezvous tracking systems in the 1986-95 time period are given in Table 6. The figures given should be considered as tentative at this time and used only to aid in establishing the overall requirements of rendezvous, station-keeping and docking sensors rather than as specific characteristics of the listed spacecraft, vehicles and other concepts.

TENTATIVE

Table 6

Typical Characteristics of Selected Spacecraft, Vehicles and Other Concepts Related to Advanced Multipurpose Rendezvous Tracking Systems - 1986 to 1995

	Mass, kg	Dimen., LxWxH , m	Thrust, N	Orbit		Interceptor(I) or Target(T)	IOC, CY
				Alt, km	Incl, deg		
Shuttle Orbiter	$2x10^6$	37x24x23	$24.5x10^6$	200-1000	23 to 103	Both	1982
Wide Body Centaur	$12x10^3$	8.8x4.4D	$89x10^3$	200 & Up	All	I	(1987)
Advanced Chemical Rocket OTV-Initial	$24x10^3$	12x4.4D	$67x10^3$	200 & Up	All	I	(1990)
Electric Rocket OTV	3500	10x100x10	10	200 & Up	All	I	(1986)
Extravehicular Mobility Unit (EMU)	150	0.7x0.5x2	0	Near Orbiter		T	1982
Manned Maneuvering Unit (MMU)	150	0.7x0.8x1.3	24x7.6	Near Orbiter		Both	1983
Small Payload Maneuvering System (SPMS)	226	1x0.7x0.6	10	Near Orbiter		I	(1987)
Teleoperator Maneuvering Systems (TMS)	3550	1x4D	4022	200 & Up	All	I	(1990)
Typical Low Earth Orbit (LEO) Spacecraft (S/C)	1 to 50 x 10^3	1 to 60x4.5D	1000 to 20000	200-1000	All	T	1983 et seq.
Typical LEO Space Platforms	10 to 200 x 10^3	10x100x5	-	200-1000	All	T	(1990)
Science and Applications Space Platforms - Unmanned (SASP)	1.6-16.2 x 10^3	30x100x10	-	200-1000	All	T	(1990)
Space Operations Center (SOC)	2600	50x150x20	-	500-1000	23 to 103	T	(1990)
Various Geostationary Orbit (GSO) S/C	1to10x10^3	1 to 60x4.5D	-	$36.7x10^3$	Equa.	T	1986
Typical GSO Platforms, Stations and Bases	10 to 200 x 10^3	30x100x10	-	$36.7x10^3$	Equa.	T	(After 1995)
Solar System Exploration S/C	$5x10^3$	10x30x7	900	Helio	Ecliptic	Both	(1990)

REFERENCES

1. Tong, D., Study of the Potential Impact of Large Multifunctional Space Platforms on Canadian Satellite Systems, Canadian Department of Communications Report No. DOC-CR-SP-80-008, July 1980.

2. Nein, M. and Runge, F., Science and Applications Space Platform, AIAA Large Space Structures Conference, January 1981.

3. Chase, R. L., Potential Military Space System Applications for Advanced Electric Propulsion Systems, AIAA 81-1536, 29 July 1981.

4. Cager, R. H., Jr., LaFlame, D. T. and Pardoe, L. C., Orbiter Ku-Band Integrated Radar and Communications Subsystem, IEEE Transactions on Communications, Vo. COM-26, No. 11, November 1978.

5. Calousi, V. A., Orbital Transfer Vehicle - Concept Defintion Study Final Report, Vols, 1-6, Boeing Aerospace Co. Report No. 180-26090, 1980.

6. Anon., Briefing on Teleoperator Maneuvering System, Vought, Spring 1981.

7. Stofan, A. J. et al., NASA's Next Decade in Space, National Space Club, June 1981.

8. Covington, C., et al., Space Operations Center - A Concept Analysis, NASA Johnson Space Center Report No. JSC-16277, November 29, 1979.

9. Reactor, W. F. III, and Bowman, R. M., Global Satellite Communications System Using Geostationary Platforms, IAF 81-52, September 1981.